

https://dspace.org/

Development of a high pressure hydrometallurgical process for the extraction of iron from iron oxide bearing materials

Rolfe, Wesley

2016

http://hdl.handle.net/10539/22608

Rolfe, Wesley (2016) Development of a high pressure hydrometallurgical process for the extraction of iron from iron oxide bearing materials, University of the Witwatersrand, Johannesburg, <http://hdl.handle.net/10539/22608>

Downloaded from a DSpace repository. https://dspace.org/



DEVELOPMENT OF A HIGH PRESSURE HYDROMETALLURGICAL PROCESS FOR THE EXTRACTION OF IRON FROM IRON OXIDE BEARING MATERIALS

Wesley Rolfe

A dissertation submitted to the Faculty of Engineering and the Built Environment, University of the Witwatersrand, in fulfilment of the requirements for the degree of Master of Science in Engineering.

Johannesburg, 2016

The financial assistance of the National Research Foundation (NRF) towards this research is hereby acknowledged. Opinions expressed and conclusions arrived at, are those of the author and are not necessarily attributed to the NRF.

DECLARATION

I declare that this dissertation is my own unaided work. It is being submitted for the degree of Master of Science in Engineering to the University of the Witwatersrand, Johannesburg. It has not been submitted before for any other degree or examination in any other University.

……

Wesley Rolfe

28th day of October, 2016

ABSTRACT

The feasibility of extracting iron from iron(III) oxide bearing materials with acetylacetone has been under investigation for many years. This is an alternate, environmentally friendly process for the recovery of iron compared to conventional processes that are energy intensive, have numerous costly process steps and produce large quantities of greenhouse gases. Iron(III) oxide bearing waste materials can be used in this process which reduces its environmental impact as it would not require waste storage.

This study investigated the feasibility of reducing the reaction time of the liquid phase extraction of iron from iron ore fines by performing the extraction at elevated pressures and temperatures. It was found that that the extraction under pressure was dependent on temperature, pressure, particle size and solid to liquid ratio. It was found that at high temperatures and long extraction times, an unknown secondary reaction occurs that consumes the desired product, iron(III) acetylacetonate, and inhibits the recovery of these crystals. This results in lower extraction yields. It was found that the side reaction was largely dependent on the temperature of the system and the amount of iron(III) acetylacetonate present. The effects of the side reaction could be limited by lower operating temperatures and reducing the total reaction times.

An optimum conversion of iron(III) oxide to iron(III) acetylacetonate of 47.2% was achieved for synthetic iron (III) oxide (> 95 wt% Fe_2O_3) at a total extraction time of 4 h, 160 °C, 0.025 g:1 mL, operating pressure of 1700 kPa, initial N_2 feed pressure of 1010 kPa and 375 rpm stirrer speed. The optimum extraction of iron from iron ore fines (> 93 wt% Fe_2O_3) to iron(III) acetylacetonate was found to be 20.7% at 4 h, 180 °C, 0.025 g:1 mL and operating pressure of 1900 kPa, initial N_2 feed pressure of 1010 kPa and 375 rpm stirrer speed. These are the optimum conditions where the side reaction is limited to improve the recovery and desired reaction conversion capabilities of the process.

The operation under pressure yielded lower conversions than that of the atmospheric leaching process developed by Tshofu (acetylacetone water system under reflux). It was also found that it was not possible to reduce the extraction time and achieve comparable extractions when operating at higher temperatures and pressures. The formation of an additional unwanted product would also lead to unnecessary treatment costs in an industrial process. Hence, it was found that pressure leaching as an alternative is not currently viable

due to the lower yields and associated high costs. Atmospheric leaching seems to be the most economically feasible option until a better alternative is found.

Dedication

To my family and friends for all their support and getting me through everything, especially my parents who have supported me throughout everything that I have done.

Acknowledgements

My sincere thanks are given to the following people and organisations that have provided input of some kind to the completion of this project:

- The National Research Fund (NRF) for providing the funding that made this project possible.
- The School of Chemical and Metallurgical Engineering for hosting me and my experimental work.
- My Supervisor Dr Lizelle van Dyk who was an invaluable part of my research. Her guidance and support throughout the project was a driving force towards the end completion.
- Marco Pires and Celsius Scientific for the Autoclave and for dealing with any problems experienced while the autoclave was in operation.
- Glawdis Tshofu for his initial inputs and training at the beginning of the project.
- Prof. Herman Potgieter and Prof. Sanja Potgieter for their advice and offered knowledge.
- Bruce Mothibedi, Doctor Mbense and Xolani Mdletshe for help with equipment, laboratory problems and other help offered.
- Reghana Daniels and Sibongile Maswanganye for dealing with all my orders
- Rhod McRae-Samuel and his team (Rodney Gurney, Phathu Sikhwari and Hopewell Gumede) in the Workshop for all their help with equipment problems
- The staff of the Chemical and Metallurgical Engineering School for being there if any help was needed
- Dr Caren Billing for her help regarding statistics and chemistry insight
- Rudolph Erasmus for performing the Raman Spectroscopy on the samples
- Tumelo Phaahlamohlaka for performing the FTIR scans
- My colleagues in the School of Chemistry and Metallurgical Engineering for being the support needed to finish this project and offer advice when it was needed.
- My vacation work student, Megan Blignaut for her vital help in the laboratory during the last stages of investigation that made it possible for the project to proceed.
- Michiel Wessels for his assistance in the laboratory.

- Finally, my friends and family that were my support and strength needed to complete this project. Especially my parents that were with me every step of the way and whom without I would not have been able to achieve what I did.

Contents

Page

DECLARATION I
ABSTRACT II
DEDICATION IV
ACKNOWLEDGEMENTS V
CONTENTS VII
LIST OF FIGURES IX
LIST OF TABLES XIII
LIST OF SYMBOLS XVI

1 INTRODUCTION 1
1.1 Motivation and Background 1
1.2 Research Aim and Objectives 3
1.3 Dissertation Layout 4

2 LITERATURE REVIEW 5
2.1 Introduction 5
2.2 Conventional methods for iron extraction 5
2.2.1 Blast furnace 6
2.2.2 Direct reduction 7
2.2.3 Smelting reduction 9
2.2.4 Sintering and pelletisation 10
2.3 Ligands and metal complexes 11
2.4 Alternatives and advances in iron extraction techniques 12
2.5 Pressure leaching 15
2.5.1 Overview 16
2.5.2 Technical details 17
Types 17
Equipment and operation 17
2.6 Vapour pressure 18

3 EXPERIMENTAL METHODS 21

3.1 High pressure autoclave 21
3.2 Determination of experimental operating space 23
3.2.1 Solubility analysis of iron(III) acetylacetonate in acetylacetone 23
3.2.2 Measurement of pure and mixture vapour pressures 24
3.3 Extraction of iron from synthetic iron(III) oxide and iron ore fines 24
3.3.1 Initial extraction of iron from iron ore fines 24
3.3.2 Extraction of iron from synthetic iron(III) oxide 25
3.3.3 Extraction of iron from iron ore fines 26
3.4 Analysis of results 27
3.4.1 Spectroquant Pharo 300 Spectrophotometer analysis (UV-Vis) 27
3.4.2 Fourier transform infrared spectroscopy (FTIR) 28
3.5 Recovery of crystals and unreacted acetylacetone 28

4 EXPERIMENTAL RESULTS AND DISCUSSION 30
4.1 Determination of experimental operating space 30
4.1.1 Solubility analysis of iron(III) acetylacetonate in acetylacetone 30
4.1.2 Measurement of pure and mixture vapour pressures 33
4.2 Extraction of iron from synthetic iron(III) oxide and iron ore fines 36
4.2.1 Initial extraction of iron from iron ore fines 36
4.2.2 Extraction of iron from synthetic iron(III) oxide 38
4.2.3 Extraction of iron from iron ore fines 53

5 CONCLUSIONS 63

6 RECOMMENDATIONS 66

7 REFERENCES 67

APPENDIX A: MATERIALS 73
APPENDIX B: AUTOCLAVE DETAILS 77
APPENDIX C: SPECTROQUANT ANALYSIS 82
APPENDIX D: SOLUBILITY RESULTS 85
APPENDIX E: VAPOUR PRESSURE RESULTS AND CALCULATIONS 86
APPENDIX F: RESULTS AND CALCULATIONS 94

List of figures

Page

Figure 1.1: Proposed process block flow diagram of the extraction of iron from iron(III) oxide bearing materials and the recovery of iron(III) acetylacetonate. 3
Figure 2.1: Schematic diagram of steel production technologies from iron (blast furnace, direct reduction and smelting reduction) or scrap steel (Stahl, 2013). 6
Figure 2.2: Schematic diagram of a blast furnace (Shah, n.d.). 7
Figure 2.3: Schematic diagram of the MIDREX Process (Downstream Consulting Pty Ltd, 2013). 8
Figure 2.4: FINMET process schematic diagram (Feinman, 1999).....9
Figure 2.5: Schematic diagram of the COREX process (Gojić and Kožuh, 2006).....10
Figure 2.6: Acetylacetone structure (Binnemans, 2005).....11
Figure 2.7: Keto-enol equilibrium of acetylacetone (Binnemans, 2005).....12
Figure 2.8: Horizontal autoclave with four-compartments, mechanical stirrers, gas injectors and heat exchangers (Vignes, 2011). 18
Figure 2.9: Vapour pressure data for various metal(acetylacetonates) (Berg and Truemper, 1965). 20
Figure 3.1: Autoclave with N_2 feed, temperature controllers and magnetic stirrer. 22
Figure 3.2: Disassembled autoclave.....22
Figure 3.3: Solubility of iron(III) acetylacetonate in acetylacetone experimental setup. .23
Figure 3.4: Heidolph Rotary Evaporator setup used for recovery. 29
Figure 4.1: Solubility of iron(III) acetylacetonate in acetylacetone performed with two different light bulbs (i.e. energy saver 9 W bulb and a 100 W bulb).....31
Figure 4.2: Vapour pressure of acetylacetone and water in the presence of nitrogen plotted with the pure component Antoine predicted curves (Yaws, 2015).....33
Figure 4.3: Vapour pressure of acetylacetone, water and a 9:1 solution of acetylacetone and water in the presence of nitrogen and an ASPEN Plus simulation of the mixture. 34
Figure 4.4: UV-Vis scan for the initial study at varying N_2 loaded pressures of 7.5 g of iron ore fines (>93 %) at 220 °C with 300 mL solution (270 mL acetylacetone and 30 mL water), solid to liquid ratio of 0.025 g:1 mL, total time 18 h, particle size of +106 - 150 µm and stirrer speed of 375 rpm. 37
Figure 4.5: UV-Vis analysis results of 5 g of synthetic iron oxide at solid to liquid ratio of 0.025 g:1 mL, 1000 kPa N_2, total time of 3 h and varying temperature. 39

Figure 4.6: UV-Vis scan results for the iron(III) acetylacetonate standards shown in terms of iron concentrations. 40
Figure 4.7: UV-Vis analysis results of 5 g of synthetic iron oxide at solid to liquid ratio of 0.025 g:1 mL, 1000 kPa N_2, total time of 4 h and varying temperature. 41
Figure 4.8: UV-Vis analysis results of 5 g of synthetic iron oxide at solid to liquid ratio of 0.025 g:1 mL, 1000 kPa N_2, total time of 6 h and varying temperature. 42
Figure 4.9: UV-Vis analysis results of 5 g of synthetic iron oxide at solid to liquid ratio of 0.025 g:1 mL, 1000 kPa N_2, total time of 8 h and varying temperature. 42
Figure 4.10: UV-Vis analysis results of 5 g of synthetic iron oxide at solid to liquid ratio of 0.025 g:1 mL, 1000 kPa N_2, total time of 10 h and varying temperature. 43
Figure 4.11: UV-Vis analysis results of 5 g of synthetic iron oxide at solid to liquid ratio of 0.025 g:1 mL, 1000 kPa N_2, total time of 18 h and varying temperature. 44
Figure 4.12: UV-Vis analysis results of 10 g of synthetic iron(III) acetylacetonate in 200 mL of solution (9:1 acetylacetone:water), 1000 kPa N_2, total time of 8 h and at 220 °C. 45
Figure 4.13: Results for the temperature study of 5 g of synthetic iron oxide (>95 %) with 200 mL solution (180 mL acetylacetone and 20 mL water), 1010 kPa N_2 loaded, solid to liquid ratio of 0.025 g:1 mL and stirrer speed of 375 rpm. 46
Figure 4.14: Recovered iron(III) acetylacetonate crystals. 48
Figure 4.15: FTIR scan results for the synthetic iron oxide experiment performed at 140 °C, total time of 4 h, 9:1 ratio of acetylacetone: water, 0.025 g/mL and 5 g of iron oxide. 50
Figure 4.16: FTIR scan results for the synthetic iron oxide experiment performed at 180 °C, total time of 8 h, 9:1 ratio of acetylacetone: water, 0.025 g/mL and 5 g of iron oxide. 51
Figure 4.17: FTIR scan of acetylacetone (National Institute of Standards and Technology, 2016b). 51
Figure 4.18: FTIR scan of iron(III) acetylacetonate (National Institute of Standards and Technology, 2016c). 52
Figure 4.19: UV-Vis analysis results for the reaction rate study of 5 g of iron ore fines (>93 %) at 140 °C with 200 mL solution (180 mL acetylacetone and 20 mL water), 1010 kPa N_2 loaded, solid to liquid ratio of 0.025 g:1 mL, particle size of +106 -150 µm and stirrer speed of 375 rpm. 54

Figure 4.20: Comparison of the Tshofu's (2014) 140 °C liquid phase experiment with synthetic iron(III) oxide (< 1 µm) and iron ore fines (+106 -150 µm) at 140 °C with 200 mL solution (180 mL acetylacetone and 20 mL water), 1010 kPa N_2 loaded, solid to liquid ratio of 0.025 g:1 mL, and stirrer speed of 375 rpm. 55
Figure 4.21: UV-Vis results for iron ore fines at 4 h, 5 g, 1000 kPa N_2 initial pressure, 106 -150 µm and 0.025 g:1 mL solid to liquid ratio at varying temperature 56
Figure 4.22: Results for the particle size and temperature study of 5 g of iron ore fines (>93 %) with 200 mL solution (180 mL acetylacetone and 20 mL water), 1010 kPa N_2 loaded, solid to liquid ratio of 0.025 g:1 mL, total time 4 h and stirrer speed of 375 rpm. 57
Figure 4.23: UV-Vis analysis results for the pressure study of 5 g of iron ore fines (>93 %) at 180 °C with 200 mL solution (180 mL acetylacetone and 20 mL water), solid to liquid ratio of 0.025 g:1 mL, particle size of +45-75 µm, total time 4 h and stirrer speed of 375 rpm. 58
Figure 4.24: Results for the pressure study of 5 g of iron ore fines (>93 %) at 180 °C with 200 mL solution (180 mL acetylacetone and 20 mL water), solid to liquid ratio of 0.025 g:1 mL, particle size of +45-75 µm, total time 4 h and stirrer speed of 375 rpm. 59
Figure 4.25: UV-Vis analysis results for the solid to liquid ratio study of iron ore fines (>93 %) at 180 °C with 200 mL solution (180 mL acetylacetone and 20 mL water), 1010 kPa N_2 loaded, particle size of +45-75 µm, total time 4 h, and stirrer speed of 375 rpm. 60
Figure 4.26: Results for the solid to liquid ratio study of iron ore fines (>93 %) at 180 °C with 200 mL solution (180 mL acetylacetone and 20 mL water), 1010 kPa N_2 loaded, particle size of +45-75 µm, total time 4 h, and stirrer speed of 375 rpm. 61

Figure A.1: Particle size distribution of iron ore fines (Tshofu, 2014). 75
Figure B.1: Engineering drawing of the autoclave. 78
Figure F.1: UV-Vis scan results for the iron(III) acetylacetonate standards shown in terms of iron concentrations (scanned on 06/01/2016). 94
Figure F.2: Calibration curve for the iron(III) acetylacetonate standards represented in terms of iron concentration present (scanned on 06/01/2016). 95
Figure F.3: UV-Vis analysis results temperature study of 5 g of iron ore fines (>93 %) with 200 mL solution (180 mL acetylacetone and 20 mL water), 1010 kPa N_2 loaded,

solid to liquid ratio of 0.025 g: 1 mL, particle size of +45-75 µm, total time 4 h and stirrer speed of 375 rpm. 107
Figure F.4: UV-Vis scan results of varying acetylacetone volumes into ethanol with solution total volume of 50 mL. 111
Figure F.5: Results of varying acetylacetone volumes into ethanol with solution total volume of 50 mL. 112
Figure F.6: FTIR scan results for the synthetic iron oxide experiment performed at 140 °C, total time of 8 h, 9:1 ratio of acetylacetone: water, 0.025 g:1 mL and 5 g of iron oxide. 112
Figure F.7: FTIR scan results for the synthetic iron oxide experiment performed at 140 °C, total time of 4 h, 9:1 ratio of acetylacetone: water, 0.025 g:1 mL and 5 g of iron oxide. 113

List of tables

Page

Table 2.1: Antoine coefficients for acetylacetone and water (Yaws, 2015). 19
Table 4.1: Fitted model to experimental vapour pressure of acetylacetone, water and a mixture of acetylacetone and water (9:1) in the presence of nitrogen. 34
Table 4.2: Crystal recovery results for 5 g of synthetic iron oxide at 1010 kPa N_2, solid to liquid ratio of 0.025 g:1 mL, and stirrer speed of 375 rpm. 49
Table 4.3: Crystal recovery results for 5 g of iron ore fines at 1010 kPa N_2, solid to liquid ratio of 0.025 g: 1mL, and stirrer speed of 375 rpm. 62

Table A.1: Acetylacetone chemical and physical properties (Sigma-Aldrich, 2015a). 73
Table A.2: Ethanol chemical and physical properties (Sigma-Aldrich, 2015b). 73
Table A.3: Iron(III) acetylacetonate chemical and physical properties (Kabemba, 2005; Sigma-Aldrich, 2012). 74
Table A.4: Chemical composition of iron ore fines (weight %) (Tshofu, 2014). 75
Table A.5: Crystalline composition of iron ore fines (weight %) (Tshofu, 2014). 75
Table A.6: Iron(III) oxide chemical and physical properties (Sigma-Aldrich, 2016). 76
Table A.7: Nitrogen chemical and physical properties (Afrox, 2015; Felder and Rousseau, 2005). 76
Table A.8: Water chemical and physical properties (Felder and Rousseau, 2005). 76
Table B.1: Heating jacket heating conditions. 81
Table C.1: Volume of 100 ppm Fe solution required to make the desired Spectroquant standard solutions. 83
Table D.1: Solubility of iron(III) acetylacetonate in acetylacetone performed with two different light bulbs (i.e. energy saver 9 W bulb and a 100 W bulb). 85
Table E.1: Vapour pressure results for acetylacetone and water mixture (9:1 acetylacetone:water) in presence on N_2. 86
Table E.2: Vapour pressure results for acetylacetone in presence on N_2. 89
Table E.3: Vapour pressure results for water in presence on N_2. 90
Table F.1: Iron(III) acetylacetonate standard calibration results (scanned on 06/01/2016). 95

Table F.2: Iron(III) acetylacetonate standard calibration results (scanned on 08/01/2016). 96
Table F.3: Iron(III) acetylacetonate standard calibration results (scanned on 15/01/2016). 96
Table F.4: Iron(III) acetylacetonate standard calibration results (scanned on 22/01/2016). 97
Table F.5: Iron(III) acetylacetonate standard calibration results (scanned on 29/01/2016). 97
Table F.6: Iron(III) acetylacetonate standard calibration results (scanned on 04/02/2016). 98
Table F.7: Iron(III) acetylacetonate standard calibration results (scanned on 19/02/2016). 98
Table F.8: Iron(III) acetylacetonate standard calibration results (scanned on 26/02/2016). 99
Table F.9: Iron(III) acetylacetonate standard calibration results (scanned on 03/03/2016). 99
Table F.10: Iron(III) acetylacetonate standard calibration results (scanned on 07/03/2016). 100
Table F.11: Iron(III) acetylacetonate standard calibration results (scanned on 08/03/2016). 100
Table F.12: Iron(III) acetylacetonate standard calibration results (scanned on 11/03/2016). 101
Table F.13: Iron(III) acetylacetonate standard calibration results (scanned on 16/03/2016). 101
Table F.14: Results for the initial study at varying N_2 loaded pressures of 7.5 g of iron ore fines (>93 %) at 220 °C with 300 mL solution (270 mL acetylacetone and 30 mL water), solid to liquid ratio of 0.025 g:1 mL, total time 18 h, particle size of +106 - 150 µm and stirrer speed of 375 rpm. 104
Table F.15: Results for the temperature study of 5 g of synthetic iron oxide (>95 %) with 200 mL solution (180 mL acetylacetone and 20 mL water), 1010 kPa N_2 loaded, solid to liquid ratio of 0.025 g:1 mL and stirrer speed of 375 rpm. 105
Table F.16: Results for the reaction rate study of 5 g of iron ore fines (>93 %) at 140 °C with 200 mL solution (180 mL acetylacetone and 20 mL water), 1010 kPa N_2 loaded,

solid to liquid ratio of 0.025 g:1 mL, particle size of +106 -150 µm and stirrer speed of 375 rpm. 108
Table F.17: Results for the particle size and temperature study of 5 g of iron ore fines (>93 %) with 200 mL solution (180 mL acetylacetone and 20 mL water), 1010 kPa N_2 loaded, solid to liquid ratio of 0.025 g:1 mL, total time 4 h and stirrer speed of 375 rpm. 109
Table F.18: Results for the pressure study of 5 g of iron ore fines (>93 %) at 180 °C with 200 mL solution (180 mL acetylacetone and 20 mL water), solid to liquid ratio of 0.025 g:1 mL, particle size of +45-75 µm, total time 4 h and stirrer speed of 375 rpm. 110
Table F.19: Results for the solid to liquid ratio study of iron ore fines (>93 %) at 180 °C with 200 mL solution (180 mL acetylacetone and 20 mL water), 1010 kPa N_2 loaded, particle size of +45-75 µm, total time 4 h, and stirrer speed of 375 rpm. 110
Table F.20: Calculated yield of iron(III) acetylacetonate for the solid to liquid ratio study of iron ore fines (>93 %) at 180 °C with 200 mL solution (180 mL acetylacetone and 20 mL water), 1010 kPa N_2 loaded, particle size of +45-75 µm, total time 4 h, and stirrer speed of 375 rpm. 114

List of symbols

Symbol	Unit	Property
a	-	Antoine coefficient
b	-	Antoine coefficient
c	-	Antoine coefficient
C	ppm	Concentration
	$g.mL^{-1}$	
d_{50}	µm	50 % cumulative passing (i.e. mean particle size)
D	-	Dilution ratio
m	g	Mass
M	$g.mol^{-1}$	Molecular weight
n	mol	Moles
N	-	Number of terms
p^*	kPa	Partial pressure
P	kPa	Pressure
S_x	-	Standard deviation
t	s	Time
T	°C	Temperature
V	mL	Volume
$\bar{X}$	-	Arithmetic mean
X_i	-	Any given value from sample

Subscripts:

1	Substance 1
2	Substance 2
actual	The actual component (i.e. what was actually achieved)
calc	Calculated value
cool	Cooling stage of reaction in autoclave
dil	Diluted sample aspects
Fe	Iron
$Fe(acac)_3$	Iron(III) acetylacetonate
Fe_2O_3	Iron(III) oxide
heat	Heating stage of reaction in autoclave
loaded	Initial loaded component into autoclave
max	Maximum
min	Minimum
react	Main reaction stage of reaction in autoclave
sample	Sample (i.e. liquid from autoclave experimental run)
T	Total
weighed	Weighed sample

Note: The units given above are those used unless otherwise stated

1 INTRODUCTION

1.1 Motivation and Background

Iron production (blast furnace and direct reduction iron) has almost doubled over the last 15 years from 620 Mt in 2000 to 1 212 Mt in 2015 due to an increased need for steel. Steel demand is forecast to increase 1.5 times that of the current demand (1.6 billion tonnes of steel produced in 2013) (World Steel Association, 2015). This is resulting in the depletion of high grade iron ore deposits (Beyeme Zogo, 2010). The demand for iron will likely continue to increase but the high grade iron ore deposits will only keep decreasing. In future it might become necessary to develop techniques that can process under-utilised and/or low grade resources (classified as waste material in some cases) which are being stockpiled. Iron ore fines is one such potential under-utilised resource. Iron ore that is smaller than 4.75 mm is classified as fines (IEA ETSAP, 2010). It is mostly used as mining back fill or stockpiled in large quantities around iron ore mining operations (Beyeme Zogo, 2010).

An additional rise in environmental awareness has also driven industry to explore alternate process routes to those that have been used for decades. Conventional extraction processes have proven to be energy intensive, harmful to the environment due to the production of greenhouse gases, and/or are known to produce large quantities of waste which would need to be stored or contained accordingly. Conventional iron ore processing techniques such as blast furnace processing, direct or smelting reduction are key examples of environmentally harmful processes as they contribute to all three of the factors listed above (United States Environmental Protection Agency, 1994).

Van Dyk and co-workers (2012) have been developing an environmentally friendly process to extract iron from iron ore fines which utilises acetylacetone as a reagent. In the aforementioned process, which utilises acetylacetone as the leaching agent, there is potential to recover the reagent during the recovery of the metal (Tshofu, 2014). Furthermore, the only by-product of the iron and acetylacetone process is water and as it is a relatively low temperature process (<300 °C) greenhouse gas production will be limited to the energy requirements of the process. The gas phase

extraction technique was found to be viable for a synthetic iron oxide mixture (87% extraction achieved) and low iron(III) oxide concentrations; however, when applied to an industrial sample of iron ore fines inhibiting factors were observed (Tshofu, 2014). Tshofu (2014) performed extraction experiments with iron ore fines (hematite) and acetylacetone in a fluidised bed gas phase reactor and found that surface passivation occurred due to the possible formation of a product layer during the extraction process. It caused a significant reduction in the extraction rate due to diffusion limitations and ultimately stopped the reaction from occurring. This meant that the iron ore fines could not be processed via the gas phase technique.

To overcome this problem, a liquid phase process was investigated as it was found from literature that metal(acetylacetonates) are soluble in liquid acetylacetone (Apblett and Barber, 2010). In such a process the product layer would dissolve in the liquid extractant. This proved to be a viable process option as 97.7% of the iron was extracted after 48 h at 140 °C. The only drawback of this process compared with the gas phase process was a significant increase in extraction time.

Consequently this study proposes the use of a pressure leaching process to decrease the reaction rate. By increasing the pressure it should be possible to suppress the boiling point of acetylacetone, which would allow the process to occur in liquid phase at higher temperatures. Previous studies have found that the rate of reaction between iron(III) oxide and acetylacetone increases with an increase in temperature (Tshofu, 2014; van Dyk et al., 2010). Consequently, it is proposed to carry out the extraction in a high pressure autoclave loaded with nitrogen gas and operated at higher temperatures. Iron(III) oxide bearing materials (such as synthetic iron(III) oxide and iron ore fines composed of mostly hematite) will be reacted with acetylacetone to form iron(III) acetylacetonate and water. The reaction is shown in Equation (1.1) below.

$$Fe_2O_{3_{(s)}} + 6H(C_5H_7O_2)_{(f)} \rightarrow 2Fe(C_5H_7O_2)_{3_{(dissolved)}} + 3H_2O_{(l)} \quad (1.1)$$

This proposed process for the extraction of iron and recovery of iron(III) acetylacetonate is given in Figure 1.1 below. The feed to the reactor would consist of acetylacetone and water (9:1 volume ratio) and some iron oxide bearing material.

Apblett and Barber (2010) showed that the addition of about 10 % of water to the acetylacetone catalyses the reaction with iron oxide. The product stream from the high pressure autoclave would consist of unreacted acetylacetone and iron oxide, iron(III) acetylacetonate and water. The unreacted iron oxide is separated from the dissolved product, acetylacetone and water by solid-liquid separation (the solids sent for further processing). The dissolved iron(III) acetylacetonate in water and acetylacetone is then concentrated by evaporating the excess water and acetylacetone to recover the product from the liquid solution. The concentrated iron(III) acetylacetonate may then be dried further to recover the crystal product. The evaporated acetylacetone and water would need to be cooled and the acetylacetone recovered from the water. The acetylacetone can be recycled back into the process for further extraction with the iron oxides.

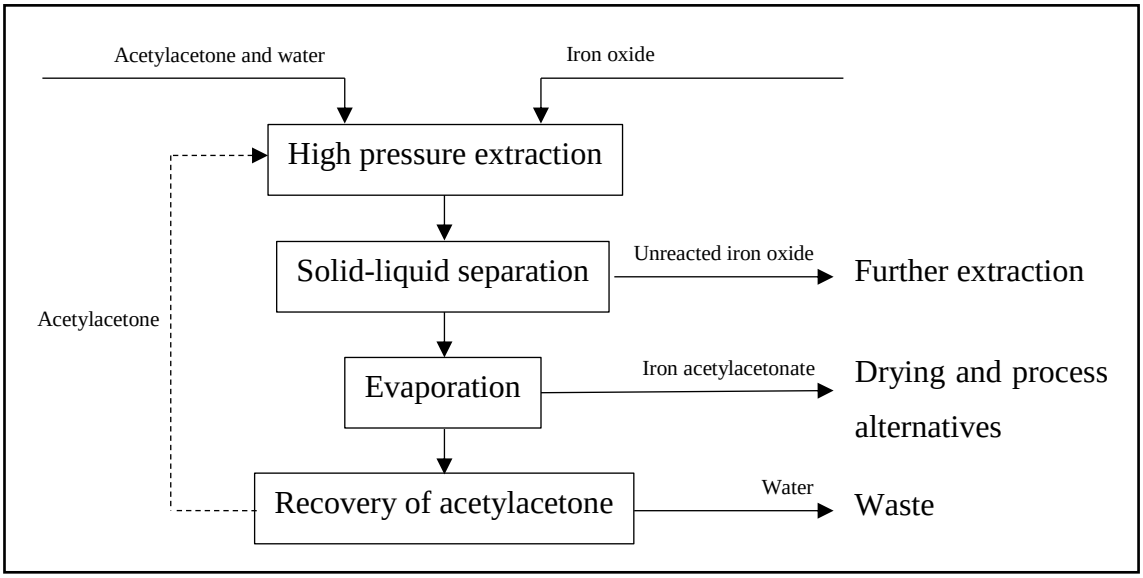


Figure 1.1: Proposed process block flow diagram of the extraction of iron from iron(III) oxide bearing materials and the recovery of iron(III) acetylacetonate.

1.2 Research Aim and Objectives

The principle objective of this study was to investigate the feasibility of utilising a high pressure process to extract iron from iron bearing materials with acetylacetone (2,4-pentanedione). This was to be achieved by:

1. Studying the solubility of iron(III) acetylacetonate in acetylacetone.

2. Studying the vapour pressure of acetylacetone at potential reaction conditions.
3. Studying the extraction of iron from iron oxide bearing materials in a pressure leaching vessel under different conditions by investigating the effect of temperature, particle size, pressure and iron to acetylacetone (solid to liquid) ratio on the extraction rate.

This investigation will extend the research already conducted by Tshofu (2014) and van Dyk and co-workers (2012).

1.3 Dissertation Layout

This dissertation comprises of 6 chapters and 6 appendices. Chapter 2 is a literature review highlighting the conventional iron extraction methods, ligand chemistry, advances in iron extraction technology, and pressure leaching technology with its applications in extraction. Chapter 3 describes the experimental setups and experimental methods used. Chapter 4 presents the main results and discusses the findings. The conclusions and recommendations from the study are given in Chapters 5 and 6 respectively. A list of references is given at the end of the dissertation followed by the appendices.

2 LITERATURE REVIEW

2.1 Introduction

Iron (Fe) is one of the most common elements on earth and is a key component of steel (an alloy of carbon and iron) and wrought or cast iron. These metals are utilised for numerous purposes, including weaponry, construction, transportation, and art to name a few. (Minerals Council of Australia, 2012; Tata Steel Europe Limited, n.d.)

Iron is found in nature in many forms (i.e. as a chloride, oxide, sulphide, etc.), but the most abundant form is as an oxide. Common iron oxide ores include: hematite (Fe_2O_3), magnetite (Fe_3O_4) and goethite ($Fe_2O_3H_2O$) which contain on average 70, 72 and 63 wt% iron respectively (Minerals Council of Australia, 2012). These ores are the key sources of iron; however, there are also alternate waste sources that are being utilised or could be utilised if economically viable. An iron source is considered viable when the iron content is greater than 25% (United States Environmental Protection Agency, 1994). These sources are iron ore fines, fines from the sinter processing plants, waste chloride pickle liquor and blue dust (BlueScope Steel, n.d.; National Metallurgical Laboratory, 2010; World Steel Association, 2010). Iron is also recovered from scrap steel (National Metallurgical Laboratory, 2010).

2.2 Conventional methods for iron extraction

Iron is conventionally extracted/ produced via pyrometallurgical based processes such as blast furnace processing, direct reduction or smelting reduction. These processes cannot be applied to all iron ores/ sources as they would need to be tailored specifically to each source. Iron ore fines, for instance, would need to be agglomerated before being used as a feed source to the blast furnace as it will be blown out of the furnace if added directly. These conventional processes are energy intensive, require numerous processing steps and result in the formation of large quantities of CO_2 and SO_2 (greenhouse gases) (IEA ETSAP, 2010).

The above mentioned processes are described in more detail below (process routes, operation, advantages and disadvantages). Figure 2.1 is a schematic diagram of different steel production technologies and includes its production from scrap steel.

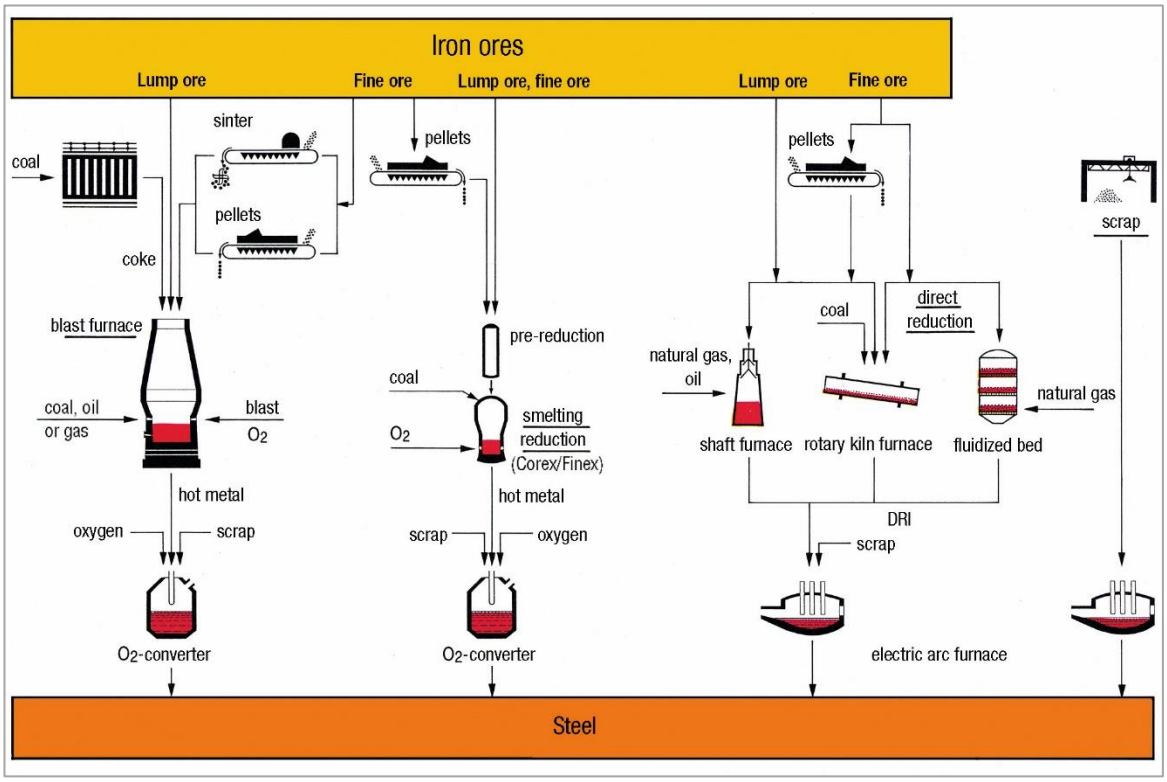


Figure 2.1: Schematic diagram of steel production technologies from iron (blast furnace, direct reduction and smelting reduction) or scrap steel (Stahl, 2013).

2.2.1 Blast furnace

Blast furnace processing produces a molten iron mixture called pig iron by smelting pellets or sinter in a reducing environment created by the combustion of coke or coal respectively. Figure 2.2 is a schematic diagram of the production blast furnace iron (BFI), slag and blast furnace gas. The iron ore and fuel (coke) is fed in through the top of the furnace and as in proceeds down the furnace the ore is reduced to remove oxygen (O_2). Hot O_2 enriched air is pumped in from the bottom (IEA ETSAP, 2010).

The feed to the furnace is typically hematite (Fe_2O_3) and sometime magnetite (Fe_3O_4) (5-10% SiO_2 and Al_2O_3 and the remainder is hematite), metallurgical coke (90 % C, 10 % ash, 0.5-1 % S and dry basis 5-10 % H_2O), and calcium oxide (CaO)

and magnesium oxide (MgO). The CaO and MgO acts as a flux for the silica and alumina impurities (Peacey and Davenport, 2013). The Fe_2O_3 undergoes step wise reduction to Fe_3O_4 and then FeO and finally Fe (Feinman, 1999).

The process creates a large amount of gases (1 200 to 2000 Nm^3/t of pig iron) with the average composition of CO (20-28%), H_2 (1-5%), N_2 (50-55%), CO_2 (17-25%), sulphur and cyanide, as well as dust and other impurities resulting from the ore and coal. This process is energy intensive and with the large quantities of gas produced it is necessary to further reduce the emissions and energy consumption by improving the efficiencies of the process (IEA ETSAP, 2010).

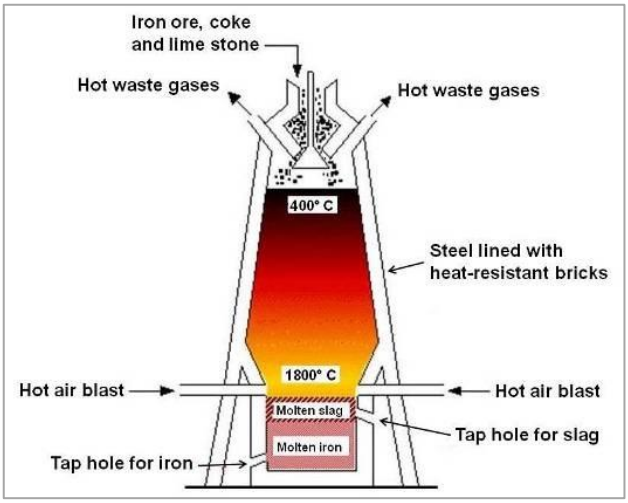


Figure 2.2: Schematic diagram of a blast furnace (Shah, n.d.).

2.2.2 Direct reduction

Direct reduction (direct reduced iron - DRI) is the removal of oxygen by reducing the ore with natural gas. The product (metallic iron referred to as sponge iron) is the feed source to electric arc furnaces (EAF) used in steel production. The feed to the process can consist of lump iron ore, iron ore fines, pellets and coal which unlike the blast furnace operation does not require previous preparation. This process has a lower investment cost than that of blast furnaces. However, blast furnaces are still the primary means to produce iron due to the production ability (output of 10000 t/d of pig iron) (Gojić and Kožuh, 2006).

Numerous direct reduction processes exist, including MIDREX, FINMET, HyL and SL/RN. These four are currently in industrial operation and are part of about

30 different DRI processes identified by Gojić and Kožuh (2006). The MIDREX process is the leading technology in terms of direct reduction. This process is shown below and consists of four stages namely: reduction gas, reforming, heat recovery and briquette making.

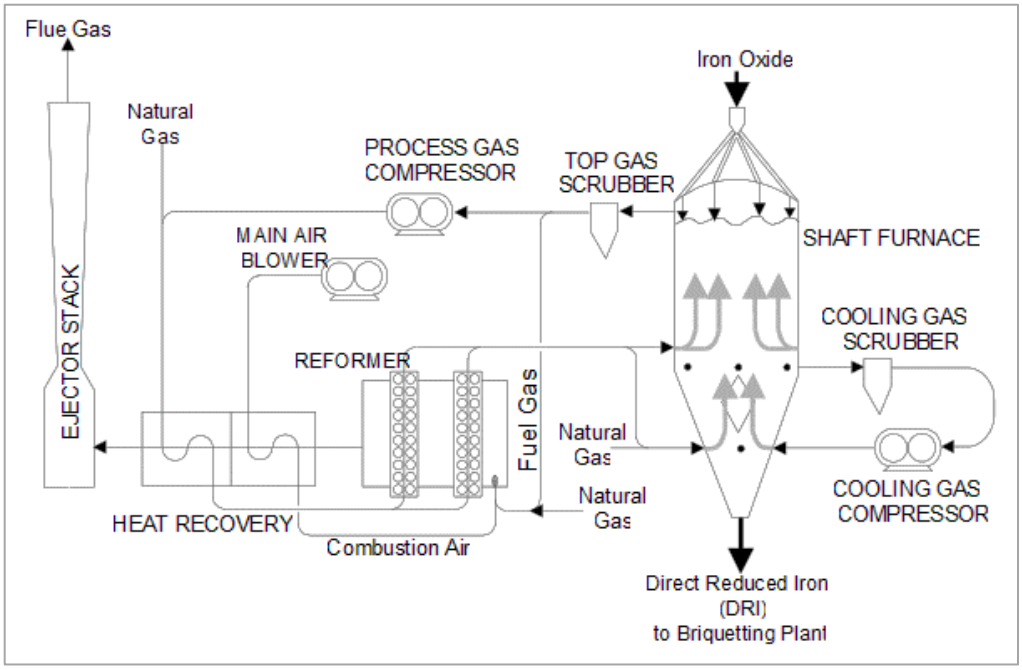


Figure 2.3: Schematic diagram of the MIDREX Process (Downstream Consulting Pty Ltd, 2013).

The FINMET process mentioned above is also a form of direct reduction; however, it utilises fluidised bed technology for the reactors. The process allows for the use of fines without any other form of preparation such as sintering or pelletisation. These fines flow counter-current to the reducing gas (Feinman, 1999). The schematic diagram for the production of iron using the FINMET process is shown below.

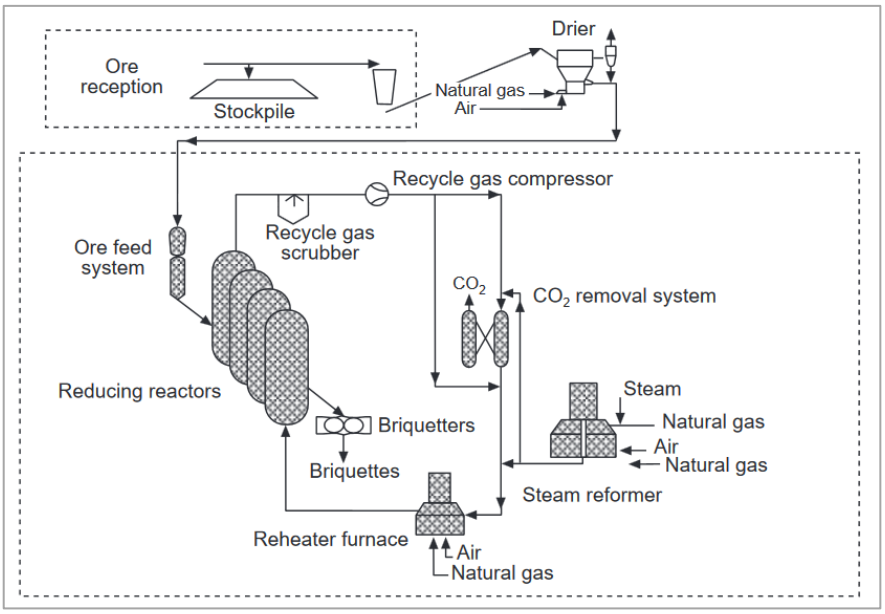


Figure 2.4: FINMET process schematic diagram (Feinman, 1999).

The FINMET process is still a developing technology (Gojić and Kožuh, 2006).

2.2.3 Smelting reduction

Smelting reduction (smelting reduction iron – SRI) like blast furnace processing creates pig iron but without the use of metallurgical coke. These are alternative processes being developed that use coal as the reducing agent instead. The iron ore feed is processed in two separate reactors. Pre-reduction occurs in the reduction shaft and the product from this is then conveyed by discharge screws to the smelter gasifier for the final reduction and melting. The most well-known and used SRI is the COREX process (schematic shown in Figure 2.5) (Gojić and Kožuh, 2006).

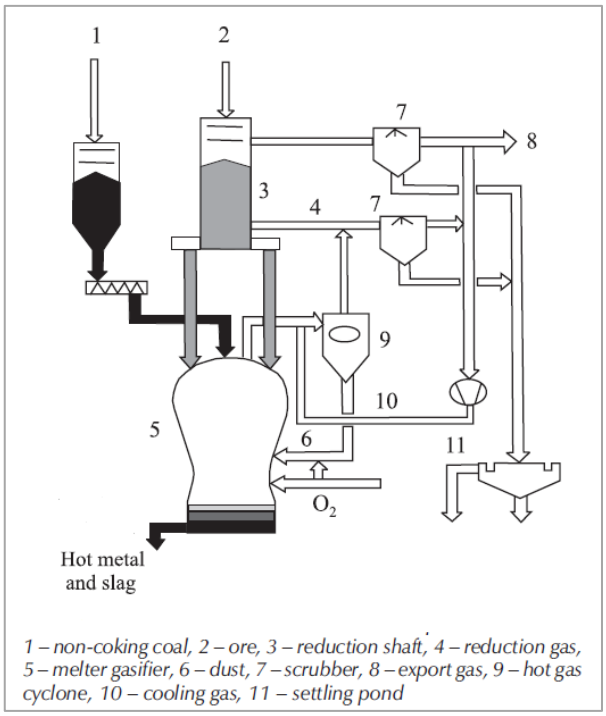


Figure 2.5: Schematic diagram of the COREX process (Gojić and Kožuh, 2006).

2.2.4 Sintering and pelletisation

A limitation of the processes above is that they cannot process iron ore fines directly as they could be blown out the furnace with the waste gases, reduce permeability and gas flow inside the furnace (Biswas, 1981). Fines need to undergo an agglomerisation process such as sintering or pelletisation before being utilised. Sintering entails combining the iron ore with additives, coke breeze and recycled sinter into a mixing drum which is then being ignited and crushed to form sinters. Pelletising entails upgrading the iron ore content and converting the fines into small balls of 9 - 16 mm. This is done by combing the fines with additives and heating and cooling the mixture. This pelletisation process transforms all magnetite to hematite and requires large amounts of heat (IEA ETSAP, 2010).

These conventional processes are energy intensive, require numerous processing steps and result in the formation of large quantities of CO_2 and SO_2 (greenhouse gases) (IEA ETSAP, 2010). Hence, an increased interest in developing alternative processes that are less harmful to the environment and are less energy intensive. Advances have been made in the extraction of metals using ligands and metal

complexes. The following section gives a brief description regarding ligands and metal complexes.

2.3 Ligands and metal complexes

Ligands are ions or molecules that act as Lewis bases in that they can donate a pair of unshared electrons to a metal ion (Lewis acid) to form a complex. This is possible as the metal has empty valence orbitals that accept the donated electron pair. A metal complex is formed when a central metal ion is bonded to a group of surrounding ions or molecules. A ligand bonding with a metal ion forms a metal-ligand bond that would exhibit chemical properties that are significantly different to those of the original metal. This could be a change in colour, reactivity and other factors. Furthermore, it is possible to have monodentate (single donor electron pair) or polydentate (two or more donor electron pairs) ligands. The polydentate ligands are also referred to as chelating agents due to their ability to bond with the metal between their donor sights similar to that of how a "claw" grabs something. These complexes and bonds formed between chelating agents and metal ions result in complexes that are more stable than those of the monodentate variety. EDTA (ethylene diamine tetra acetic acid) is a common example of a chelating agent that is used in the food industry as well as in medicines and other processes (Brown et al., 2009).

β-diketones (i.e. 1,3-diketones) are a group of chelating agents that are readily available in industry and have been/ are being intensively studied. The β-diketones are a set of chemicals that are characterised by a carbon atom separating two carbonyl groups. Acetylacetone (2,4-pentanedione and abbreviated as Hacac) is an example of this group and is also the simplest structure as its substituents on the carbonyl groups are methyl groups (Binnemans, 2005). It is given by the following structure:

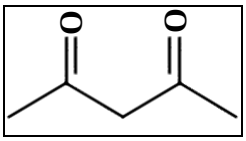


Figure 2.6: Acetylacetone structure (Binnemans, 2005).

Acetylacetone is able to bond via both oxygens and is hence classified as a bidentate ligand. Another key aspect of β-diketones is that they experience keto-enol tautomerism and these are in equilibrium with each other (Binnemans, 2005). The keto-enol tautomerism structures of acetylacetone are shown below.

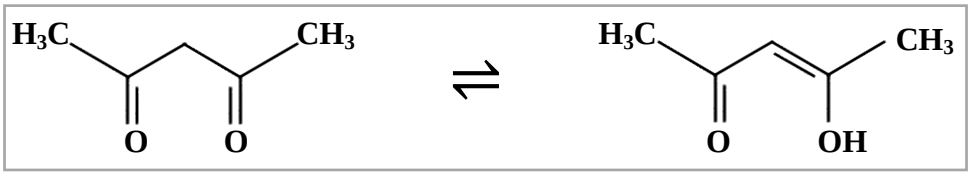


Figure 2.7: Keto-enol equilibrium of acetylacetone (Binnemans, 2005).

The β-diketones react with metals to form β-diketonate complexes that are more stable, volatile and hydrophobic (hence insoluble in water) (Binnemans, 2005). An example of such a reaction is the one between ionic iron and acetylacetone to form iron(III) acetylacetonate ($Fe(acac)_3$). The formation of iron(III) acetylacetonate forms the basis of the section that follows.

2.4 Alternatives and advances in iron extraction techniques

β-diketones are receiving a lot of attention due to their reactive ability and stability. These compounds are able to effectively extract a variety of metals. Starý and Hladký (1963) studied how the properties of four β-diketones affected the extraction of 30 metal ions (including but not limited to Be(II), Ca(II), Fe(III), Mg(II) and Sr(II)) and from this they determined the optimum extraction conditions. The β-diketones that were investigated were acetylacetone, thenoyltrifluoroacetone, benzoylacetone and dibenzoylmethane. All the Fe(III) ions (10^{-3} – 10^{-4} M) that were initially present in the testing solutions were readily extracted by all four of the β-diketones. Specifically, all of the iron was extracted by 0.100 M acetylacetone between the pH range of 2.5 – 7.

A key feature of the reaction between metal complexes and β-diketones is that these form a product that exhibits properties similar to that of a pure organic compound in that they are insoluble in water, soluble in non-polar solvents and volatile (Berg and Truemper, 1960). The volatility of these compounds and the ability of the solvent to readily react with the metal became a driving force in the development

of direct extraction processes to extract a metal from its ore or a waste material. The Selective Extraction and Recovery using Volatile Organic compounds (SERVO) process is one such process. This is a gas phase process whereby the feed material (i.e. metal containing material) is heated and contacted with the volatile organic chelating agent (i.e. the β-diketone). This whole process occurs within a fluidised bed and the resulting product is a volatile metal complex which can be drawn from the reaction zone and the metal recovered. This process has been used to extract chromium, vanadium, iron and other metals from a variety of sources, including low grade ore, sediment, soil, spent catalyst and industrial waste (Allimann-Lecourt, 2004; Mariba, 2010; Potgieter et al., 2006; van Dyk et al., 2012).

The applications and benefits of the SERVO process led to further investigations. Potgieter and co-workers (2006) investigated the feasibility of using gas phase extraction in a fluidised bed to recover valuable metals (aluminium, chromium, iron and vanadium) from their synthetic solid oxide compounds. Acetylacetone was used as the reagent. This study showed that the recovery of these metals was dependent on the temperature and the reaction time (acetylacetone flowrate was kept constant). The percentage recovery was 63.7, 48.2, 75.2, and 63.0 % respectively (after 105, 150, 45 and 120 min respectively). This proved that the applied process could be feasible as a means to recover the metals from their solid oxide materials.

A benefit of the gas phase process is that it is a greener alternative to conventional extraction processes as the reagents can potentially be recovered and recycled. The recovery of the reagent reduces the amount of waste produced as so reduces the environmental impact of the process. Coupling this with the fact that when acetylacetone reacts with the metal oxide the only products are the volatile metal complex and water, additional studies was conducted to develop green extraction techniques for iron and other metals such as aluminium, lead and copper (Apblett and Barber, 2010; Potgieter et al., 2006; Shemi et al., 2012; van Dyk et al., 2010, 2012).

van Dyk and co-workers (2012) worked on a gas phase extraction method in a fluidised bed reactor to extract iron from a synthetic iron oxide and silica mixture, and similarly to extract lead from a synthetic lead oxide and silica mixture. It was found that 87 % of the iron could be recovered from this mixture by acetylacetone. This was achieved at 250 °C, acetylacetone flow rate of 1 mL/min (at 25 °C), 1 wt% synthetic Fe_2O_3 mixture after 4 hours. To establish whether the same principles could be applied to actual iron ore samples further testing was done by Tshofu (2014) with iron ore fines. The iron ore fines were from Kumba Iron Ore and were found to contain a far higher percentage of iron oxide (hematite), 93 % in a solid matrix ore. The highest percentage extraction achieved was only 3.9 % at an acetylacetone flow of 9 mL/min after 6 hours at 250 °C. This is significantly lower than that of the synthetic testing extraction. It was concluded that there was likely a passivation layer forming which inhibited the reaction/diffusion process (i.e. diffusion through the layer was not fast enough). The limitations of the process led to an investigation into the possible leaching of the iron ore fines with acetylacetone instead in an attempt to overcome the formation of a product layer, by dissolving it in the liquid extractant. Better iron extraction results (97 %) were obtained after 48 hours of leaching at 140 °C and an iron fines to acetylacetone ratio of 0.025:1. However, this process could not be evaluated at higher temperatures due to the acetylacetone turning into a vapour at temperatures above 140 °C. The acetylacetone was limited to the liquid phase to ensure that the solubility limitations that were present in the aforementioned gas phase extraction did not occur (i.e. the formation of the passive layer).

Tshofu (2014) also determined that it was possible to recover unreacted acetylacetone from the reaction product solution using a Heidolph Rotary Evaporator. This yielded acetylacetone with a high purity that could be recycled back into the process. The product iron(III) acetylacetonate could be processed further or alternately used as another means to produce iron(III) acetylacetonate crystals.

Tshofu (2014) also investigated the recovery of iron from the iron(III) acetylacetonate via hydrogen reduction (Equation 2.1)

$$Fe(C_5H_7O_2)_{3(g)} + \frac{3}{2}H_{2(g)} \rightarrow Fe_{(s)} + 3H(C_5H_7O_2)_{(g)} \qquad (2.1)$$

The highest recovery, 46.4 % iron, was obtained at 250 °C at a hydrogen flowrate of 5 cm^3/min after 3 h. These results shows that the process was possible, but would need to be optimised to produce higher recoveries. This is in support of the work done by Zhang and co-workers (2011) who produced iron nano-crystals via the hydrogen reduction of iron(III) acetylacetonate in solution.

The extraction processes described above have some limitations such as only applicable to low concentration ores (gas phase) and long reaction times (liquid phase with reflux), that can potentially be overcome by reacting the reagents at high pressure. The next section will focus on pressure leaching for its potential application in this study.

2.5 Pressure leaching

Iron is typically removed as an impurity in many leaching processes. Iron is present in other metallic ores, such as zinc ores, and the ores containing Platinum Group Metals (PGMs) and base metals (like Cu, Ni and Co). These ores are treated using hydrometallurgical based processes (typically H_2SO_4 leaching) and the iron is usually precipitated out in the initial leaching stages and discarded as a waste product. The purification and removal of iron in these systems is usually a key step as the presence of iron reduces the recovery of the desired metals (Ferron, 2006; Milbourne et al., 2003; International Zinc Association, 2011).

Yu and co-workers (2011) performed pressure HCl leaching to investigate the kinetics in the removal of iron impurities from metallurgical grade silicon. This study determined the effects of temperature, particle size, total pressure and concentration of hydrochloric acid (the extractant used) on the kinetics of the process. It was found that a decrease in particle size, an increase in temperature, an increase in pressure and an increase in acid concentration all improved the extraction rate. Based on these factors it was then determined that the extraction of iron followed that of the shrinking core model with an activation energy of the leaching reaction of 46.9 kJ/mol.

Pressure leaching is used in industry to reduce reaction time as it enables operation at higher temperatures. Furthermore, most metal compounds' solubility increase as the temperature increases which results in more of the metal being dissolved into solution. This process is associated with higher costs compared to atmospheric leaching due to the increased operating temperature as well as the associated costs of the vessel which should be able to withstand high pressures (Gupta and Mukherjee, 1990). However, it has higher recovery rates and it is able to deal with complex ores. Pressure leaching is applied to nickel laterite, uranium, copper and cobalt (SGS SA, 2014).

A brief overview and technical details regarding pressure leaching is presented in the following sections.

2.5.1 Overview

Pressure leaching has been in use for over 75 years and is becoming increasingly more important as ores are becoming more complex to process. Pressure leaching was originally performed at lower temperatures on aluminium based materials such as the Bayer process whereby bauxite ores were treated. The system was operated at 143 °C and 425 kPa in a pressure vessel called a "digester" (operations based in Russia). Uranium was also processed using pressure leaching and were generally performed between 100–120 °C at pressures ranging from 200–500 kPa (operations based in the USA and some in Canada). Pressure acid leaching (PAL) was also performed on lateritic nickel-cobalt ores at temperatures between 255–270 °C and pressures of 4 000–5 300 kPa. Operation at higher temperature and pressures reduces residence time and increases conversion (Uhrie, 2015).

The technology is constantly being adapted and improved with newer designs and operations being implemented. Traditional extraction technologies are being replaced by newer pressure leaching processes, for example: Hudson Bay Mining replaced their zinc sulphide traditional roast-leach-electrowining (RLE) process with a two-stage pressure leaching process (1993) and this system is now in operation in Kazakhstan (2003) and China (2009). Traditional roasting of sulphide ores to recover gold has mostly been replaced by the pressure oxidation of the ores in acidic media (Lakshmanan et al., 2015). The aforementioned lateritic ore

systems have also had advances with pilot-scale plant studies being performed to evaluate the newly patented (2008) nitric acid pressure leaching (NAPL) technology (Ma et al., 2015).

2.5.2 Technical details

TYPES

There are two types of pressure leaching systems in use, pressure leaching in the absence of oxygen, and pressure leaching in the presence of oxygen. In the pressure systems operated without oxygen, only ore and the leaching agent is loaded into the autoclave and the reactor is operated above the boiling temperature of the leachant which increases the reaction rate. In the oxygen operated leaching systems the rate of reactions are dependent on the partial pressure of oxygen (material undergoes oxidation) and the total pressure inside the autoclave is the solution pressure plus the oxygen pressure. An example of each system is the treatment of bauxite with caustic soda in the extraction of alumina (no oxygen), and the leaching of sulphide ores such as copper (oxygen) (Gupta, 2003).

EQUIPMENT AND OPERATION

High pressure leaching can be performed in horizontal, vertical, spherical or long horizontal tube autoclave configurations. Generally horizontal arrangements are used. The autoclave is divided into multiple compartments (3 to 4) equipped with impellors, used to ensure constant agitation to reduce the settling of solids and to increase the contact between the liquid and solid reagents. Alternately the entire horizontal autoclave could be rotated about its horizontal axis. The feed stock is pumped into the autoclave under pressure and flows from one compartment to the next. The horizontal configuration can be seen in Figure 2.8 below. Typically heating is done with steam and cooling with water if and when required. Autoclaves are constructed from mild steel, stainless steel or titanium depending on the corrosive nature of the leaching zone. It is also possible to get glass fiber-reinforced plastic autoclaves.

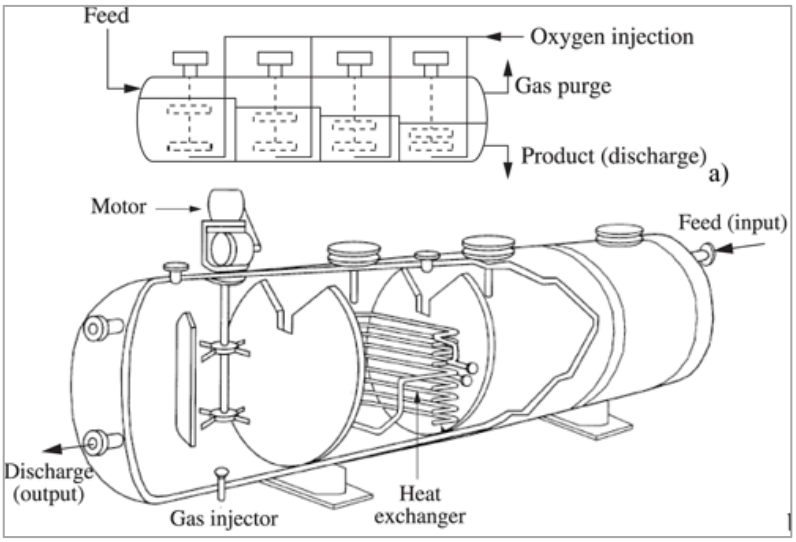


Figure 2.8: Horizontal autoclave with four-compartments, mechanical stirrers, gas injectors and heat exchangers (Vignes, 2011).

Pressure vessels are operated at higher temperatures than the standard boiling points that results in an increased reactivity (Gupta, 2003; Uhrie, 2015). Thus temperature is a key driving force in pressure leaching reactions. The pressure of the system influences the reaction rate either due to it increasing the operating temperature (oxygen free system) or the material undergoes oxidation (oxygen rich system). Thus, reaction rate is dependent on the pressure of the system. The behaviour of the materials present in the proposed process at higher temperatures and pressures need to be investigated.

2.6 Vapour pressure

Melia and Merrifield (1969) measured the vapour pressure of acetylacetone over the temperature range of 297-398 K using a Smith and Menzies isoteniscope. The following equation best summarised the results (with an estimated error of ±0.1 mm):

$$\log_{10} P\ (mmHg) = 7.902 - \frac{2.059 \times 10^3}{T} \qquad (2.2)$$

where T is temperature (K) and P is the partial pressure of acetylacetone (mm Hg). By using this equation one can calculate that the partial pressure of acetylacetone increase by 526 mmHg (70.1 kPa) from 297 to 398 K.

The Antoine equation and its parameters for water and acetylacetone is given below.

$$\log_{10} p^* = a - \frac{b}{T + c} \qquad (2.3)$$

where p^* is the partial pressure (mm Hg), T is temperature (°C) and a, b and c are the Antoine coefficients.

Table 2.1: Antoine coefficients for acetylacetone and water (Yaws, 2015).

	Formula	A	B	C	T_{min} (°C)	T_{max} (°C)
Acetylacetone	$C_5H_8O_2$	6.76192	1292.97	192.744	-5.000	373.5
Water	H_2O	8.05573	1723.64	233.076	0.01000	374.0

The experimental work in this study will be done at temperatures in the prediction range of these formulae and so the aforementioned equations can be utilised to predict the vapour pressure in this system. However, it will be necessary to study the vapour pressure of acetylacetone and the acetylacetone/ water mixture at the reaction conditions to determine how the experimental systems varies to the predicted system.

Berg and Truemper (Berg and Truemper, 1965) studied the vapour pressure of the following metal(acetylacetonates): $Al(acac)_3$, $Be(acac)_2$, $Co(acac)_2$, $Fe(acac)_3$, $Ni(acac)_2$. The results of this study are shown in the figure below.

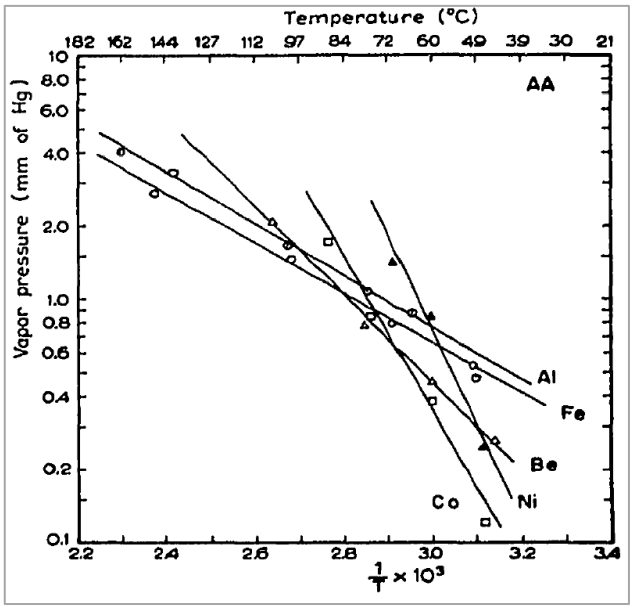


Figure 2.9: Vapour pressure data for various metal(acetylacetonates) (Berg and Truemper, 1965).

From the figure it can be seen that the vapour pressure of iron(III) acetylacetonate increases by roughly 3.5 mm Hg (0.5 kPa) over the given temperature range. This increase is significantly less than that of the pure acetylacetone. The vapour pressure of iron(III) acetylacetonate was only determined up to 179 °C. This is the melting point of iron(III) acetylacetonate (Berg and Truemper, 1965).

The vapour pressure of the proposed system would be a result of the partial pressures of all components involved. However, acetylacetone and water are in excess and based on the aforementioned details they are assumed to have the greatest effect on the system. Hence, the vapour pressure of acetylacetone and water would need to be investigated.

3 EXPERIMENTAL METHODS

This study aimed to investigate the extraction of iron from iron oxide bearing materials using a high pressure autoclave. A description of the experimental equipment and procedures are given below. The properties of all the chemicals used are given in Appendix A.

3.1 High pressure autoclave

A high pressure autoclave was used in the vapour pressure and extraction studies. The autoclave is equipped with a heating mantle and can be seen in Figure 3.1 and Figure 3.2. All wetted parts are constructed of SS316 and a Hastelloy C liner is used to protect the inside of the reactor against corrosion. The specifications are as follows:

- Design pressure: 10000 kPa
- Design temperature: 250 °C
- Vessel volume: 450 mL
- Operating volume (%): 40 - 70
- WIKA CPG500 digital pressure gauge (connected with a thermosiphon)

The autoclave temperature is controlled with a GEFRAN 600 temperature controller and temperature readings are done with two type K thermocouples, one located on the outside and another in the reactor The autoclave is placed on a magnetic stirrer IKA C-MAG HS 7 to stir its contents with a bar magnet. The engineering drawing, standard operation instructions, commissioning of the reactor and safety precautions are given in Appendix B.

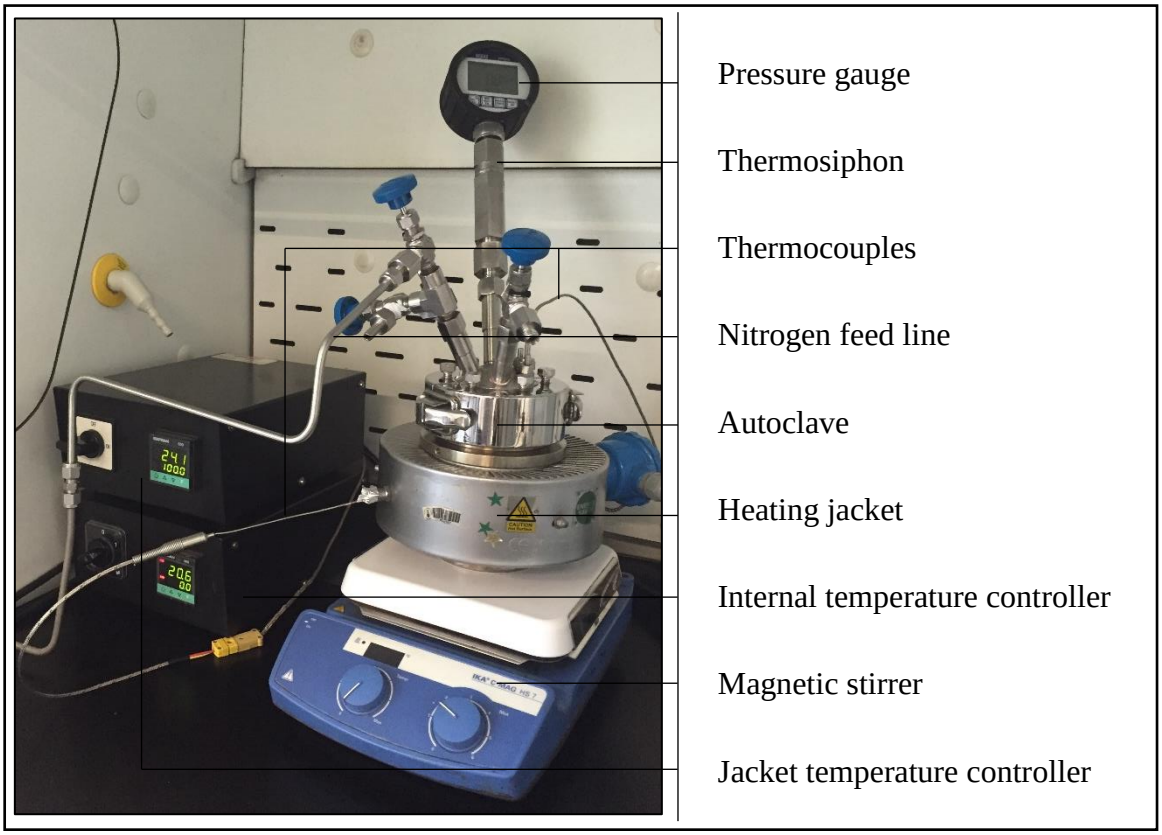


Figure 3.1: Autoclave with N_2 feed, temperature controllers and magnetic stirrer.

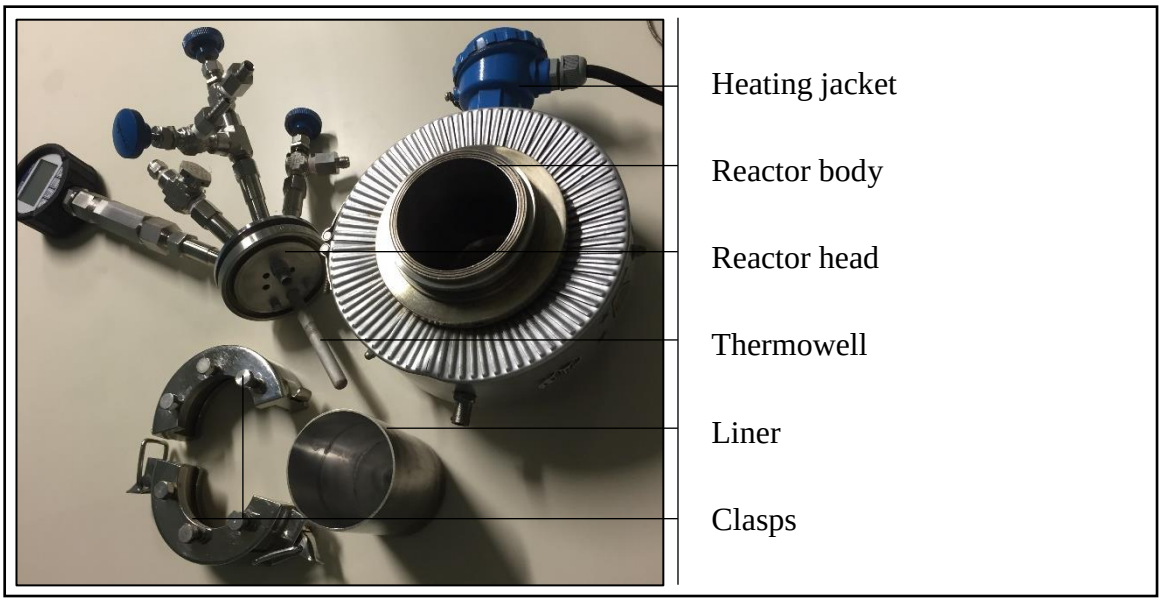


Figure 3.2: Disassembled autoclave.

3.2 Determination of experimental operating space

3.2.1 Solubility analysis of iron(III) acetylacetonate in acetylacetone

The solubility of iron(III) acetylacetonate in acetylacetone stipulates the saturation limits of the solution. Oversaturation will lead to crystallization of iron(III) acetylacetone. The crystals might deposit on the iron bearing material and prevent the reagents from reacting. This would be undesirable and hence provides the upper limit of the operating space that the reaction can be performed in terms of solids reagent initially in solution. Results are given in section 4.1.1.

The solubility method used on the iron(III) acetylacetone/ acetylacetone mixture was adapted from that used by students at Calvin College, Michigan (Wolthuis et al., 1960). A visual method was utilised whereby light was shone through the solution and the dissolution or formation of crystals was observed. Two different light bulbs were used, namely an energy saver 9 W and a 100 W bulb. These were used to determine the effect of lightbulb brightness on the solubility. A known amount of iron(III) acetylacetonate crystals was placed inside a test tube filled with 10 mL of acetylacetone. Setup shown in Figure 3.3 below. The solution was heated until all the crystals had dissolved and then cooled. The point at which the first crystal formed was observed is the saturation temperature. The mass of crystals in the test tube was increased and the process repeated. A type K thermocouple and GEFRAN 600 temperature controller were used to measure the temperature of the solution.

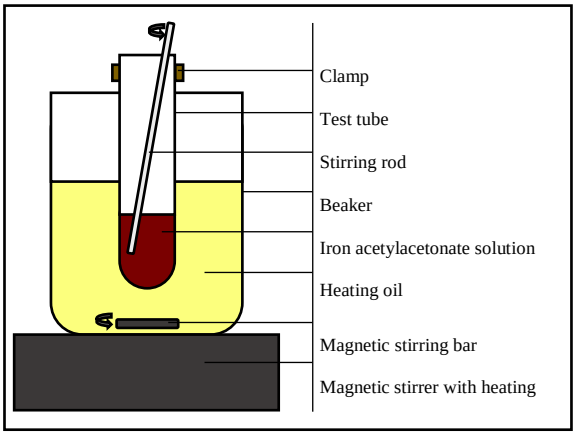


Figure 3.3: Solubility of iron(III) acetylacetonate in acetylacetone experimental setup.

3.2.2 Measurement of pure and mixture vapour pressures

The vapour pressure of the system gives an indication as to the boiling conditions of the solution. The vapour pressure of the acetylacetone and water system was determined using an adaptation of the Isoteniscope method (Smith and Menzies, 1910) and is described below. The reactor was loaded with a 9:1 ratio solution of acetylacetone to water (i.e. 180 mL acetylacetone and 20 mL water which is the operating volume used in proceeding experiments) (Apblett and Barber, 2010). The system was purged for 5 min using N_2 (inert) and once this was done the excess pressure resulting from the N_2 purge released until 0 kPa was recorded on the pressure gauge. The temperature controller was turned on and the solution heated up gradually to 240 °C (based on internal thermocouple temperature reading). The heating jacket was then kept at a constant temperature to ensure the internal temperature remained constant at 240 °C. The setup was kept at this temperature for 30 min to ensure the system pressure was stable. The heating arrangement was then turned off to allow the system to cool down naturally. The temperature readings were recorded at 20 kPa intervals starting at the pressure correlating to ± 235 °C. The pressure readings were taken using a WIKA CPG500 digital pressure gauge and temperature using GEFRAN 600 temperature controller and type K thermocouple. This was repeated three times.

A comparison between the vapour pressure data of the liquid extractant (9:1 acetylacetone:water) and its pure constituents was achieved by repeating the above experiment with 200 mL acetylacetone and 200 mL water respectively. Results are given in section 4.1.2.

3.3 Extraction of iron from synthetic iron(III) oxide and iron ore fines

3.3.1 Initial extraction of iron from iron ore fines

Initial testing of the system was done to evaluate how the chemicals behaved under pressure and to establish a direction forward with the development of the new process.

The autoclave was loaded with 7.5 g of iron ore fines (composition and other details are given in Appendix A) at a solid to liquid ratio of 0.025 g:1 mL with 270 mL acetylacetone and 30 mL water (9:1 ratio of acetylacetone to water). The particle size of the fines were between 106 and 150 µm (i.e. +106 –150 µm). A magnetic stirring bar was placed in the solution. The reactor was sealed and purged with N_2 for 5 minutes and then pressurised to 1000, 2000 or 3000 kPa (initial pressure before heating). The initial temperature of the solution was kept as constant as possible (deviation ± 5 °C). The stirring speed was set to 375 rpm. The solution was heated to the desired reaction temperature of 220 °C (± 2 °C) over the course of an hour (Δt_{heat}). This was done using a stepped heating method that can be found in Appendix B. Once the desired reaction time (Δt_{react}) was reached, the reactor and solution was cooled over the course of an hour (Δt_{cool}) to 80°C. The total time (Δt_T) was taken as:

$$\Delta t_T = \Delta t_{heat} + \Delta t_{react} + \Delta t_{cool} \qquad (3.1)$$

The total time for each experiment was chosen as 18 hours to significantly reduce the residence time in the original liquid phase reaction performed by Tshofu (2014).

The cooled solutions (i.e. 80 °C solutions) were filtered and the liner and filtration setups washed with excess pure acetylacetone to ensure minimal loss of material. The final volume of solution (combing the rinse with the reactor solution) was 300 mL (the volume taken once the solution had reached room temperature). These solutions were analysed using a Spectroquant Pharo 300 Spectrophotometer as per the method discussed in section 3.4.1. Results are given in section 4.2.1.

The volume of the reaction was then changed to 200 mL such that a comparison could be made between these results and those of Tshofu (2014).

3.3.2 Extraction of iron from synthetic iron(III) oxide

The effects of temperature on iron extraction was studied using synthetic iron oxide (95% Fe_2O_3). The reaction was studied at 120, 140, 150, 160, 180 and 220 °C. The autoclave was loaded with 180 mL of acetylacetone, 20 mL of water (i.e. 9:1) and 5 g of synthetic iron oxide (i.e. solid to liquid ratio of 0.025 g:1 mL). A magnetic stirring bar was placed in the solution. The reactor was sealed and purged with N_2

for 5 minutes and then pressurised to 1000 kPa (initial pressurisation and starting temperature of solution kept as constant as possible, pressure within ± 10 kPa and temperature within ± 5 °C). The stirring speed was set to 375 rpm. The reactor was heated for an hour to the desired temperature (refer to Appendix B for heating rates), kept at this temperature for the duration of the allotted reaction time and cooled for an hour to 80 °C. The reactions were studied at total times of 3, 4, 6, 8, 10 and 18 h for each temperature. The cooled solution was filtered and prepared following the same procedure as given above with the exception that final volume of solution was 250 mL unless otherwise specified. Results are given in section 4.2.2.

3.3.3 Extraction of iron from iron ore fines

Iron ore fines was reacted at 140 °C and total times of 4, 6, 8 and 10 h. The system was loaded with 5 g of +106 –150 µm iron ore fines with a solid to liquid ratio of 0.025 g:1 mL (180 mL acetylacetone and 20 mL water, i.e. 9:1). The autoclave was sealed, purged with N_2 and pressurised to 1000 kPa with excess N_2. Stirring speed was set to 375 rpm. The desired internal temperature of 140 °C was achieved after heating the solution for an hour (refer to Appendix B for heating rates), and the solution kept at this temperature (± 2 °C) for the desired reaction time. The solution was cooled for an hour to 80 °C and the same procedure followed as above regarding filtration and analysis.

Two particle size ranges, namely +45 – 5 µm and +106 –150 µm were evaluated at the desired reaction temperatures of 120, 140, 160 and 180 °C. The total time per experiment was chosen as 4 h. The system was loaded according to the same procedure and conditions above at the varying particle size and temperatures. Furthermore, a third particle size range of +212 –300 µm was evaluated at 180 °C, total time of 4 h and all other conditions the same. Stirring speed was set to 375 rpm. The solutions were heated and cooled for an hour and the final solutions filtered and prepared for analysis as per the same conditions given above.

Pressure of the autoclave was varied at 0, 1000, 2000 and 3000 kPa N_2 initial loading pressure. The system was loaded exactly the same as above with 5 g of iron ore fines, 180 mL acetylacetone, 20 mL water, the optimised temperature of 180 °C and particle size range of +45 –75 µm and with total time of 4 h. Stirring

speed was set to 375 rpm. The solutions were heated and cooled for an hour and the final solutions filtered and prepared for analysis as per the same conditions given above.

Solid to liquid ratios were varied to 0.025, 0.050 and 0.100 g : 1 mL accordingly (i.e. 5, 10 and 20 g of iron ore fines into 180 mL acetylacetone and 20 mL water). The system was loaded exactly the same as above with particle size range of +45 – 75 µm, N_2 initial loading pressure of 1000 kPa, desired reaction temperature of 180 °C and with total time of 4 h. The solutions were heated and cooled for an hour and the final solutions filtered and prepared for analysis as per the same conditions given above.

3.4 Analysis of results

3.4.1 Spectroquant Pharo 300 Spectrophotometer analysis (UV-Vis)

An analytical method was needed that gave a means to assess whether the desired products were formed and at what concentration. UV-Vis spectrophotometry was chosen as the different peaks represent the compounds that are present. Atomic Absorption Spectrometry (AAS) could not be applied to all the samples generated due to some solutions being more viscous than others which blocked the feed tubing. It was necessary to identify the peaks associated to those of acetylacetone and iron(III) acetylacetonate. These peaks are roughly 307 nm for acetylacetone (Abood et al., 1992) and a double set of peaks at roughly 360 and 440 nm for iron(III) acetylacetonate (Meneses et al., 2014).

All experimental solutions were analysed using a Spectroquant Pharo 300 Spectrophotometer. The solutions were scanned at a wavelength range 190 and 600 nm. Peak absorbance readings were taken at 351 nm (maximum peak determined from calibration data shown in Appendix F). The ultraviolet-visible spectrum (UV-Vis) scans and readings were repeated three times and an average taken per each standard and solution.

Calibration curves were constructed using prepared standard solutions of known iron (III) acetylacetonate concentration. The standards were made using iron (III) acetylacetonate crystals (>99.9 %), acetylacetone and ethanol. The blank consisted

of ethanol and acetylacetone. More detail on the preparation of the standards and blank solutions can be obtained from Appendix C. Before each analysis a calibration curve was constructed and the blank run.

The samples were diluted 1000 times (dilution procedure given in Appendix C) and the diluted sample was analysed.

Grade A glassware and micropipettes were used for all solution preparation.

3.4.2 Fourier transform infrared spectroscopy (FTIR)

Fourier transform infrared spectroscopy (FTIR) is utilised to identify functional groups present in solutions and solids. This makes it possible to predict the composition of the material (Coates, 2000). The solutions were scanned using a Bruker Tensor 27 FTIR equipped with OPUS software. The solutions were analysed using the standard operating procedure of the Chemistry Department of the University of the Witwatersrand. A ZnSe crystal tip was used and the percentage transmittance was measured over the wavelength range of 550 – 4000 cm^{-1}.

3.5 Recovery of crystals and unreacted acetylacetone

In an industrial process the unreacted acetylacetone and iron (III) acetylacetonate will be recovered and so a protocol was developed to recover these chemicals on a laboratory scale. A question that needed to be answered was, “Is it possible to recover all the iron(III) acetylacetone as crystal product?” and so crystals were recovered from some of the liquid products of the experimental runs.

A Heidolph rotary evaporator fitted with A KNF N022AN.18 vacuum pump was used (Figure 3.4) for the recovery of the crystals. The vacuum pump was connected to the evaporator at the top of the condenser via an ice trap and two addition cooling zones to reduce the operating pressure and hence the boiling points of water and acetylacetone. The evaporator was heated with paraffin oil and operated at a rotating speed of 90 rpm. The recovery was done in two stages. During the first stage the bulk of the crystals were recovered with the evaporator operated at 105 °C. The distillate from the first stage was then evaporated again at 100 °C to recover

any additional crystals. The distillate from this batch process (2nd stage) was placed in a liquid-liquid separator and allowed to separate into acetylacetone and water as their densities differ and the solubility of water in acetylacetone is poor. The recovered crystals were collected at the bottom of the evaporation flask during each run and dried in an oven at 100 °C for 2 h. The crystals were then stored in a desiccator overnight before weighing it.

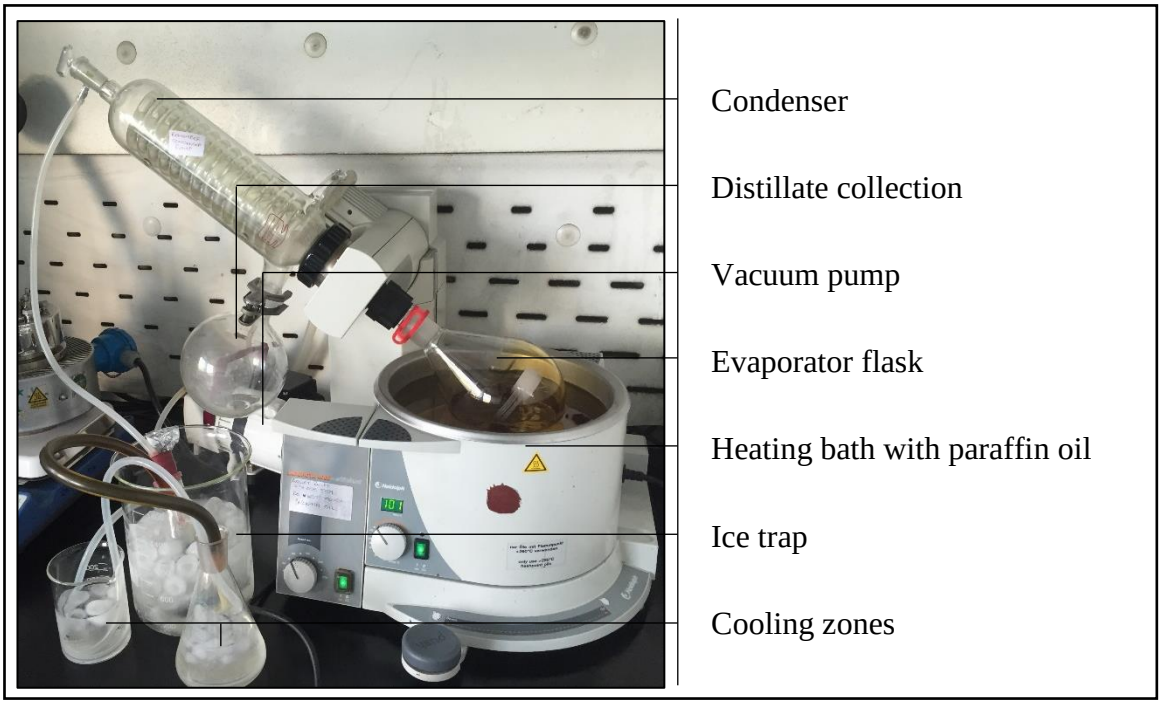


Figure 3.4: Heidolph Rotary Evaporator setup used for recovery.

4 EXPERIMENTAL RESULTS AND DISCUSSION

The process under investigation was the reaction of iron(III) oxide and acetylacetone to iron(III) acetylacetonate and water inside a high pressure autoclave and pressurised with N_2 (inert). The results from the experimental work are presented and discussed below.

A new pressure reactor/ autoclave was purchased and hence needed to be commissioned accordingly before experimentation could commence. This was done following the instructions given by the manufacturer (summarised in Appendix B)(AmAr Equipments PVT. LTD., n.d.). All parts were checked to be in the right working order and all safety precautions followed.

4.1 Determination of experimental operating space

There are two important factors, namely solubility of iron(III) acetylacetonate in acetylacetone and the vapour pressure of the solvents, that determine the operational space of the extraction process. These factors are investigated below.

4.1.1 Solubility analysis of iron(III) acetylacetonate in acetylacetone

Information about the solubility of iron (III) acetylacetonate in acetylacetone is important as an oversaturation of the reaction solution will lead to crystallization of iron(III) acetylacetone. The crystals might deposit on the iron bearing material and prevent the reagents from reacting. When Tshofu (2014) increased the solid to liquid ratio to 0.127:1 crystals formed in the reaction solution which reduced the extraction significantly. No solubility data could be found in literature for this system, hence it was investigated. The results are shown below (refer to Appendix D for tabulated results).

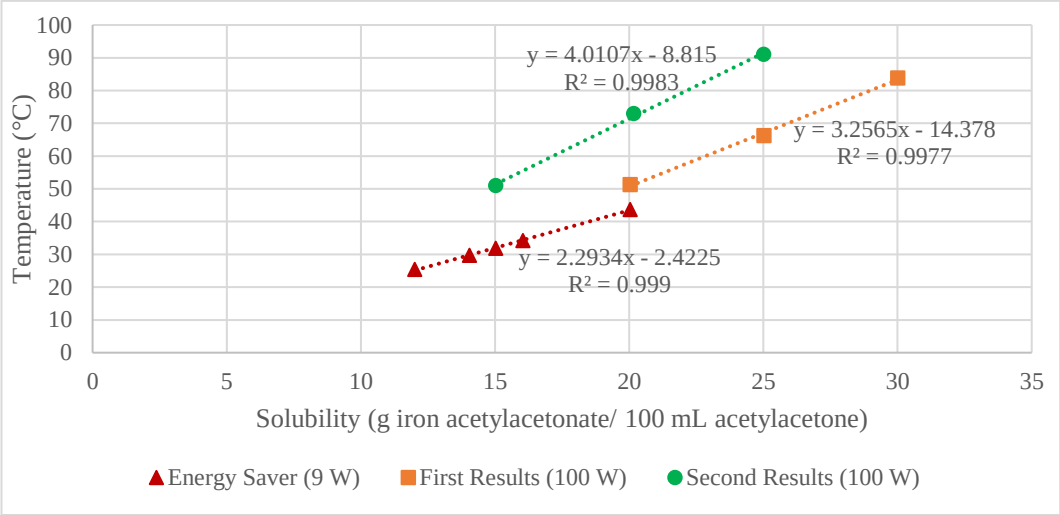


Figure 4.1: Solubility of iron(III) acetylacetonate in acetylacetone performed with two different light bulbs (i.e. energy saver 9 W bulb and a 100 W bulb).

It can be seen from the results that there is no agreement in the solubility results between the different runs. A possible reason for this is the method itself which relies heavily on the observer's ability to identify when the first crystal starts to form. Initially an energy saver bulb was used, but it did not provide enough light through the solution. At any concentration higher than 20 g/100 mL it became increasingly difficult to see the crystals as the solution became darker red. A higher wattage and brighter bulb was implemented to overcome the limitation of the energy saver. The light was easily shone through the solution. However, it also meant that originally when it was perceived that there were no longer crystals present and all had dissolved when viewing with the energy saver bulb was no longer the case. This meant a great difference in the results obtained using an energy saving light vs a 100 W light.

It can be seen from the results above that there are some limitations to the visual method utilised. The main limitation being the subjectivity of results. Another limitation was that the use of a test tube meant that there was a potential for foreign particles to be suspended in the solution (even with every precautionary measure taken such as sealing the top of the test tube, very clean glass ware, etc.). The presence of any foreign items would result in crystals forming before they should as the foreign body would act as a crystallisation point. The foreign bodies could

also have been perceived as undissolved crystals which could be why it was found that the crystals weren't dissolving properly.

Taking the above into account the method utilised above gives an estimate of the solubility and some predictions could be made. Based on the trends straight lines were fitted to the data and the solubility equations for the 100 W experiments are given below.

First results:

$$sol.\left(\frac{g\ Fe(acac)_3}{100\ mL\ Hacac}\right) = \frac{T\ (°C) + 14.378}{3.2565} \qquad (4.1)$$

Second results:

$$sol.\left(\frac{g\ Fe(acac)_3}{100\ mL\ Hacac}\right) = \frac{T\ (°C) + 8.815}{4.0107} \qquad (4.2)$$

Tshofu (2014) found with the 0.127:1 experiment that 35.49 g of iron(III) acetylacetonate was formed and resulted in some crystallising when the solution was filtered at room temperature. The 0.025:1 experiment yielded 20.09 g of iron(III) acetylacetonate and did not crystallise out during filtration. The solubility results above support this as it can be seen that at 25 °C the solubility based on the 100 W bulb results (1st and 2nd), extrapolating the fitted straight lines, were 12.1 or 8.4 g per 100 mL of solution respectively. The filtered solutions had a volume of 250 mL, taking this into account then solutions above 30.2 (from 1st results) or 21.0 g (from 2nd results) would crystallise out which was the case above. If the reactor is operated below the estimated solubility crystallisation should not occur. Thus, the systems that follow were based on an initial solid to liquid ratio of 0.025:1 to reduce the likelihood of crystal formation. The higher the temperature, the higher the saturation. Hence, to further reduce the loss of product the filtration temperature of 80 °C was chosen.

The solubility method above can only give a rough estimate of the operation limits around the loading of solids in the reactor. A more accurate method would need to be investigated

4.1.2 Measurement of pure and mixture vapour pressures

The pure and mixture vapour pressures of acetylacetone and water were measured over the temperature range of the extraction studies. The results are given below (tables given in Appendix E).

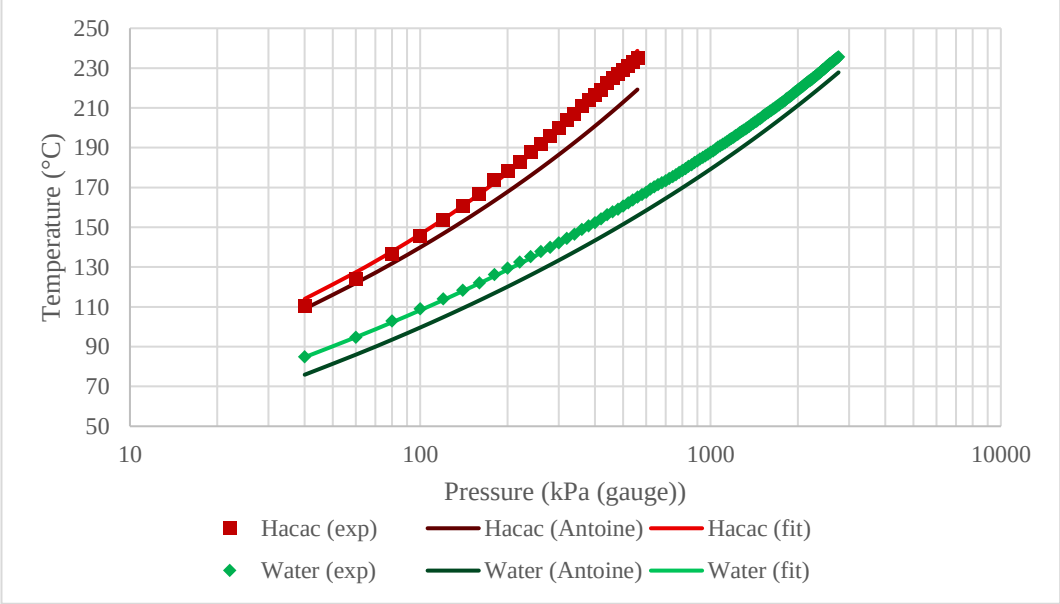


Figure 4.2: Vapour pressure of acetylacetone and water in the presence of nitrogen plotted with the pure component Antoine predicted curves (Yaws, 2015).

If one compares the experimental vapour pressure curves with those predicted by the Antoine equations of Yaws (2015) it can be seen that in our system the vapour pressures are lower than expected. A possible reason for this might be the fact that in our system a small amount of nitrogen is present compared to the method used by Yaws (2015) where the chamber was evacuated. This suggests that the pressure of the system would be slightly lower than that if only that component was present.

The experimental curves follow a similar trend as the Antoine curves hence a model was fitted using linear regression to the following $\log_{10} p^* = a - \frac{b}{T+c}$ where p^* is

the partial pressure (mmHg), T is temperature (°C) and a, b and c are the Antoine coefficients. The values for a, b and c are shown below:

Table 4.1: Fitted model to experimental vapour pressure of acetylacetone, water and a mixture of acetylacetone and water (9:1) in the presence of nitrogen.

	a	b	c	T_{min} (°C)	T_{max} (°C)
Acetylacetone	5.87654	833.051	131.055	110	236
Water	8.11796	1753.56	226.155	84	236

A comparison between the pure component systems and that of the mixture (9:1 acetylacetone:water) is presented below.

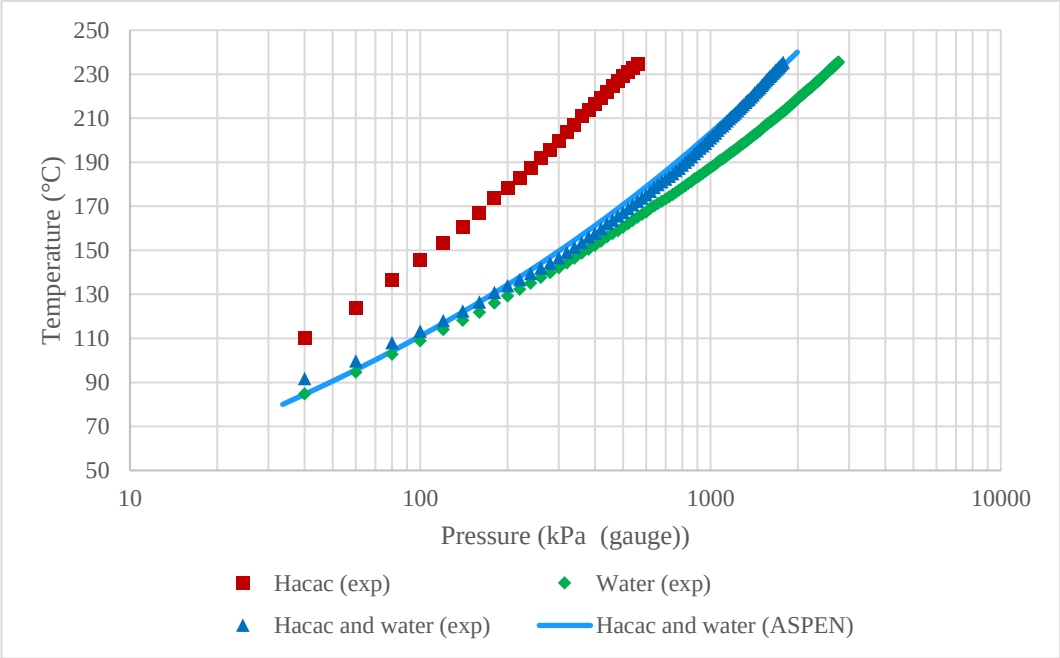


Figure 4.3: Vapour pressure of acetylacetone, water and a 9:1 solution of acetylacetone and water in the presence of nitrogen and an ASPEN Plus simulation of the mixture.

It can be seen that the water has a great influence on the vapour pressure of the mixture at temperatures below the boiling point of acetylacetone as the mixture curve tends to lie very close to that of water. As the temperature increase beyond this point and acetylacetone begins to evaporate the curve moves away from that of water and one can see that acetylacetone also contributes to the vapour pressure of the system.

The experimental results shown above are the average results per experimental set with a relative standard deviation range of 0 – 1.1, 0 – 3.7, and 0.6 – 12.1 % for the acetylacetone, water, and acetylacetone and water experimental sets respectively. The higher relative deviations (i.e. 0.5 – 1.1, 1.4 – 3.7, and 3.0 – 12.1 % respectively) occur as the pressure drops below 300 kPa which is likely due to the fact that the pressure gauge and temperature controller cannot respond quickly enough to very small changes in pressure and temperature. Higher temperatures and pressures have far smaller relative standard deviations (0– 0.5, 0 – 1.4, and 0.6 – 3.0 % respectively). Since the proposed process is a high temperature and pressure system these are more important and need a far more accurate representation.

An ASPEN Plus model was fitted to the mixture system based on the following: UNIFAC property method, nitrogen as a Henry's component, modelled using a sensitivity analysis around a flash drum that had two feeds (namely the mixture – acetylacetone and water – and nitrogen), the feeds were fed in proportion to the system loading conditions by setting the standard volume flows (this takes the volume as if the two components are immiscible) – i.e. 180, 20 and 250 L/h for acetylacetone, water and nitrogen respectively. The flash drum was operated at varying temperatures and vapour fraction of 0.5656 (ASPEN required info). The pressure was calculated for the system.

The proposed experimental reaction temperatures are 120, 140, 150, 160, 180, and 220 °C and from the curve of the mixture above, the vapour pressures are 130, 240, 320, 420, 660 and 1400 kPa respectively. In order to keep as much of the solution in liquid phase as possible the total pressure inside the reactor would need to be higher than these vapour pressures. This is supported by bubble point calculations. This was achieved by using excess nitrogen. The effects of higher pressure on the extraction of iron from iron bearing materials is investigated in the sections that follow

4.2 Extraction of iron from synthetic iron(III) oxide and iron ore fines

4.2.1 Initial extraction of iron from iron ore fines

Initial extraction experiments were conducted with iron ore fines (93% Fe_2O_3) and acetylacetone in the high pressure autoclave to determine an operating regime. The reactor was loaded to 66.7% (300 mL) of its capacity which was below the maximum recommended loading of 70% and above the minimum of 40 % (AmAr Equipments PVT. LTD., n.d.). It was shown by Mariba (2010) and Tshofu (2014) that the reaction of iron oxide and acetylacetone achieved higher extraction rates at higher temperatures. Furthermore, Mariba (2010) showed that when one performs the extraction at temperatures greater than 210 °C there is a significant increase in extraction compared to those performed at lower temperatures. Thus, the initial testing of the reactor was performed at an internal reactor temperature of 220 °C. This temperature was also chosen to ensure that the reactor was operated with about a 10 % temperature safety margin between the operated and design temperature of the reactor. It also ensured that internal pressure of the reactor did not exceed the maximum design pressure as the system was loaded with excess N_2 before heating. The system was loaded with 1000, 2000 and 3000 kPa of N_2 initially and then heated. The final pressures at the reaction temperature were 2600, 4300 and 6000 respectively. These pressures are significantly higher than the vapour pressures of the original system above. The reactor was run for a total of 18 h with 7.5 g of iron ore fines and a solid to liquid ratio of 0.025 g:1 mL. The results were analysed with the Spectroquant Pharo 300 Spectrophotometer and the spectra of the three samples are shown in Figure 4.4.

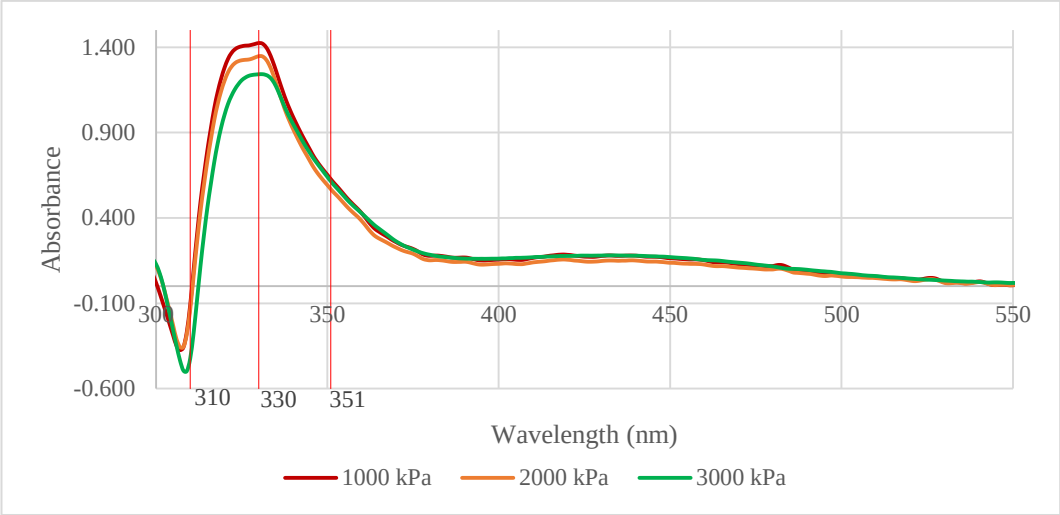


Figure 4.4: UV-Vis scan for the initial study at varying N_2 loaded pressures of 7.5 g of iron ore fines (>93 %) at 220 °C with 300 mL solution (270 mL acetylacetone and 30 mL water), solid to liquid ratio of 0.025 g:1 mL, total time 18 h, particle size of +106 -150 µm and stirrer speed of 375 rpm.

It can be seen from the UV-Vis scan that the maximum peak is at 330 nm and another peak at 438 nm. The UV-Vis curves of the standards (Appendix F) show that the peaks for iron(III) acetylacetonate are at 351 and 438 nm. The shift in the maximum peak from 351 nm to 330 nm shows that the reaction mixtures did not contain pure iron(III) acetylacetonate in solution and that another organometallic compound could have been present. Based on the wavelength the compound is likely a conjugated olefin with the form $(-HC = CH-)_2$ (Robinson et al., 2004). This meant that the reaction had likely undergone a polymerisation reaction.

In order to test this theory it was decided to recover the iron(III) acetylacetonate formed as crystals. The Heidolph rotary evaporator was loaded with 200 mL of solution and operated accordingly at 105 °C. It was observed that after 3 h no more vapour was forming in the distillate flask and being pulled into the condenser. A substantial amount of liquid was still present in the evaporation flask. The solution was heated further until evaporation took place again up to a maximum of 160 °C. Tshofu (2014) was able to completely recover the acetylacetone and crystals at 160 °C. The amount of solution present in the evaporator flask reduced but no crystals formed. A viscous material remained in the flask. No viscous material was noted

by Tshofu (2014) and since complete recovery was possible it suggests that no side reaction occurred in the atmospheric liquid phase experiments operated with condensing reflux.

The absence of crystal formation and the presence of the viscous material supports the results of the UV-Vis scans. This made it impossible to quantify the results and it was concluded that these operating conditions were not conducive for the formation of the desired iron(III) acetylacetonate product.

From an industrial perspective the occurrence of a side reaction and formation of the unwanted product would lead to additional waste being produced. This means that the aim to create a greener process whereby a waste material is utilised and overall waste reduced, would not be occurring as a new source of waste is being added. It was therefore necessary to find operating conditions where the occurrence of any side reactions would be avoided.

It was noted that the spectra was similar for all pressures which likely suggested that the resulting phenomena was caused by other factors. However, since no side reaction was observed for the atmospheric liquid phase experimentation performed by Tshofu (2014) it suggests that operating in a sealed vessel may have an effect that is increased by other factors. The iron ore fines contains impurities such as quartz (3.92 %) and muscovite (2.17 %) which may be a potential cause (Tshofu, 2014). The operating temperature and reaction time could also have an effect. Further experimentation was needed to find the conditions whereby the desired product is formed and the side reaction is limited. Utilising a purer synthetic iron oxide in the extraction provided a means to assess the effect of impurities and by varying the operating temperatures the effect of temperature could be evaluated as well. The results of this study follows.

4.2.2 Extraction of iron from synthetic iron(III) oxide

It was discovered that an unknown side reaction occurred that reduced the formation and prevented the recovery of iron(III) acetylacetonate crystals. It is necessary to evaluate what factors influence this side reaction and determine at what conditions the pressure leaching process can be operated at to have the desired product formed.

The interference of other species is limited by performing the extraction experiments on a synthetic iron(III) oxide that is of a higher purity (> 95 %). The effects of temperature and time on both the desired and undesired reactions were evaluated. The aim is to reduce the side reaction, identify what affects it the most and increase the desired reaction/ extraction of the iron in the form of iron(III) acetylacetonate).

The reaction of the synthetic iron(III) oxide with acetylacetone was studied at 120, 140, 150, 160, 180 and 220 °C for total time of 3, 4, 6, 8, 10 and 18 h when deemed necessary. The system was operated to coincide with the experiments above an initial nitrogen pressure of 1000 kPa. The total pressures inside the reactor at the desired reaction temperatures were higher than those of the vapour pressures of the original system. The resulting operating pressures were 1380, 1500, 1610, 1700, 1900 and 2600 for the above temperatures respectively. The analysis of the experiments was done as before and the UV-Vis results was used as a means to study the formation of an undesired product. The results of these spectra are given below.

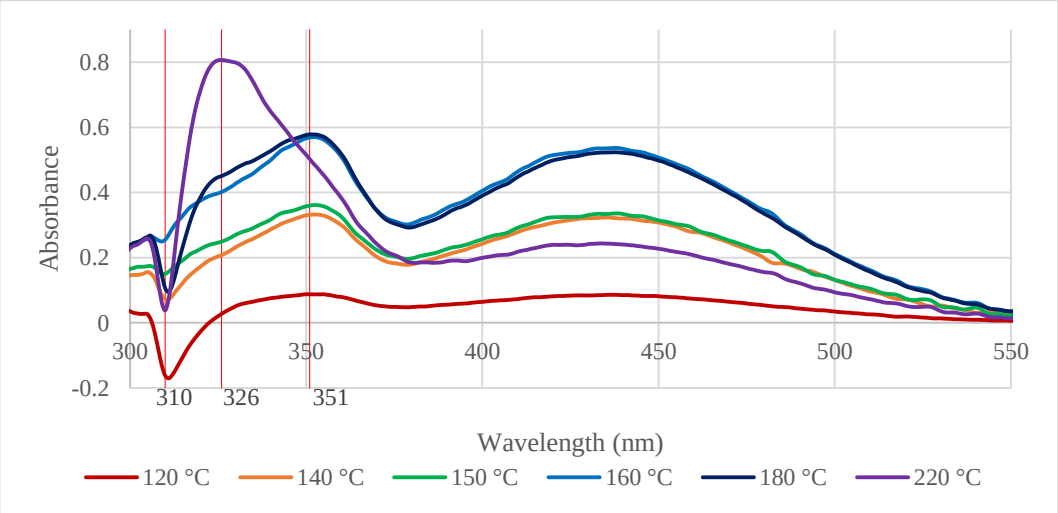


Figure 4.5: UV-Vis analysis results of 5 g of synthetic iron oxide at solid to liquid ratio of 0.025 g:1 mL, 1000 kPa N_2, total time of 3 h and varying temperature.

The shortest time of 3 h was initially evaluated at varying temperatures. There is a clear difference in the shape of the peaks and in the case of the 220 °C the maximum peak location. The peaks for 120-180 °C exhibit a similar form as those of the

calibration/ standard solution UV-Vis curves given in Appendix F. These peaks have the signatory wavelengths matching those of iron(III) acetylacetonate 351 and 438 nm. This implies that the desired product is formed. The amplitude of these peaks increase from 120 to 180 °C which shows that the concentration of iron(III) acetylacetonate increases and hence the desired product formation increases with temperature. There is a shift in the maximum peak of the 220 °C to 326 nm which is similar to that of the previous fines experiments. This suggests that the side reaction has taken preference. Another difference in the above spectra to those of the standard solutions UV-Vis curves is that there is a drop in absorbance around 310 nm. An example of the calibration UV-Vis curves is shown in Figure 4.6 below for comparison purposes (full details regarding this curve are given in Appendix F). The drop occurs at the wavelength that represents pure acetylacetone and the decrease in absorbance is due to the concentration of acetylacetone present in the sample solutions analysed. The acetylacetone concentration present in the blank and standards is slightly higher than that of the samples above. Its effects are investigated and are given in Appendix F.2.5. The concentration does not influence the peaks of the iron(III) acetylacetonate or unknown material unless in extreme excess.

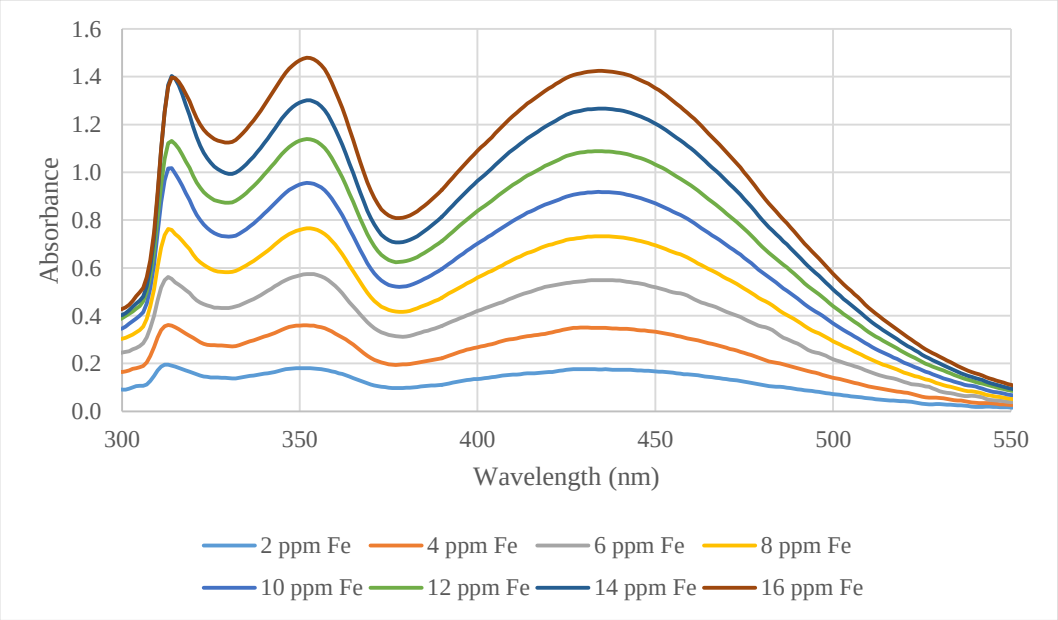


Figure 4.6: UV-Vis scan results for the iron(III) acetylacetonate standards shown in terms of iron concentrations.

The curves for the 120-180 °C exhibit a slight peak at 326 nm which suggests that the side reaction is taking place but has not surpassed that of the desired reaction.

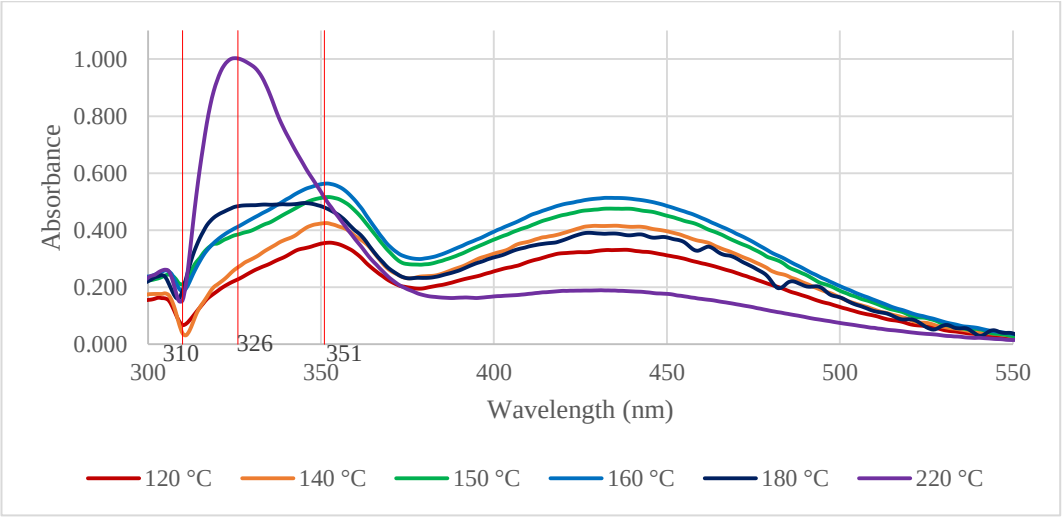


Figure 4.7: UV-Vis analysis results of 5 g of synthetic iron oxide at solid to liquid ratio of 0.025 g:1 mL, 1000 kPa N_2, total time of 4 h and varying temperature.

The same temperatures were investigated at a longer total time of 4 h. The 120-160 °C curves like those above show the notable peaks of iron(III) acetylacetonate and hence its formation. There is a significant change in the curve of the 180 °C sample. The maximum peak has transformed and spans between 326-351 nm. This suggests that the side reaction is beginning to take preference. The 220 °C sample has its maximum peak at 326 nm but has a higher absorbance than that of the other temperatures. The increase in the formation of the unknown material means an increased difficulty to quantify the results as its formation took preference. The maximum peaks of the 120-160 °C samples increase with temperature; however, that of the 180 °C has decreased. This signifies that the side reaction is likely competing with the formation of iron(III) acetylacetonate.

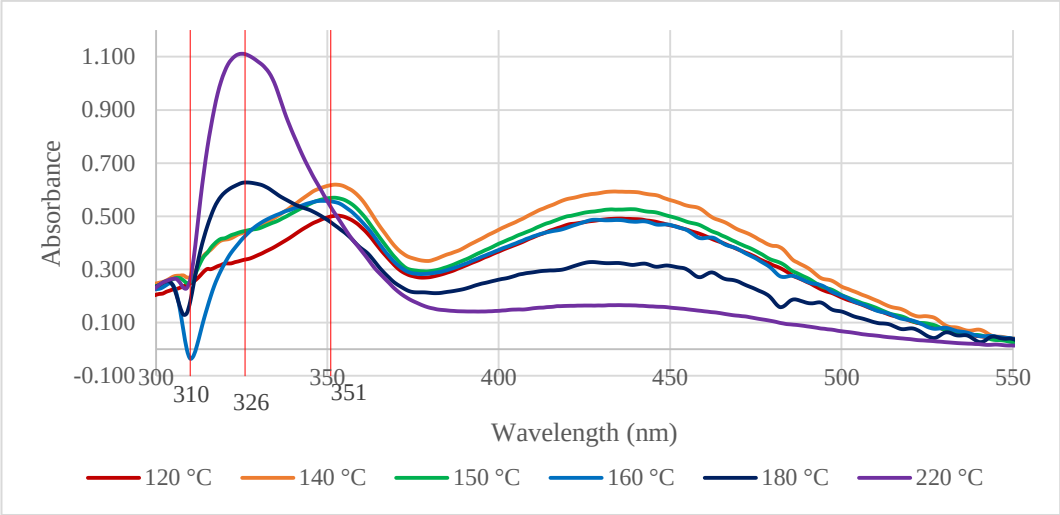


Figure 4.8: UV-Vis analysis results of 5 g of synthetic iron oxide at solid to liquid ratio of 0.025 g:1 mL, 1000 kPa N_2, total time of 6 h and varying temperature.

The total time was increased further to 6 h at the same operating conditions. The maximum peak of the 180 °C sample has now completely shifted to 326 nm with only a slight peak at 351 nm. The 120-160 °C curves still have their maximum peaks at 351 nm but there is an increase in the amplitude of the peak at 326 nm. This suggests that the desired reaction is still favourable but with the increased time the side reaction is increasing as well. The amplitude of the 220 °C maximum peak is increasing while the peak's wavelength has remained constantly at 326 nm.

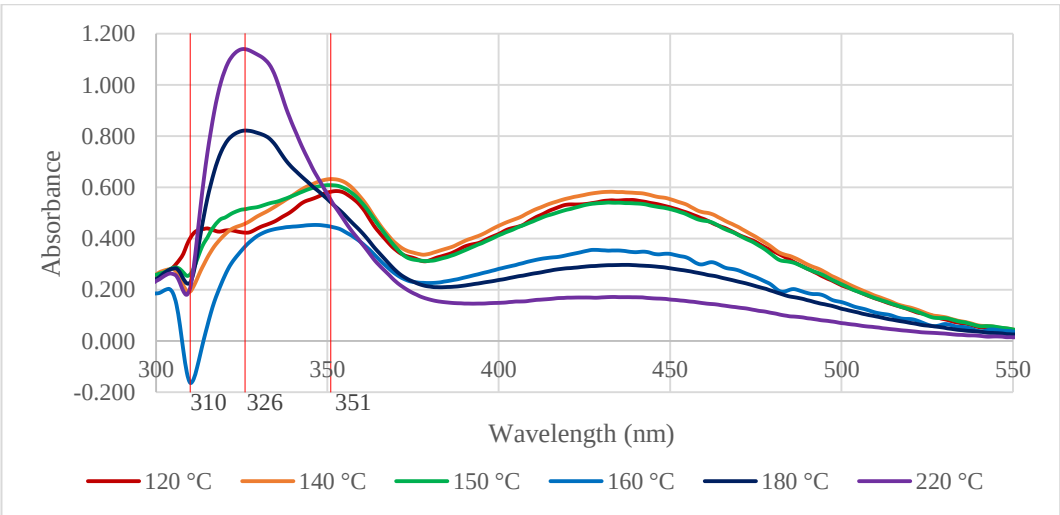


Figure 4.9: UV-Vis analysis results of 5 g of synthetic iron oxide at solid to liquid ratio of 0.025 g:1 mL, 1000 kPa N_2, total time of 8 h and varying temperature.

An additional 2 h was added to the total time and the effect of temperature becoming more evident on the progression of the side reaction. The 160 °C sample's curve maximum peak, like that of the 180 °C sample's curve previously, now spans the wavelength range of 326-351 nm. This implies that the side reaction is becoming more favourable. Iron(III) acetylacetonate is still being formed in the 120-150 °C experiments while the side reaction is slowly increasing. The 180 and 220 °C solutions are dominated by the side reaction and their results are difficult to assess. These two solutions have shown that over the increased reaction time that the side reaction increases and the maximum peak remains constant at 326 nm. These two reaction temperatures at extended times favoured the formation of the unknown material and the total amount of iron(III) acetylacetonate in solution could not be determined. Hence, no further experiments were conducted at these temperatures for the synthetic iron(III) oxide.

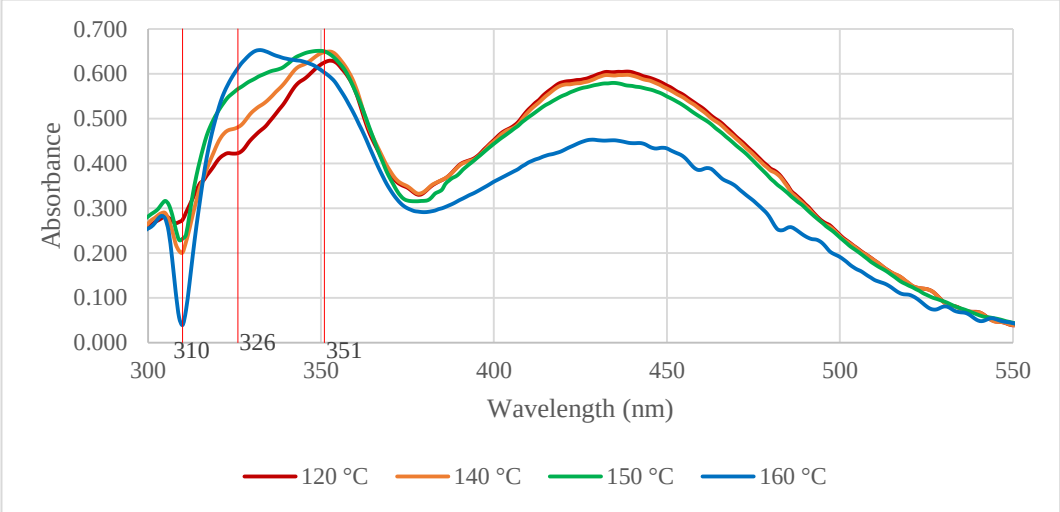


Figure 4.10: UV-Vis analysis results of 5 g of synthetic iron oxide at solid to liquid ratio of 0.025 g:1 mL, 1000 kPa N_2, total time of 10 h and varying temperature.

It can be seen in the figure above that at the total time of 10 h that the 160 °C experiment experiences the shift of peak to 330 nm. The other temperatures (120, 140, and 150 °C) show the peaks typical of iron(III) acetylacetonate. However, it can also be seen that there is a further increase in the peak size at 326 nm compared to the previous scan which signifies that the side reaction is increasing. Since the 160 °C reaction has proceeded from the formation of iron(III) acetylacetonate to

the unknown material it was deemed that it would not be tested at longer time periods as it would follow the trend of the 180 and 220 °C samples.

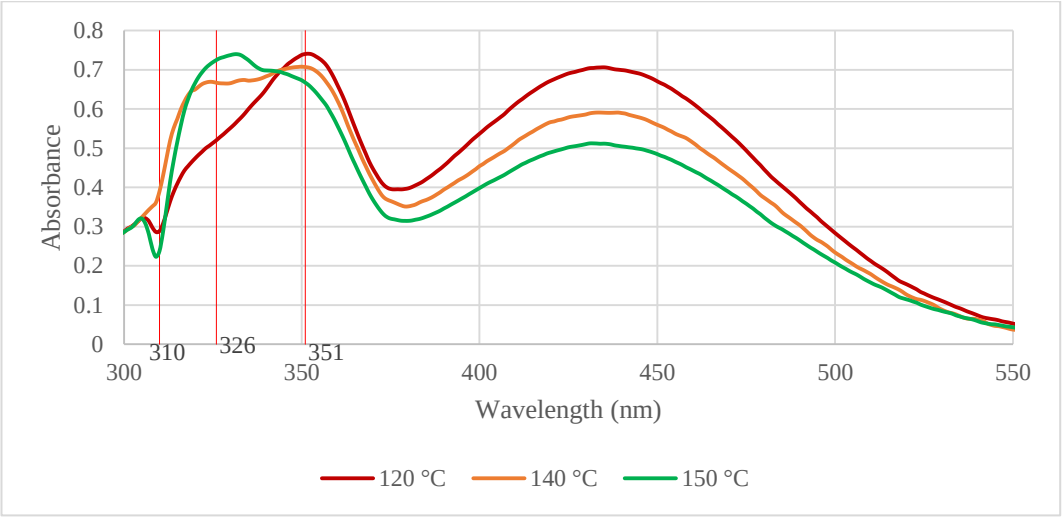


Figure 4.11: UV-Vis analysis results of 5 g of synthetic iron oxide at solid to liquid ratio of 0.025 g:1 mL, 1000 kPa N_2, total time of 18 h and varying temperature.

It can be seen from the figure above that only the 120 °C experiment at 18 h is showing reduced signs of the iron(III) acetylacetonate converting. The 140 and 150 °C experiments show the max peak shifting to 326 nm.

From the UV-Vis analysis results it is evident that there is an increase in peak shift as the time of reaction increases. Furthermore, the peak shift is dependent on the reaction temperature. The longer the reaction proceeds the increased likelihood of the side reaction occurring. Although the 220 °C experiments were performed for shorter times than those with the iron ore fines they exhibited the same trends. This suggests that the peak shift and formation of the unknown material is more dependent on the reaction temperature and time rather than the impurities present. The increase in amplitude of the 326 nm peaks as total time increased, coupled with the broadening of the maximum peaks to span 326-351 nm suggests that the side reaction is dependent on the iron(III) acetylacetonate present as well.

Similarly to those of the initial iron ore fines experiments the shifted wavelength peak at 326 nm suggests a conjugated olefin forming (Robinson et al., 2004). This means that the reaction has likely undergone a polymerisation reaction.

To evaluate whether the side reaction was consuming the iron(III) acetylacetonate an experiment using only iron(III) acetylacetonate (10 g at 99.99 wt% purity) and the solvent solution was done. The reaction was performed at the same operating conditions as those above at a temperature of 220 °C and total time of 8 h. The UV-Vis results are given below.

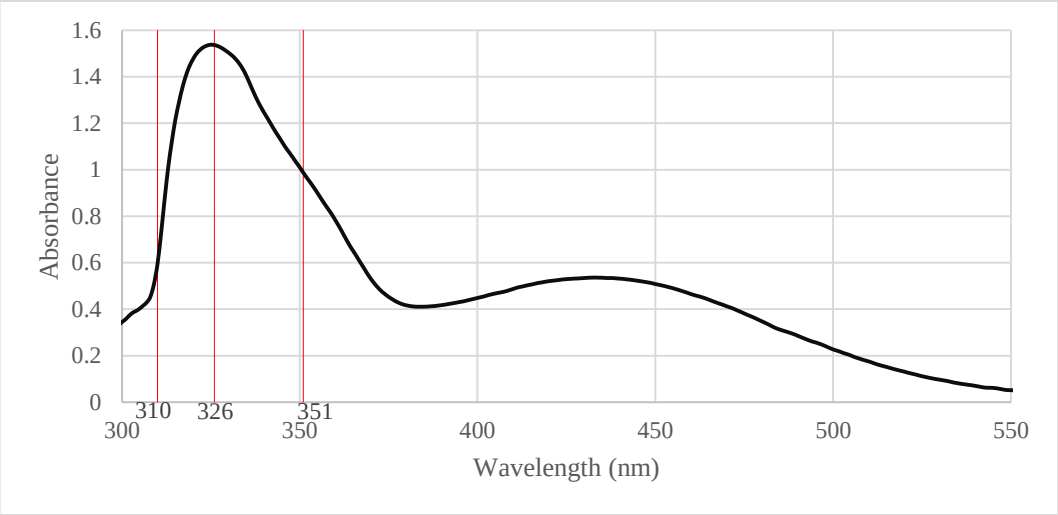


Figure 4.12: UV-Vis analysis results of 10 g of synthetic iron(III) acetylacetonate in 200 mL of solution (9:1 acetylacetone:water), 1000 kPa N_2, total time of 8 h and at 220 °C.

The reaction was performed in the absence of iron(III) oxide but it can be seen that the same peak shift phenomena occurred as in previous systems. There is no definite peak at 351 nm even though only iron(III) acetylacetonate was loaded. This suggests that the iron(III) acetylacetonate was consumed during the side reaction. This means that a consecutive not a parallel reaction is occurring.

Another possibility is that the iron(III) acetylacetonate or acetylacetone decomposed. The key components of iron(III) acetylacetonate decomposition are acetone, carbon dioxide and iron (Hoene et al., 1958). Acetone's maximum UV-Vis peak is typically around 265 nm (National Institute of Standards and Technology, 2016a), while the other components would not show up on an UV-Vis. This suggests that a different side reaction is occurring as the maximum peak above does not correlate to that of acetone.

The UV-Vis curves above only show the compounds and functional groups present but when coupled with the calibration curves (refer to Appendix F for calibration data and the calculations regarding the synthetic iron(III) oxide) it is possible to determine the concentrations of the iron in the form of iron(III) acetylacetonate present in each solution. With the concentration it was then possible to calculate the amount of iron that was converted from iron(III) oxide to iron(III) acetylacetonate using the iron(III) acetylacetonate peak maximum at 351 nm. The results of which are shown in the figure below.

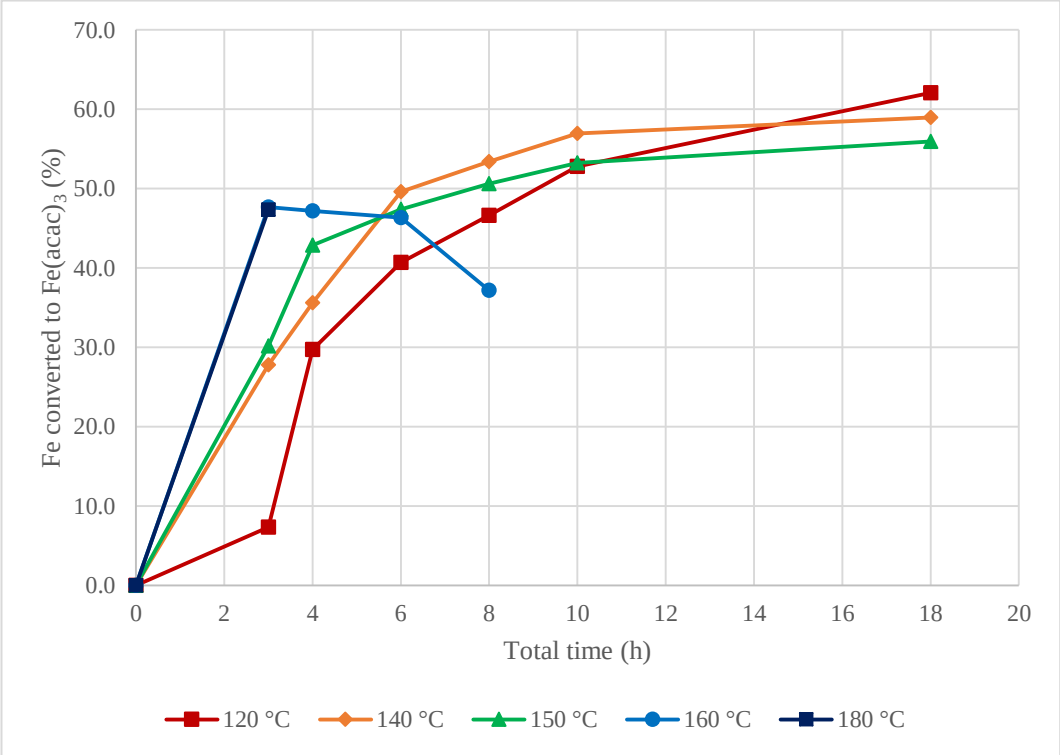


Figure 4.13: Results for the temperature study of 5 g of synthetic iron oxide (>95 %) with 200 mL solution (180 mL acetylacetone and 20 mL water), 1010 kPa N_2 loaded, solid to liquid ratio of 0.025 g:1 mL and stirrer speed of 375 rpm.

It can be seen in the figure above that as time progresses the conversion increases, except for the conversion of iron to iron(III) acetylacetonate taking place at 160 and 180 °C. The conversion at 160 °C decreases as time proceeds due to the side reaction that occurs that competes with the formation of iron(III) acetylacetonate. The 180 °C is only shown at one point as 3 h is the only time that the iron(III) acetylacetonate formation hasn't been surpassed by the side reaction. The 120, 140

and 150 °C curves cross each other as time proceeds and the side reactions begin to dominate the 140 and 150 °C runs. Maximum conversion of 62.1 % is achieved at 120 °C after 18 h. The 140 and 150 °C conversion at 18 h is only slightly lower at 59.0 and 55.9 % respectively.

Taking into account the peak shifts and the results above it is evident that the 4 h experiments have the least signs of side reaction occurring and conversions greater than 30 %. Comparing the 4 h experiments with those of the 18 h experiments (3.5 times the duration) the 120, 140 and 150 °C conversions have only increased from 29.7 to 62.1, 35.6 to 59.0, and 42.9 to 55.9 % respectively. The results suggest that a multi-reactor system might offer a solution to prevent/ minimise the formation of a polymer in solution. If the 4 h experiment was performed in a two stage process, whereby the unreacted iron oxide from the first reactor was fed into the system of the second reactor with fresh acetylacetone and working with the assumption that the reactors would operate similarly then higher conversions (59.4, 71.2 and 85.8 % respectively) could be achieved after 8 h rather than allowing the one reactor run for 12 h. The 160 °C experiment could achieve 94.4 % conversion using two reactors in series operated for 4 h each.

The aforementioned conversion results and operating conditions are only viable if the iron(III) acetylacetonate crystals can be recovered from their solutions. The method used to recover the crystals was an optimised version of the one utilised by Tshofu (2014) by using vacuum pressure to reduce the boiling points of the solvents. This also resulted in the recovery proceeding a lot faster as the vapour was drawn from the evaporator flask into the condenser. The recoveries took between 1-2 h per stage for the solutions that were able to be crystallised. The 1st stage distillate was found to be slightly yellow in colour showing that it contained some dissolved iron(III) acetylacetonate. The 2nd stage distillate was completely clear. The 2nd stage distillate was placed in a liquid-liquid separator. The water and acetylacetone separated into two layers due to their difference in densities (i.e. water being slightly heavier than acetylacetone at 0.997 and 0.975 g/mL at 25 °C respectively (Felder and Rousseau, 2005; Sigma-Aldrich, 2015a)). Some acetylacetone was found to be trapped in the bottom water layer and was tapped off

with the water as waste. The acetylacetone was bottled for future use. Some of the recovered iron(III) acetylacetonate crystals are shown below.



Figure 4.14: Recovered iron(III) acetylacetonate crystals.

Crystal recovery was performed using 200 mL of the original solution. The recovery was performed on the synthetic iron oxide samples at total times of 4, 6, 8 and 10 h at temperatures of 120 and 140 °C; as well as total time of 4 h for 150, 160, 180 and 220 °C. The recovery was performed on the 120 and 140 °C solutions over the entire reaction time range to determine the effect of an increased side reaction on the recovery of the crystals. The other solutions were evaluated at the time that the extraction would be operated at if a multi-phase system was utilised. The results of these recoveries are given in Table 4.2 (refer to Appendix F for calculations).

Table 4.2: Crystal recovery results for 5 g of synthetic iron oxide at 1010 kPa N_2, solid to liquid ratio of 0.025 g:1 mL, and stirrer speed of 375 rpm.

Temperature (°C)	Total time (h)	Mass of Fe extracted (g) as iron(III) acetylacetonate	Mass of $Fe(acac)_3$ in solution (g)	$Fe(acac)_3$ Crystals recovered (g)	Crystals recovered (%)	Uncrystallised liquid mass (g)
220	4	-	-	-	-	9.96
180	4	-	-	-	-	8.56
160	4	1.569	9.920	8.612	86.8	3.49
150	4	1.425	9.014	7.892	87.5	2.39
140	10	1.893	11.972	11.692	97.7	3.62
140	8	1.774	11.222	10.732	95.6	2.66
140	6	1.649	10.430	9.782	93.8	2.12
140	4	1.183	7.483	7.247	96.9	0.70
120	10	1.755	11.097	10.052	90.6	1.54
120	8	1.549	9.798	9.323	95.2	1.33
120	6	1.352	8.549	7.687	89.9	1.16
120	4	0.988	6.249	5.933	94.9	0.86

It was found that crystals could not be recovered from the 220 °C solutions even when the temperature was increased to 160 °C. This supports the findings with the initial fines experiments. A viscous liquid formed in the evaporator flask. Similarly the crystals could not be recovered from the 180 °C experiment. This was due to the large quantity of a polymer present. However, crystals could be recovered for all other samples in excess of 86 % recovery. It can be seen that the mass of crystals recovered increases both with an increase in temperature as well as with time which is in support of the conversion findings for these experiments. Furthermore, it can be seen as the time and conversion increased the mass of uncrystallised liquid that remained in the evaporator flask increased as well. The side reaction converts the iron(III) acetylacetonate formed in the desired reaction. As time progress more of the reaction takes place, which has been seen before; however, the side reaction also increases. An attempt to recover the loaded iron(III) acetylacetonate crystals from the iron(III) acetylacetonate experiment yielded only a viscous black liquid

and no crystals were formed. This further supports that the side reaction is the second stage of a series reaction.

Another analytical technique, namely Fourier Transforms Infrared Spectroscopy (FTIR), was utilised to determine the composition of the product solutions. FTIR was performed on four samples namely the 140 and 180 °C experiments performed at total times of 4 and 8 h. These experiments were chosen as it was shown above that they showed the conversion of iron(III) acetylacetonate to the unknown chemical. The FTIR was performed as a means to identify the functional groups and to increase the understanding of the final solutions composition in the reactor. Shown below are the results for the 140 °C at 4 h experiment as well as the 180 °C at 8 h experiment. The other two curves are given in Appendix F.3.

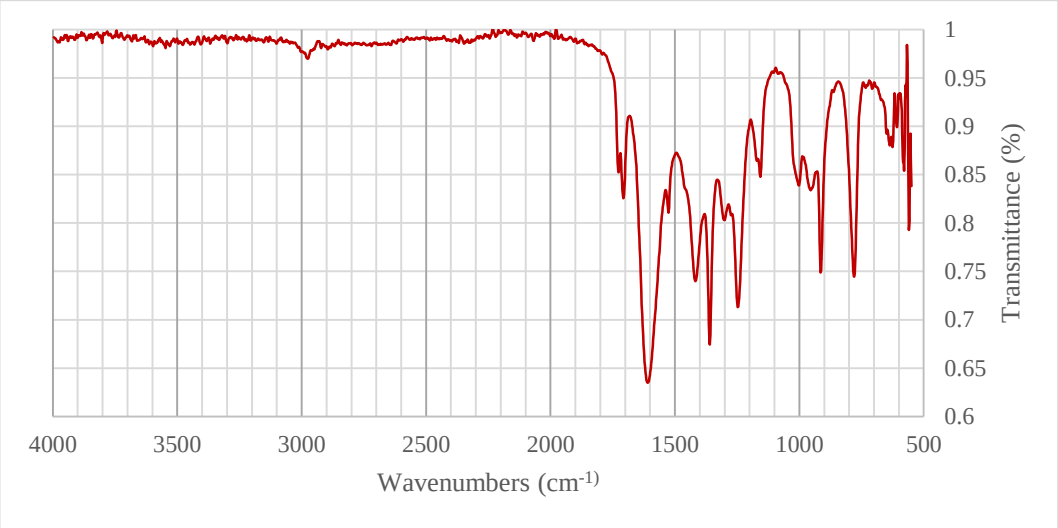


Figure 4.15: FTIR scan results for the synthetic iron oxide experiment performed at 140 °C, total time of 4 h, 9:1 ratio of acetylacetone: water, 0.025 g/mL and 5 g of iron oxide.

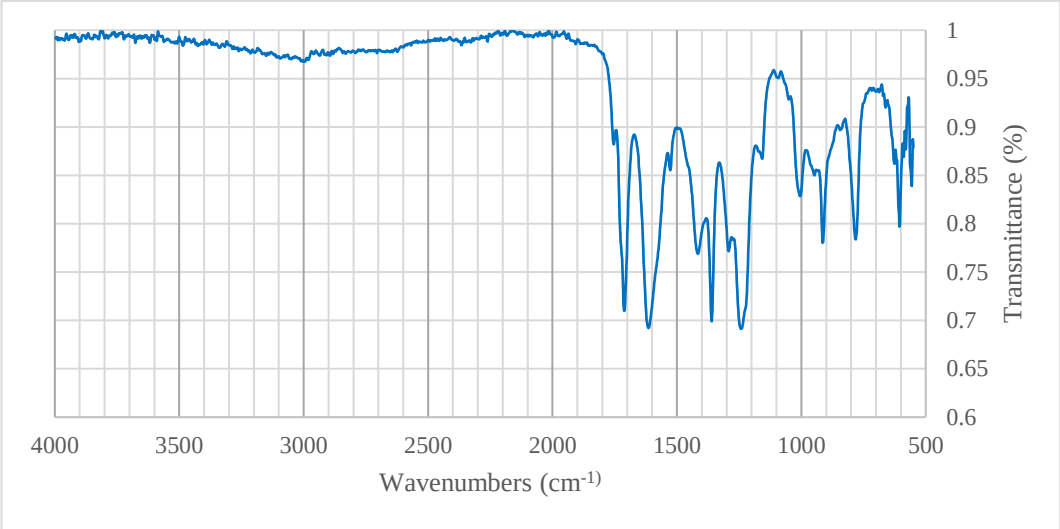


Figure 4.16: FTIR scan results for the synthetic iron oxide experiment performed at 180 °C, total time of 8 h, 9:1 ratio of acetylacetone: water, 0.025 g/mL and 5 g of iron oxide.

In order to accurately assess the above scans it was necessary to compare them to standard curves of the main constituents of the solution. These are acetylacetone and iron(III) acetylacetonate. The FTIR standard curves of these chemicals are also given below.

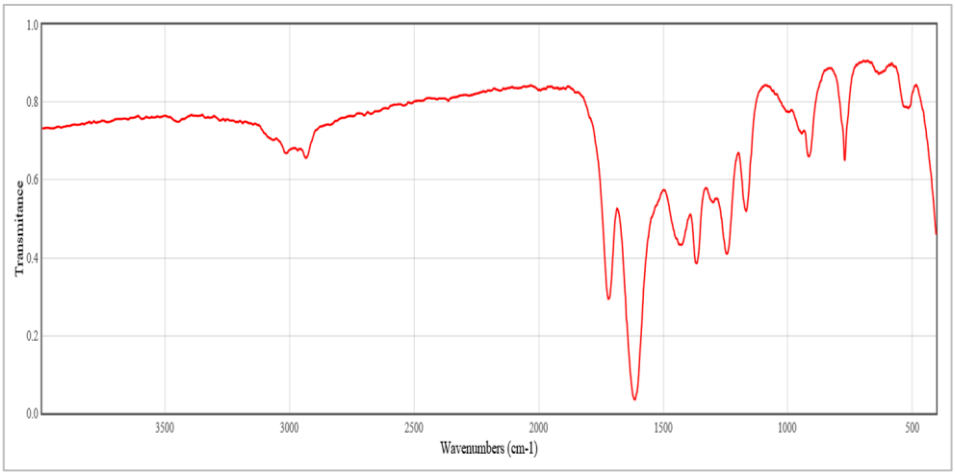


Figure 4.17: FTIR scan of acetylacetone (National Institute of Standards and Technology, 2016b).

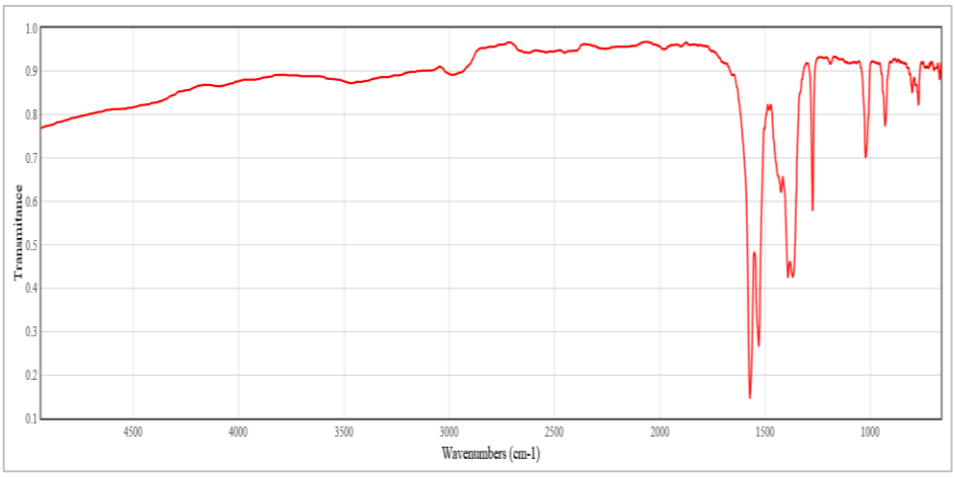


Figure 4.18: FTIR scan of iron(III) acetylacetonate (National Institute of Standards and Technology, 2016c).

Comparing the experimental scans to those of the pure component scans above it is evident that the scan results are dominated by the presence of the acetylacetone. This can be seen by the fact that the peaks shown in the acetylacetone scan are graphically similar to those of the experimental scans and locations of peaks match. There are some similarities to the iron(III) acetylacetonate scan but these are not as clear as the acetylacetone peaks. The experimental results have the peak by 3000 cm^{-1} that represents the C – H bond, the typical peak representing ketones between 1725 – 1705 cm^{-1} that is the C = O bond and also shows the C – C stretch bond (aromatic ring) between 1615 – 1450 cm^{-1} that highlights the keto-enol tautomerism of the acetylacetone (Coates, 2000).

The aim was to utilise the more precise FTIR scan to establish what the unknown material formed in the side reaction was. However, this could not be done as the large quantity of acetylacetone present in the final solutions masked the other materials present in the solution.

All the curves and results gathered from the synthetic iron(III) oxide experiments showed that there was a positive correlation and trend with the side reaction, temperature, time and amount of iron(III) acetylacetonate present in the solution. The results from the product recovery supported those of the UV-Vis scans and FTIR scans. It is evident that lower times and temperatures reduced the formation of a polymer but also reduced the conversion to the desired product, iron(III)

acetylacetonate. The side reaction also occurred despite the use of the synthetic oxide being a purer sample. This suggests that the impurities have a limited effect in comparison to the temperature, reaction rate of iron(III) acetylacetonate and amount of iron(III) acetylacetonate present.

The aforementioned temperature based experiments gave an indication of the operating range where the polymer formation is reduced and the conversion of iron(III) oxide to iron(III) acetylacetonate is improved. The system can be operated at 120 and 140 ° to a maximum total time of 18 h, at 150 °C to 10 h and 160 °C to 10 h. In order to reduce the side reaction it was found that the best suited total time for reaction should be 4 h for temperatures of 120-160 °C.

4.2.3 Extraction of iron from iron ore fines

The aim of this study was to determine whether it is possible to reduce the reaction time of the liquid phase extraction process developed by Tshofu (2014) by operating at higher operating temperatures and pressures in a high pressure reactor. In order for this to be achieved it was necessary to determine the effects of various operational conditions on the extraction of iron from iron ore fines as iron(III) acetylacetonate such as temperature (synthetic results gave an indication of viable temperature range), particle size, pressure and finally solid to liquid ratio. The effect of these variables on the polymerisation reaction was also investigated.

The rate of reaction of the iron ore fines system was studied at 140 °C and total times of 4, 6, 8 and 10 h at the initial loaded N_2 pressure of 1010 kPa which resulted in an operating pressure of 1500 kPa. The experimental conditions were chosen to agree with those used in the reflux liquid phase extraction experiments of Tshofu (2014) with iron ore fines. The UV-Vis curve of the experiment is given below.

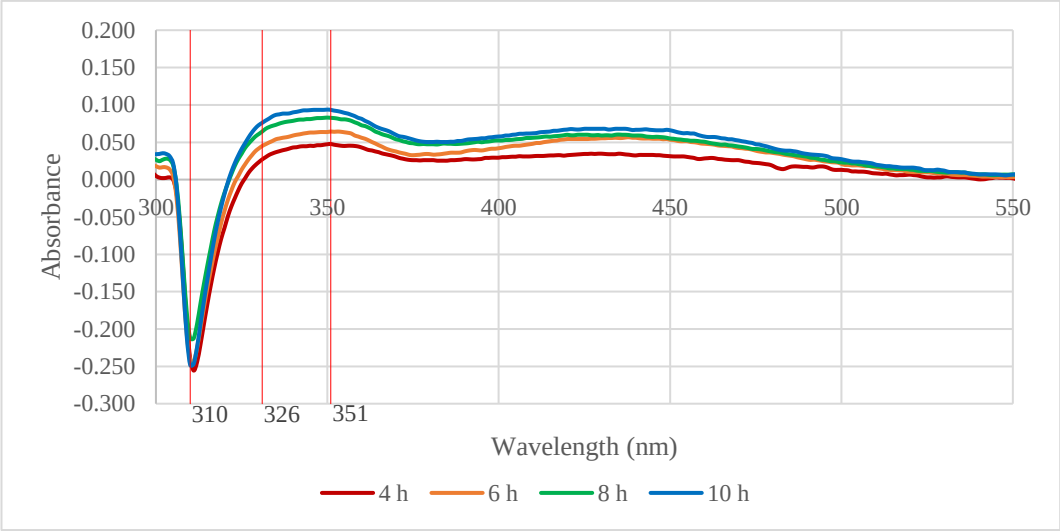


Figure 4.19: UV-Vis analysis results for the reaction rate study of 5 g of iron ore fines (>93 %) at 140 °C with 200 mL solution (180 mL acetylacetone and 20 mL water), 1010 kPa N_2 loaded, solid to liquid ratio of 0.025 g:1 mL, particle size of +106 -150 µm and stirrer speed of 375 rpm.

The analysis results given above all exhibit a similar form and have the signatory peaks associated to iron(III) acetylacetonate at 351 and 438 nm. However, it is also evident that there are no definite sharp peaks at 351 nm but rather broad peaks are present. The maximum peaks span the wavelength range of 326-351 nm. This phenomena has occurred far sooner with the industrial sample than it did for the synthetic sample. This suggests that the polymerisation reaction occurs faster with the fines. The crest of the maximum peaks are at 351 nm which implies that the desired product, iron(III) acetylacetonate is still being formed. The amplitude of the peaks increases with total time which means that the longer the reaction proceeds the more extraction is achieved.

The conversion of the iron ore fines was quantified by coupling the UV-Vis scan with the calibrations curves. The results are given below (tabulated results and calculations are given in Appendix F). The results for the iron ore fines are plotted with those of the corresponding synthetic iron(III) oxide and Tshofu's (2014) liquid phase experiments.

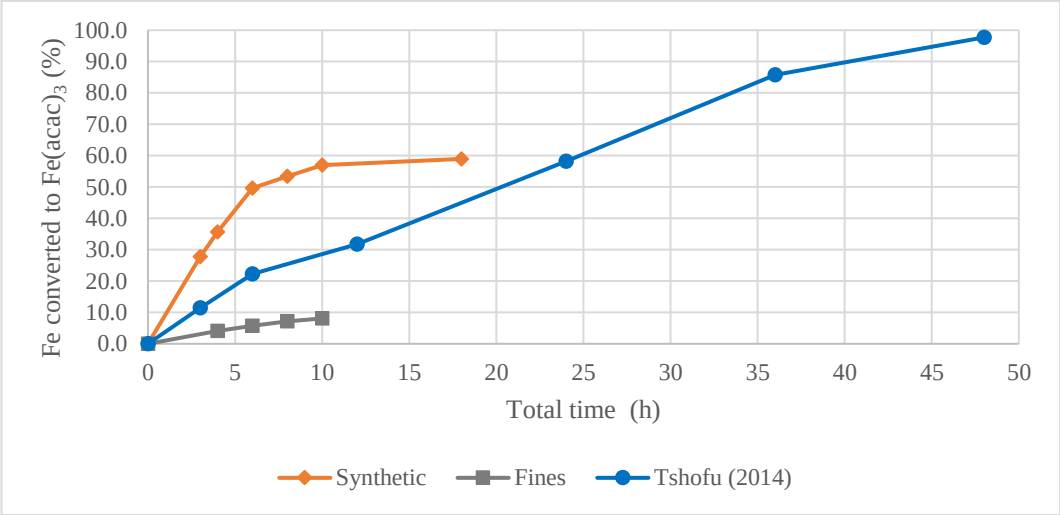


Figure 4.20: Comparison of the Tshofu's (2014) 140 °C liquid phase experiment with synthetic iron(III) oxide (< 1 µm) and iron ore fines (+106 -150 µm) at 140 °C with 200 mL solution (180 mL acetylacetone and 20 mL water), 1010 kPa N_2 loaded, solid to liquid ratio of 0.025 g:1 mL, and stirrer speed of 375 rpm.

It is evident that there is a significant difference between the synthetic and fines samples. The conversion of fines at 10 h was 8.1 % while the synthetic was 56.9 %. This significant difference could be attributed to the synthetic having far smaller particle size (< 1 µm) which is 106 - 150 times smaller than that of the fines. This means that the synthetic has a far greater surface area to react with the acetylacetone. Another factor could be that the fines's reaction is inhibited by the presence of other metal oxide species in the ore. The results from Tshofu are also higher than those of the fines. A likely explanation could be that the operation of the reactor using a reflux and in the presence of oxygen may catalyse the reaction. It could also be due to better mass transfer/ reaction rate differences. That reactor was also operated at atmospheric conditions which could also have contributed to the difference in results. Furthermore, no side reaction was noted with that system, hence no iron(III) acetylacetonate was consumed which also influences the desired product extraction rates. This also suggests that the resultant pressure of operating in the sealed vessel has an influence on the side reaction.

The effect of particle size and temperature on the system was evaluated. Two particle size ranges, namely 45 – 75 µm and 106 – 150 µm, were used to evaluate

the effect of temperature and particle size on the system. The desired reaction temperatures studied were 120, 140, 160 and 180 °C. The total time per experiment was chosen as 4 h based on the synthetic system results. The system was loaded according to the same procedure and conditions above at the varying particle size and temperatures. The UV-Vis results for the 106 – 150 µm particle size range is given below and the results for the 45 -75 µm particle size range are given in Appendix F.

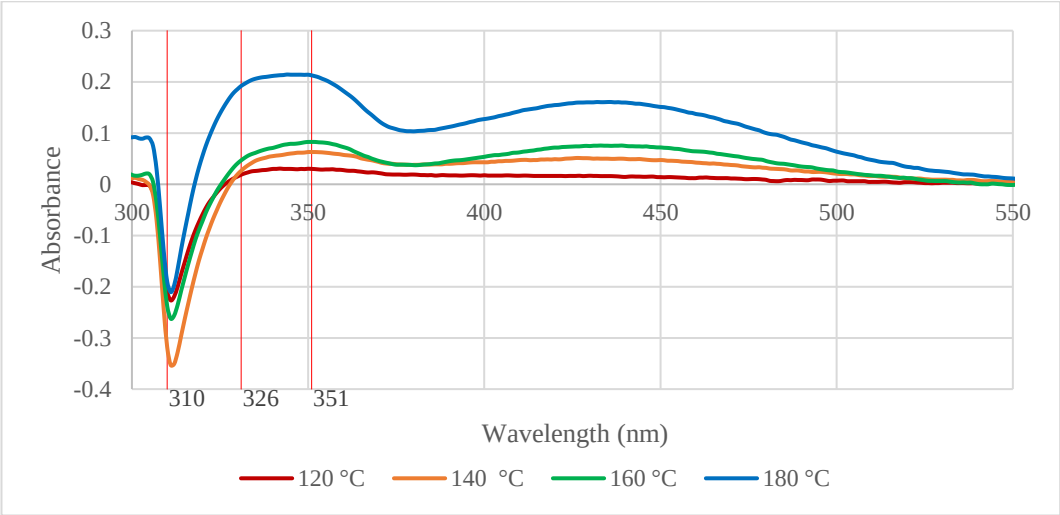


Figure 4.21: UV-Vis results for iron ore fines at 4 h, 5 g, 1000 kPa N_2 initial pressure, 106 -150 µm and 0.025 g:1 mL solid to liquid ratio at varying temperature

It can be seen from the UV-Vis results above that the curves (as well as the 45-75 µm curves) exhibit a similar relationship to those of the synthetic sample at the different temperatures but with broader peaks. The 120, 140 and 160 °C curves have their peaks at 351 and 438 nm in signifying iron(III) acetylacetonate. The 180 °C curve has a max peak spread between 326 and 351 nm. This suggests that the iron(III) acetylacetonate is beginning to convert but hasn't converted completely unlike that of the synthetic sample at the same conditions. This likely means that due to there being less iron(III) acetylacetonate present the side reaction is slowed down. The conversion results for the temperature and particle size range study are shown below.

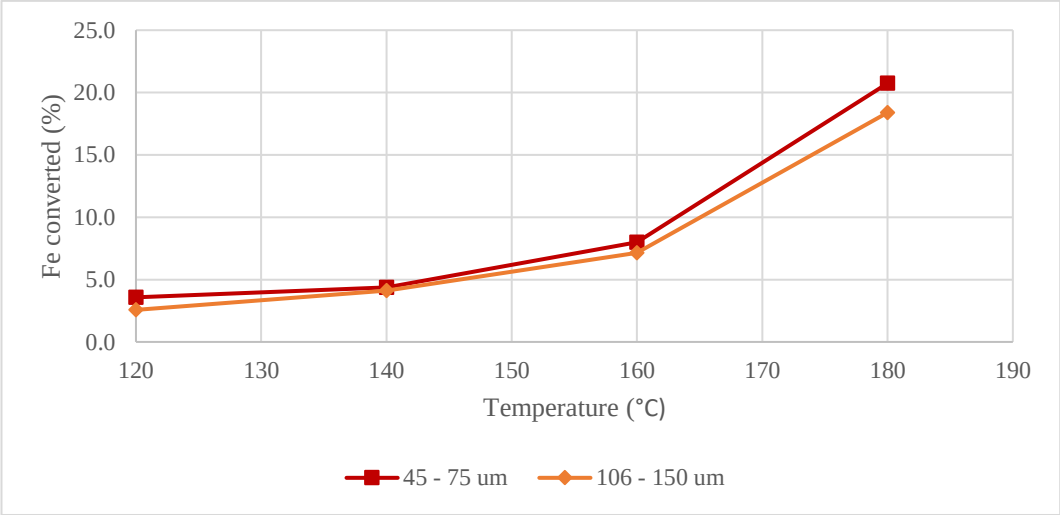


Figure 4.22: Results for the particle size and temperature study of 5 g of iron ore fines (>93 %) with 200 mL solution (180 mL acetylacetone and 20 mL water), 1010 kPa N_2 loaded, solid to liquid ratio of 0.025 g:1 mL, total time 4 h and stirrer speed of 375 rpm.

It can be seen that as temperature increases so does the conversion. This is due to an increase in system energy which means more reaction potential. This is in support of the results seen with the synthetic iron(III) oxide. The maximum conversion was achieved at 180 °C giving 20.7 and 18.4 % at particle sizes of 45 – 75 and 106 – 150 µm respectively. There is a significant increase in conversion from 160 to 180 °C by about 2.5 times. This means that a likely energy barrier has been overcome similarly to the discoveries made by Mariba (2010) in the gas phase system.

It can also be seen that the smaller the particle the higher the reaction conversion. This result was confirmed by performing a third experiment under the same conditions at 180 °C with particle size range of 212 – 300 µm which gave 17.2 % conversion. However, there was not a very prominent change. The increased conversion with smaller particle size is due to an increased surface area which means more contact between the acetylacetone and the surface of the iron ore fines. Hence, particle size is probably an influencing factor on the difference between the fines and the synthetic as the synthetic particles were significantly smaller than

those of the fines (i.e. < 1 µm). The effect of temperature and particle size are in support of those found by Mariba (2010) and Tshofu (2014).

Maximum conversion of 20.7 % was achieved at 180 °C, total time of 4 h, and particle size range of 45 – 75 µm. Hence these conditions were carried through to the next evaluation stage and the effect of pressure on the system was assessed. The effect of pressure on the system was evaluated at varying N_2 initial loading pressures of 0, 1010, 2010 and 3010 kPa. This resulted in final operating pressure of 750, 1900, 3350 and 4600 kPa respectively. The UV-Vis results are shown below.

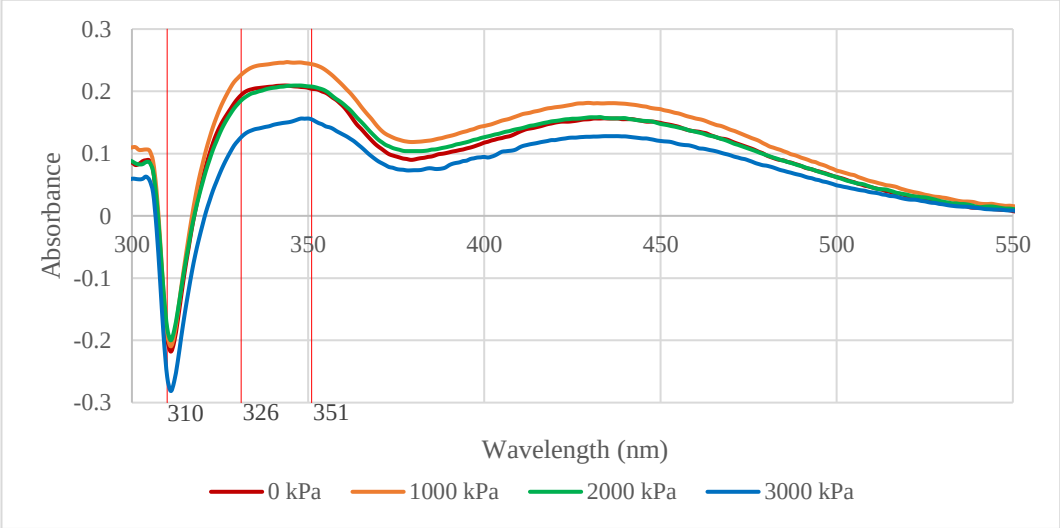


Figure 4.23: UV-Vis analysis results for the pressure study of 5 g of iron ore fines (>93 %) at 180 °C with 200 mL solution (180 mL acetylacetone and 20 mL water), solid to liquid ratio of 0.025 g:1 mL, particle size of +45-75 µm, total time 4 h and stirrer speed of 375 rpm.

All the curves exhibit a similar shape and trend to those of the previous studies with peaks at 351 and 438 nm. The peaks are broader but unlike the synthetic the unknown side reaction hasn't taken preference and made the determination of iron(III) acetylacetonate formed unquantifiable. The trend of the peaks is similar which suggests the additional pressure has limited effect on the side reaction compared to the pressure effects experienced where no additional nitrogen was used. This could mean that these conditions could form part of a viable process.

Intriguingly the 1000 kPa sample has the highest peak and hence conversion. This is shown in the results below.

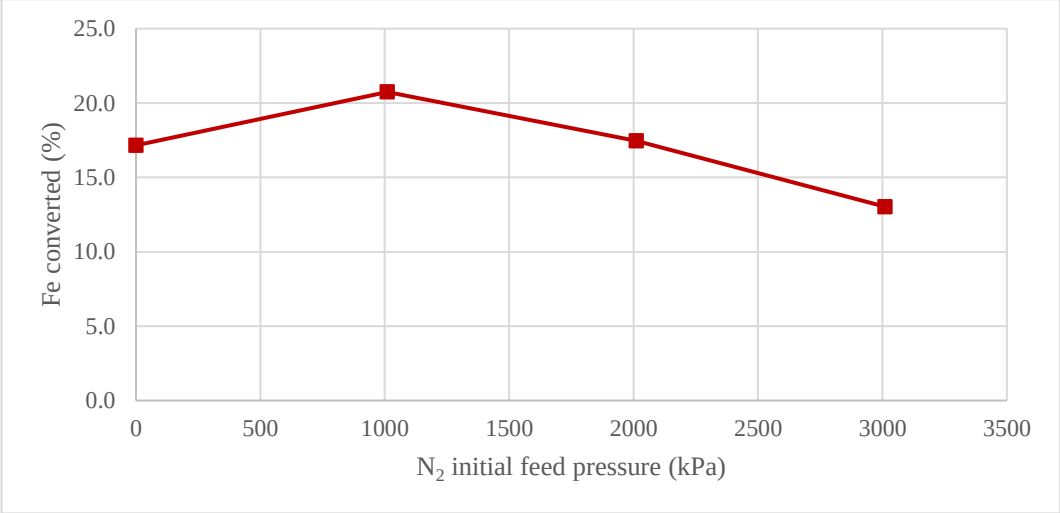


Figure 4.24: Results for the pressure study of 5 g of iron ore fines (>93 %) at 180 °C with 200 mL solution (180 mL acetylacetone and 20 mL water), solid to liquid ratio of 0.025 g:1 mL, particle size of +45-75 µm, total time 4 h and stirrer speed of 375 rpm.

It can be seen that the conversion increases from 17.1 to 20.7 % from 0 to 1000 kPa, while the conversion decreases after 1000 kPa to 17.5 to 13.0 % at 2000 and 3000 kPa respectively. This shows that the conversion peaks at 1000 kPa N_2 initial loading pressure and hence it is the optimum pressure for the system. The increase in conversion between 0 and 1000 kPa could be due to the acetylacetone existing more in the liquid phase at the slightly higher pressure as the total pressure of the system is 2600 ± 200 kPa which is significantly higher than that of the vapour pressure at this temperature of 660 ± 60 kPa. The decrease in conversion as the pressure is increased further could be attributed to the reaction forming water. The higher the water content the higher the resulting internal vapour pressure would be as water dominates the vapour pressure in comparison to acetylacetone (as shown in the vapour pressure results). Hence, at too high an initial pressure the system would favour the reaction whereby pressure is reduced (i.e. acetylacetone reacting with iron(III) oxide would be limited) based on the Le Chatelier's principle.

The optimum pressure was determined to be 1000 kPa of N_2 initially loaded (i.e. operating pressure of 1900 kPa) and other optimum values were 180 °C and particle size range of 45 – 75 µm. The final extraction stage studied was achieved by varying the solid to liquid ratio of iron ore fines loaded. This was achieved by loading the system with solid to liquid ratios of 0.025, 0.050 and 0.100 g: 1 mL accordingly (i.e. 5, 10 and 20 g of fines). The results of this study are shown below.

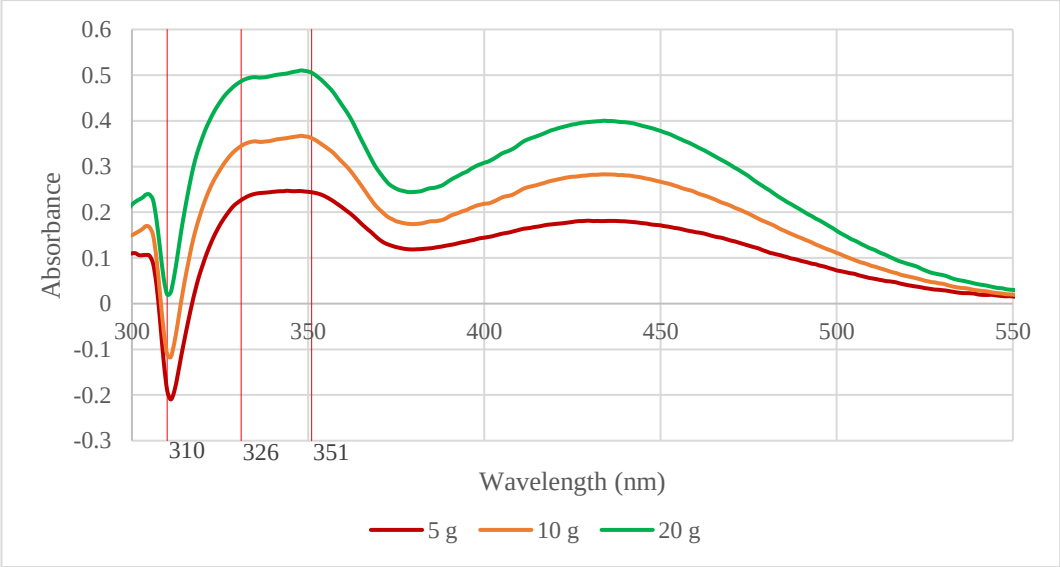


Figure 4.25: UV-Vis analysis results for the solid to liquid ratio study of iron ore fines (>93 %) at 180 °C with 200 mL solution (180 mL acetylacetone and 20 mL water), 1010 kPa N_2 loaded, particle size of +45-75 µm, total time 4 h, and stirrer speed of 375 rpm.

The UV-Vis curves above show an increase in peak magnitude as the mass of iron ore fines is increased. This means that more iron(III) acetylacetonate is formed (peaks at 351 and 438 nm present). As the iron(III) acetylacetonate increases the peak shift phenomena becomes more advanced. This suggests that there may be more polymer produced and hence a difficulty in the recovery is expected. From these results it is possible to determine the percentage conversions as presented in the figure below.

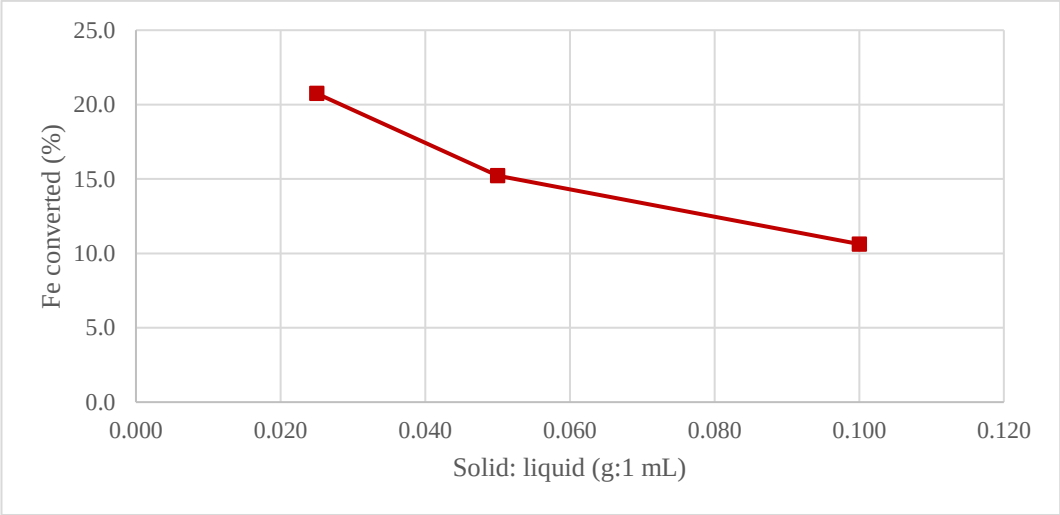


Figure 4.26: Results for the solid to liquid ratio study of iron ore fines (>93 %) at 180 °C with 200 mL solution (180 mL acetylacetone and 20 mL water), 1010 kPa N_2 loaded, particle size of +45-75 µm, total time 4 h, and stirrer speed of 375 rpm.

It can be seen from the results above that the increase in loaded fines resulted in a decrease in conversion from 20.7, 15.2 and 10.6 % for 0.025, 0.050 and 0.100 g : 1 mL systems respectively. However, the yields of the higher solid to liquid ratio are far higher due to the increase in iron ore fines available to react. This is shown by the calculated amount of iron(III) acetylacetonate that could be formed of 4.27, 6.26 and 8.74 g respectively (refer to Appendix F.4 for the calculation). This shows that although the conversion is lower, the production rate is higher for higher solid to liquid ratios which could make it a process alternative.

The presence of the unknown polymer means that the viability of the process cannot be solely based on the UV-Vis results. Hence the recovery of iron(III) acetylacetonate from some of the solutions was necessary. Recovery was performed on the two most likely viable process operating condition samples, namely the 5 g samples operated at 180 °C, 0.025 g:1 mL solid to liquid ratio, 1010kPa N_2 initial pressure and stirrer speed of 375 rpm at the different particle sizes of 45-75 and 106-150 µm. The results are given below

Table 4.3: Crystal recovery results for 5 g of iron ore fines at 1010 kPa N_2, solid to liquid ratio of 0.025 g:1 mL, and stirrer speed of 375 rpm.

Temperature (°C)	Total time (h)	Particle size (µm)	Mass of Fe extracted (g) as iron(III) acetylacetonate	Mass of $Fe(acac)_3$ in solution (g)	$Fe(acac)_3$ Crystals recovered (g)	Crystals recovered (%)	Uncrystallised liquid mass (g)
180	4	+45-75	0.675	4.267	2.630	61.6	4.00
180	4	+106-150	0.599	3.785	2.446	64.6	4.41

The fines experiments were performed at 180 °C. The synthetic samples did not yield any crystals but crystals could be recovered from the fines. This could be attributed to the lower concentration of polymer present (as can be seen by the uncrystallised liquid mass of roughly 4.4 g in comparison to roughly 8.6 g). The lower conversion of the fines meant that less iron(III) acetylacetonate was formed which meant that there was less available to be converted in the side reaction. The yields increased with the smaller particle size which also supports the findings made earlier that smaller particles increase conversion. The recovery percentage is significantly lower than that of the synthetic sample. This could be attributed to there being a lot less crystals that could form so some could have been trapped in the polymer. Alternately, during transfer from the bottoms flask to the weighing boat losses could have occurred. These factors are the likely contributor to the lower crystal recovery with the smaller particle size given above. The key feature being that crystals were able to be recovered which means that these conditions were viable for operation but not viable with the synthetic samples.

5 CONCLUSIONS

The principle objective of this study was to determine the feasibility of a high pressure hydrometallurgical process being used to convert iron in iron oxide bearing materials to iron(III) acetylacetonate using acetylacetone (2,4-pentanedione). The conclusions of this study are presented below.

The solubility of iron(III) acetylacetonate in acetylacetone was investigated utilising a visual method based on shining light through the solution and seeing the crystals dissolving or reforming. It was found that the method had limitations that prevented it from being used to accurately predict the solubility. The method was entirely subjective and depended greatly on the amount of light.

The vapour pressure of the proposed system (acetylacetone, water and nitrogen) was investigated. It was found that the experimental vapour pressures of the pure systems (i.e. acetylacetone and water all in the presence of nitrogen) could be modelled based on the Antoine equation to give the following equations:

Acetylacetone (in the presence of nitrogen):

$$\log_{10} p^* = 5.87654 - \frac{833.051}{T + 131.055} \; for \; 110 \leq T \leq 236 \qquad (5.1)$$

Water (in the presence of nitrogen):

$$\log_{10} p^* = 8.11796 - \frac{1753.56}{T + 226.155} \; for \; 84 \leq T \leq 236 \qquad (5.2)$$

where p^* is the partial pressure (mmHg), T is temperature (°C).

It was found that the vapour pressure of the mixture of acetylacetone and water (9:1 acetylacetone:water) was largely influenced by the water below the boiling point of acetylacetone and above this acetylacetone contributed more towards the total vapour pressure.

Synthetic iron(III) oxide (95 % Fe_2O_3), and an industrial sample of iron ore fines (93 % Fe_2O_3) were utilised in the study. The reaction of each of these materials

with acetylacetone in the presence of excess N_2 were investigated. It was found that inside the high pressure autoclave there were two reactions that occurred. The desired reaction forming iron(III) acetylacetonate and an unknown side reaction that consumed the iron(III) acetylacetonate. This unknown reaction and its products would need to be investigated further. The side reaction produced a waste product which would need to be properly dealt with. Hence it was necessary to determine conditions where the side reaction was limited.

A temperature study was performed on the synthetic material and found that the highest conversion of iron(III) oxide to iron (III) acetylacetonate of 62.1 % was achieved at total reaction time of 18 h, 120 °C, 1010 kPa N_2 initial loading pressure, resulting operating pressure of 1380 kPa, 0.025 g:1 mL solid to liquid ratio and 375 rpm stirrer speed. It was found that at higher temperatures and extended times that the side reaction took preference. This occurred at temperatures of 140, 150, 160, 180 and 220 °C and total reaction times of 18, 10, 4, 3 and 3 h respectively. The side reaction could be limited at lower temperatures and shorter reaction times.

A step-wise evaluation was performed to study the effects of temperature, particle size, loaded nitrogen (i.e. pressure), and solid to liquid ratio on the iron ore fines. It was determined that increasing temperature, reducing particle size and solid to liquid ratio increased the conversion of iron(III) oxide to iron (III) acetylacetonate. The amount of nitrogen initially loaded resulted in a peak (i.e. conversion increased up until a point – 1000 kPa – and then decreased). The highest conversion to iron(III) acetylacetonate of 20.7 % was achieved at total reaction time of 4 h, temperature of 180 °C, +45 – 75 µm particle size, 0.025 g: 1 mL solid to liquid ratio and 375 rpm stirrer speed. It was found that the synthetic sample had far higher conversions than that of the fines. This could be attributed to purity as well as particle size (resulting surface area being larger therefore higher reaction potential).

The side reaction rate and formation of the unknown product was found to increase with an increase in temperature and amount of iron(III) acetylacetonate present. The additional loaded nitrogen and hence pressure had a limited effect in comparison to the pressure resulting from the solution in the sealed vessel.

The feasibility of the process was also determined by the ability to recover the acetylacetone and crystals from the reaction solutions. It was found that the presence of the side reaction created a product that limited the recovery of the iron(III) acetylacetonate crystals and in some cases prevented it entirely. At temperatures higher than 180 °C with the synthetic sample it was found that crystals could not be recovered while it was still possible with the fines. This could be attributed to the reduced conversion and iron(III) acetylacetonate to react in the side reaction. Crystals were recovered from all the 4 h synthetic solutions at 120, 140, 150 and 160 °C with yields between 86-100 %. The fines solutions had yields of about 60% for the two experiments performed with particle sizes of +45 – 75 and 106 – 150 µm at 4 h, 180 °C, 0.025 g: 1 mL solid to liquid ratio and 375 rpm.

The hypothesis that the higher conversions of iron(III) oxide to iron(III) acetylacetonate could be achieved at shorter reaction times was disproved. The iron ore fines conversions achieved in the pressure vessel were lower than those achieved in previous work by Tshofu (2014). Higher conversions were achieved at atmospheric conditions and since pressure leaching operations are considered more costly it is not viable to operate under pressure. Furthermore, the atmospheric system had no evidence of the side reaction occurring hence no additional waste produced.

6 RECOMMENDATIONS

Based on the discoveries made through the course of this project the following recommendations can be made for future research:

- Investigate a more accurate method to determine solubility of iron(III) acetylacetonate in acetylacetone.
- A kinetic model developed for the aforementioned system taking into account the side reaction.
- Investigations into the side reaction, what the product is and ways to limit it/ prevent it from occurring.
- Investigations into other gases being used to pressurise the system rather than nitrogen to determine if nitrogen has an effect on system.
- Investigations into how multiple pressure leaching stages behave with the aforementioned systems.
- Optimisation of the original liquid phase extraction system used by Tshofu (2014).
- An economic comparison between this work, and that of Tshofu (2014) is recommended in order to decide upon the best possible system and results that can be achieved with industrial iron ore fines. However, some additional work in term of the optimization of crystal recovery will be required.

7 REFERENCES

Abood NA, Aiube ZH and Saeed BA (1992) Spectroscopic Study of the New SchiffBases Derived from Dibenzoylmethane and Benzolyacetone. *Journal of the Chemical Society of Pakistan* 14(2). Available from: http://jcsp.org.pk/ArticleUpload/2026-9064-1-RV.pdf (accessed 27 March 2016).

Afrox (2015) Product Data Sheet: Nitrogen. Afrox. Available from: http://www.afrox-gas.co.za/internet.lg.lg.zaf/en/images/Nitrogen269_29641.pdf (accessed 28 March 2016).

Allimann-Lecourt C (2004) Extraction of metals from contaminated land and industrial solid waste using a novel technology (servo process). Hertfordshire: University of Hertfordshire. Available from: http://uhra.herts.ac.uk/handle/2299/14249 (accessed 29 May 2016).

AmAr Equipments PVT. LTD. (n.d.) Instruction manual for high pressure lab. autoclave: non-stirrer. Available from: www.amarequip.com.

Apblett AW and Barber K (2010) Green Technology for Extraction of Iron from Ores and Other Materials. *Advances in Materials Science for Environmental and Nuclear Technology: Ceramic Transactions* 107: 169.

Berg EW and Truemper JT (1960) A study of the volatile characteristics of various metal β-diketone chelates. *The Journal of Physical Chemistry* 64(4): 487–490.

Berg EW and Truemper JT (1965) Vapor pressure-temperature data for various metal β-diketone chelates. *Analytica Chimica Acta* 32: 245–252.

Beyeme Zogo J-C (2010) Beneficiation potential of low-grade iron ore from a discard lumpy stockpile and fines tailings dam at Beeshoek mine, Northern Cape Province, South Africa. Thesis. Available from: http://ujdigispace.uj.ac.za/handle/10210/3415 (accessed 23 June 2014).

Binnemans K (2005) Rare-earth beta-diketonates. In: *Handbook on the Physics and Chemistry of Rare Earths*, Elsevier, pp. 107–272. Available from: http://linkinghub.elsevier.com/retrieve/pii/S0168127305350033 (accessed 13 February 2014).

Biswas AK (1981) *Principles of blast furnace processing: theory and practice*. Brisbane, Australia: Cootha Publishing House.

BlueScope Steel (n.d.) Reusing the By-Products of the Steel Industry. Available from: http://www.bluescopesteel.com/media/10538/Reusing%20the%20By-Products1.pdf (accessed 17 April 2014).

Brown TL, LeMay HE, Bursten BE, Murphy CJ (2009) *Chemistry: The Central Science*. 11th ed. Pearson Prentice Hall.

Coates J (2000) Interpretation of infrared spectra, a practical approach. *Encyclopedia of analytical chemistry*. Available from: http://onlinelibrary.wiley.com/doi/10.1002/9780470027318.a5606/full (accessed 20 May 2016).

Downstream Consulting Pty Ltd (2013) Midrex Process. *Downstream Consulting*. Available from: http://downstreamconsulting.com.au/node/17 (accessed 24 March 2016).

Feinman J (1999) Direct Reduction and Smelting Processes. In: *The Making, Shaping and Treating of Steel*, Pittsburgh, PA: The AISE Steel Foundation, pp. 741 – 780. Available from: http://jpkc.lut.cn/upload/20120523/20120523181034985.pdf (accessed 24 March 2016).

Felder RM and Rousseau RW (2005) *Elementary Principles of Chemical Processes*. 3rd ed. USA: John Wiley & Sons.

Ferron CJ (2006) Iron Control in Hydrometallurgy: The Positive Side of the Coin. SGS Mineral Services.

Gojić M and Kožuh S (2006) Development of direct reduction processes and smelting reduction processes for the steel production. *Kem. Ind.* 55(1): 1 – 10.

Gupta CK (2003) *Chemical Metallurgy: Principles and Practice*. Weinheim, Germany: Wiley VCH. Available from: http://web.vscht.cz/~vun/Metallurgy.pdf (accessed 28 March 2016).

Gupta CK and Mukherjee TK (1990) *Hydrometallurgy in Extraction Processes*. CRC Press.

Hoene JV, Charles RG and Hickam WM (1958) Thermal decomposition of metal acetylacetonates: mass spectrometer studies. *The Journal of Physical Chemistry* 62(9): 1098–1101.

IEA ETSAP (2010) Iron and Steel. Available from: http://www.iea-etsap.org/web/e-techds/pdf/i02-iron&steel-gs-ad-gct.pdf (accessed 14 April 2014).

International Zinc Association (2011) Zinc Production - From Ore to Metal. Available from: http://www.zinc.org/basics/zinc_production (accessed 23 June 2014).

Kabemba MA (2005) Recovery of valuable metals from solid compounds by gas phase extraction. MSc, South Africa: Tshwane University of Technology.

Lakshmanan VI, Roy R and Ramachandran V (eds) (2015) *Innovative Process Development in Metallurgical Industry: Concept to Commission*. New York, USA: Springer International Publishing.

Lazić Z (2004) *Design of Experiments in Chemical Engineering: A Practical Guide*. Weinheim: Wiley-VCH.

Ma B, Yang W, Yang B, Wang C, Chen Y, Zhang Y (2015) Pilot-scale plant study on the innovative nitric acid pressure leaching technology for laterite ores. *Hydrometallurgy* (155): 88 – 94.

Mariba ERM (2010) Gas phase extraction of metals from oxides using the ligand acetylacetone. Faculty of Engineering and the Built Environment, University of the Witwatersrand, Johannesburg. Available from: http://146.141.12.21/handle/10539/8748 (accessed 20 March 2016).

Melia TP and Merrifield R (1969) Thermal properties of acetylacetone. *Journal of Applied Chemistry* 19(3): 79–82.

Meneses CAB, Caetano EP, Torres CER, Pizarro C, Alfonso LEZ (2014) *LACAME 2012: Proceedings of the 13th Latin American Conference on the Applications of the Mössbauer Effect, (LACAME 2012) held in Medellin, Colombia, November 11 - 16, 2012*. Medellin, Colombia: Springer Science & Business Media.

Milbourne J, Tomlinson M and Gormely L (2003) Use of hydrometallurgy in direct processing of base metal/PGM concentrates. In: *Fifth International Conference in Honor of Professor Ian Ritchie – Volume 1: Leaching and Solution Purification*, The Minerals, Metals & Materials Society, pp. 617 – 630. Available from: http://technology.infomine.com/hydrometmine/papers/j.milbourne-pgm.pdf (accessed 23 June 2014).

Minerals Council of Australia (2012) Iron Fact Sheet. *Australian atlas of minerals resources, mines and processing centres*. Available from: http://www.australianminesatlas.gov.au/education/fact_sheets/iron.html (accessed 20 April 2014).

National Institute of Standards and Technology (2016a) Acetone. *Material Measurement Laboratory*. Available from: http://webbook.nist.gov/cgi/cbook.cgi?ID=C67641&Mask=400#UV-Vis-Spec (accessed 24 October 2016).

National Institute of Standards and Technology (2016b) Acetylacetone. *Material Measurement Laboratory*. Available from: http://webbook.nist.gov/cgi/cbook.cgi?ID=C123546&Type=IR-SPEC&Index=1 (accessed 20 May 2016).

National Institute of Standards and Technology (2016c) Ferric tris(acetylacetonate). *Material Measurement Laboratory*. Available from: http://webbook.nist.gov/cgi/cbook.cgi?ID=C14024181&Mask=80 (accessed 20 May 2016).

National Metallurgical Laboratory (2010) Iron oxide from waste iron rich sources. Available from: http://www.nmlindia.org/MEF005.html (accessed 22 April 2014).

Peacey JG and Davenport WG (2013) *The Iron Blast Furnace: Theory and Practice*. Elsevier.

Potgieter JH, Kabemba MA, Teodorovic A, Potgieter-Vermaak SS, Augustyn WG (2006) An investigation into the feasibility of recovering valuable metals from solid oxide compounds by gas phase extraction in a fluidised bed. *Minerals Engineering* 19(2): 140–146.

Robinson JW, Skelly Frame EM and Frame II GM (2004) Chapter 5: Visible and Ultraviolet Molecular Spectroscopy. 6th ed. In: *Undergraduate Instrumental Analysis*, New York, USA: Marcel Dekker, pp. 317 – 384. Available from: http://www.monzir-pal.net/Poisons%20and%20Drugs/Lecture%20material/UV%20vis%20and%20Fluorescence.pdf (accessed 27 March 2016).

SGS SA (2014) Pressure and Ambient Leaching. Available from: http://www.sgs.co.za/en/Mining/Metallurgy-and-Process-Design/Unit-Operations-and-Metallurgical-Services/Pressure-and-Ambient-Leaching.aspx (accessed 24 June 2014).

Shah KP (n.d.) Iron and Steel. *Practical Maintenance*. Available from: http://practicalmaintenance.net/?p=1279 (accessed 24 March 2016).

Shemi A, Mpana RN, Ndlovu S, van Dyk LD, Sibanda V, Seepe L (2012) Alternative techniques for extracting alumina from coal fly ash. *Minerals Engineering* 34: 30–37.

Sigma-Aldrich (2012) Safety Data Sheet: Iron (III) Acetylacetonate. Available from: http://www.sigmaaldrich.com/MSDS/MSDS/DisplayMSDSPage.do?country=ZA&language=en&productNumber=517003&brand=ALDRICH&PageToGoToURL=http%3A%2F%2Fwww.sigmaaldrich.com%2Fcatalog%2Fproduct%2Faldrich%2F517003%3Flang%3Den (accessed 24 March 2016).

Sigma-Aldrich (2015a) Safety Data Sheet: Acetylacetone. Available from: http://www.sigmaaldrich.com/MSDS/MSDS/DisplayMSDSPage.do?country=ZA&language=en&productNumber=P7754&brand=SIAL&PageToGoToURL=http%3A%2F%2Fwww.sigmaaldrich.com%2Fcatalog%2Fproduct%2Fsial%2Fp7754%3Flang%3Den (accessed 21 March 2016).

Sigma-Aldrich (2015b) Safety Data Sheet: Ethanol. Available from: http://www.sigmaaldrich.com/MSDS/MSDS/DisplayMSDSPage.do?country=ZA&language=en&productNumber=32221&brand=SIAL&PageToGoToURL=http%3A%2F%2Fwww.sigmaaldrich.com%2Fcatalog%2Fproduct%2Fsial%2F32221%3Flang%3Den (accessed 26 March 2016).

Sigma-Aldrich (2016) Safety Data Sheet: Iron (III) Oxide. Available from: http://www.sigmaaldrich.com/MSDS/MSDS/PleaseWaitMSDSPage.do?language=&country=ZA&brand=SIAL&productNumber=12342&PageToGoToURL=http://www.sigmaaldrich.com/catalog/product/sial/12342?lang=en&region=ZA (accessed 24 March 2016).

Smith A and Menzies AWC (1910) Studies in vapor pressure: III. A static method for determining the vapor pressures of solids and liquids. *Journal of the American Chemical Society* 32(11): 1412–1434.

Stahl (2013) Hot Metal And Crude Steel Production. Available from: http://en.stahl-online.de/index.php/topics/technology/steelmaking/ (accessed 24 March 2016).

Starý J and Hladký E (1963) Systematic study of the solvent extraction of metal β-diketonates. *Analytica Chimica Acta* 28: 227–235.

Tata Steel Europe Limited (n.d.) The properties of cast iron, wrought iron and steel. Available from: http://www.tatasteelconstruction.com/en/reference/teaching_resources/architectural_studio_reference/history/the_technology_of_iron_and_steel/the_properties_of_cast_iron,_wrought_iron_and_steel/ (accessed 23 June 2014).

Tshofu GS (2014) Green extraction of iron from iron ore. MSc, South Africa: University of the Witwatersrand.

Uhrie JL (2015) Pressure leaching: Coming of age or has it been here a long time? *Runge Pincock Minarco Perspectives* (130): 1 – 3.

United States Environmental Protection Agency (1994) Technical Resource Document: Iron. Available from: http://www.epa.gov/osw/nonhaz/industrial/special/mining/techdocs/iron.pdf (accessed 20 April 2014).

Van Dyk LD, Mariba ERM, Chen Y, Potgieter JH (2010) Gas phase extraction of iron from its oxide in a fluidized bed reactor. *Minerals Engineering* 23(1): 58–60.

Van Dyk LD, Mariba EMR, Chen Y, Johnson A, Potgieter JH (2012) Gas-phase extraction of lead and iron from their oxides in a fluidized-bed reactor. *Journal of the Southern African Institute of Mining and Metallurgy* 112(6): 461–465.

Vignes A (2011) *Extractive Metallurgy 3: Processing Operations and Routes*. Great Britain: John Wiley & Sons. Available from: http://download.e-bookshelf.de/download/0000/8127/95/L-X-0000812795-0002038125.XHTML/index.xhtml (accessed 28 March 2016).

Wolthuis E, Pruiksma AB and Heerema RP (1960) Determination of Solubility: A laboratory experiment. *Journal of Chemical Education* 37(3): 137–138.

World Steel Association (2010) Fact Sheet: Steel industry by-products. Available from: http://www.worldsteel.org/dms/internetDocumentList/fact-sheets/Fact-sheet_By-products/document/Fact%20sheet_By-products.pdf (accessed 18 April 2014).

World Steel Association (2015) Annual iron production archive. *World Steel Association*. Available from: https://www.worldsteel.org/statistics/statistics-archive/iron-archive.html (accessed 23 March 2016).

Yaws Y (2015) *The Yaws Handbook of Vapor Pressure: Antoine Coefficients*. 2nd ed. UK: Elsevier.

Yu Z, Xie K, Ma W, Zhou Y, Xie G, Dai Y (2011) Kinetics of iron removal from metallurgical grade silicon with pressure leaching. *Rare Metals* 30(6): 688–694.

Zhang H, Wang Y, Tao G, Chai Y, Que G (2011) Chemical synthesis of Fe nanocrystals via hydrogenation of ferric acetylacetonate. In: *Materials for Renewable Energy & Environment (ICMREE), 2011 International Conference on*, IEEE, pp. 2066–2070. Available from: http://ieeexplore.ieee.org/xpls/abs_all.jsp?arnumber=5930744 (accessed 10 April 2014).

APPENDIX A: MATERIALS

A.1 Chemical and physical properties and details

The chemical properties and details for acetylacetone, ethanol, iron(III) acetylacetonate, iron ore fines, iron(III) oxide, nitrogen and water are given below. The acetylacetone, ethanol, iron(III) acetylacetonate, and iron(III) oxide were purchased from Sigma Aldrich. The iron ore fines were from the Sishen operations in South Africa (part of Kumba Iron Ore, Anglo America). Nitrogen was purchased from Afrox. Water was purified in-house using a Direct-Q 5 UV System.

A.1.1 Acetylacetone

Table A.1: Acetylacetone chemical and physical properties (Sigma-Aldrich, 2015a).

Alternate names	2,4-Pentanedione, hacac	Boiling point (°C)	140.4
Chemical formula	$C_5H_8O_2$	Melting point (°C)	-23
CAS-No.	123-54-6	Density at 25 °C (g/ml)	0.975
Molecular weight (g/mol)	100.12	pH (at 200 g/L at 20°C)	6
Purity (%)	> 99	Ignition point (°C)	350
Appearance - form (colour)	Liquid (clear/ faint yellow)	Explosive limits (vol %)	1.7 - 11.4

A.1.2 Ethanol

Table A.2: Ethanol chemical and physical properties (Sigma-Aldrich, 2015b).

Alternate names	Ethyl alcohol	Boiling point (°C)	78
Chemical formula	C_2H_5OH	Melting point (°C)	-114
CAS-No.	64-17-5	Density at 25 °C (g/ml)	0.789
Molecular weight (g/mol)	46.07	pH (at 200 g/L at 20°C)	-
Purity (%)	> 99.8	Ignition point (°C)	363
Appearance - form (colour)	Liquid (clear)	Explosive limits (vol %)	3.3 - 19

A.1.3 Iron acetylacetonate

Table A.3: Iron(III) acetylacetonate chemical and physical properties (Kabemba, 2005; Sigma-Aldrich, 2012).

Alternate names	Iron(III) 2,4-pentanedionate, ferric acetylacetonate, $Fe(acac)_3$	Thermal decomposition (°C)	182
Chemical formula	$Fe(C_5H_7O_2)_3$	Melting point (°C)	180 -182
CAS-No.	14024-18-1	Density at 25 °C (g/ml)	5.24
Molecular weight (g/mol)	353.17	Solubility in water at 20 °C	Slightly soluble
Purity (%)	> 99.9	Solubility in ethanol at 20 °C	Freely soluble
Appearance - form (colour)	Powder (dark red)		

A.1.4 Iron ore fines

The iron ore fines that were used in this study were the same as those studied by Tshofu (2014) from the Sishen operations in South Africa (part of Kumba Iron Ore, Anglo America). The iron ore fines were characterised by their particle size distribution (PSD), surface area, surface morphology (SEM) and chemical analysis. A summary of these results is shown below (note: all results shown are taken from the analysis results given by Tshofu (2014)).

PARTICLE SIZE DISTRIBUTION

The PSD was determined by sieve analysis and the results are shown in the figure below with the smallest sieve size being 45 µm and the largest 5 600 µm. The 50 % cumulative passing (d_{50}) was at 2512 µm.

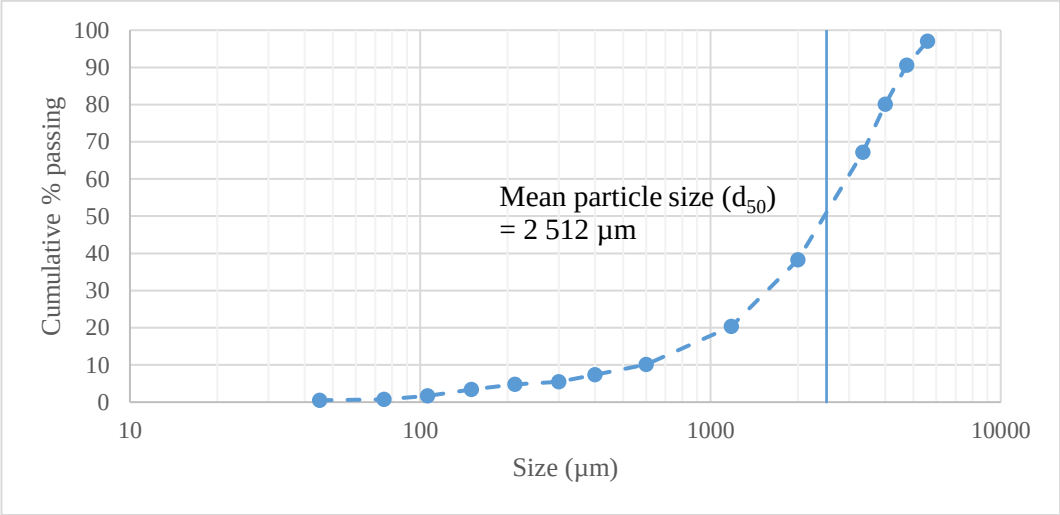


Figure A.1: Particle size distribution of iron ore fines (Tshofu, 2014).

SURFACE AREA CHARACTERISTICS

Brunauer-Emmett-Teller (BET) analysis was performed on the iron ore fies in the particle size range of 106-150, 300-400 and 1180-2000 µm. Their respective surface areas were determined to be 3.1724, 2.6450 and 1.2029 m^2/g. Hence, as particle size decreases there is an increase in available surface area (Tshofu, 2014).

CHEMICAL AND CRYSTALLINE COMPOSITION

X-ray fluorescence (XRF) and X-ray diffraction (XRD) were performed on the iron ore fines samples to determine the chemical composition and crystalline structure respectively. These results are shown in Table A.4 and Table A.5.

Table A.4: Chemical composition of iron ore fines (weight %) (Tshofu, 2014).

Chemical	Fe_2O_3	Al_2O_3	SiO_2	CaO	K_2O	P_2O_5	TiO_2	MnO	Cr_2O_3	NiO	Na_2O
Weight (%)	93.09	1.30	5.06	0.20	0.26	0.14	0.10	0.06	0.04	0.01	0.24

Table A.5: Crystalline composition of iron ore fines (weight %) (Tshofu, 2014).

Crystalline phases	Formula	Weight (%)
Hematite	Fe_2O_3	93.91
Muscovite	$KAl_2(Si_3Al)O_{10}(OH,F)_2$	2.17
Quartz	SiO_2	3.92

A.1.5 Iron oxide

Table A.6: Iron(III) oxide chemical and physical properties (Sigma-Aldrich, 2016).

Alternate names	Ferric oxide	Appearance - form (colour)	Powder (red)
Chemical formula	Fe_2O_3	Melting point (°C)	1565
CAS-No.	1309-37-1	Density at 25 °C (g/ml)	5.12
Molecular weight (g/mol)	159.69	Particle size (µm)	< 1
Purity (%)	> 95	Impurities (trace)	Ca, Cu, Mg, Zn

A.1.6 Nitrogen

Table A.7: Nitrogen chemical and physical properties (Afrox, 2015; Felder and Rousseau, 2005).

Chemical formula	N_2	Appearance - form (colour)	Gas (clear)
CAS-No.	7727-37-9	Boiling point (°C)	-195.8
Molecular weight (g/mol)	28.02	Melting point (°C)	-210
Purity (%)	99.5	Density at 25 °C (g/ml)	-

A.1.7 Water

Table A.8: Water chemical and physical properties (Felder and Rousseau, 2005).

Chemical formula	H_2O	Appearance - form (colour)	Liquid (clear)
CAS-No.	7732-18-5	Boiling point (°C)	95 - 100 (Johannesburg)
Molecular weight (g/mol)	18.02	Melting point (°C)	0
Type	Distilled	Density at 25 °C (g/ml)	0.997

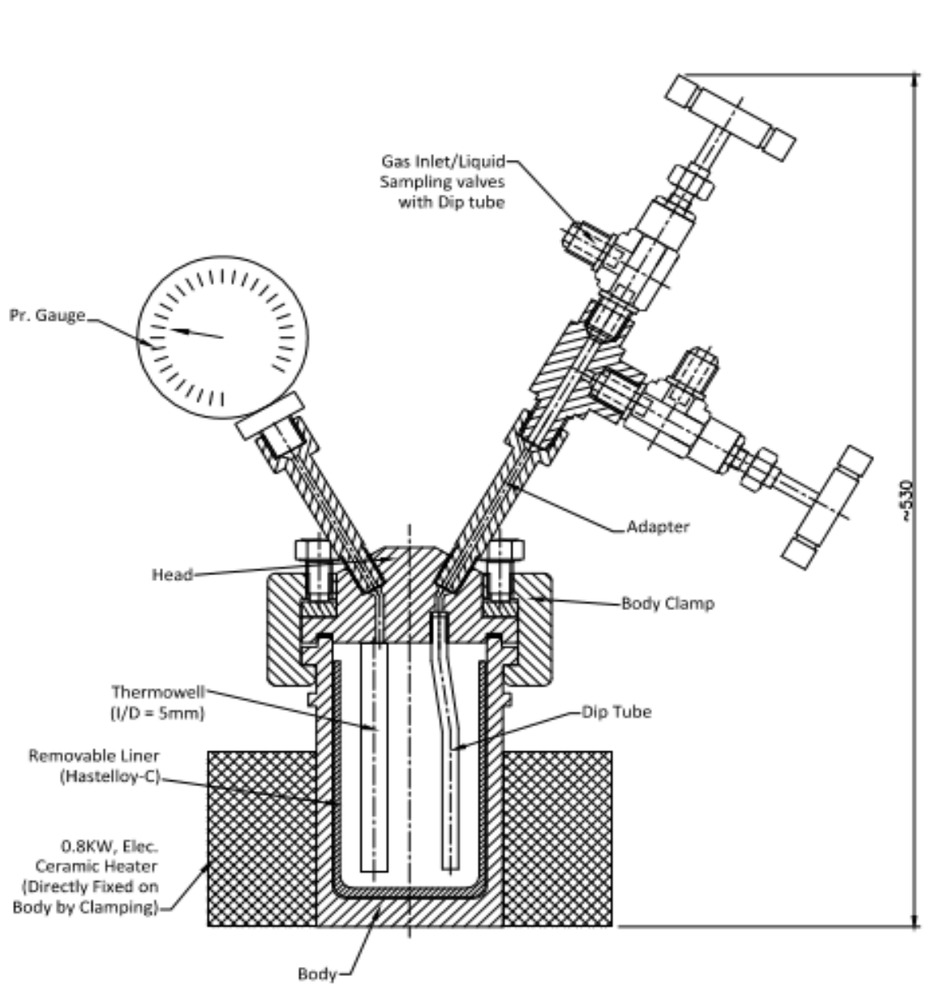
APPENDIX B: AUTOCLAVE DETAILS

B.1 Autoclave description

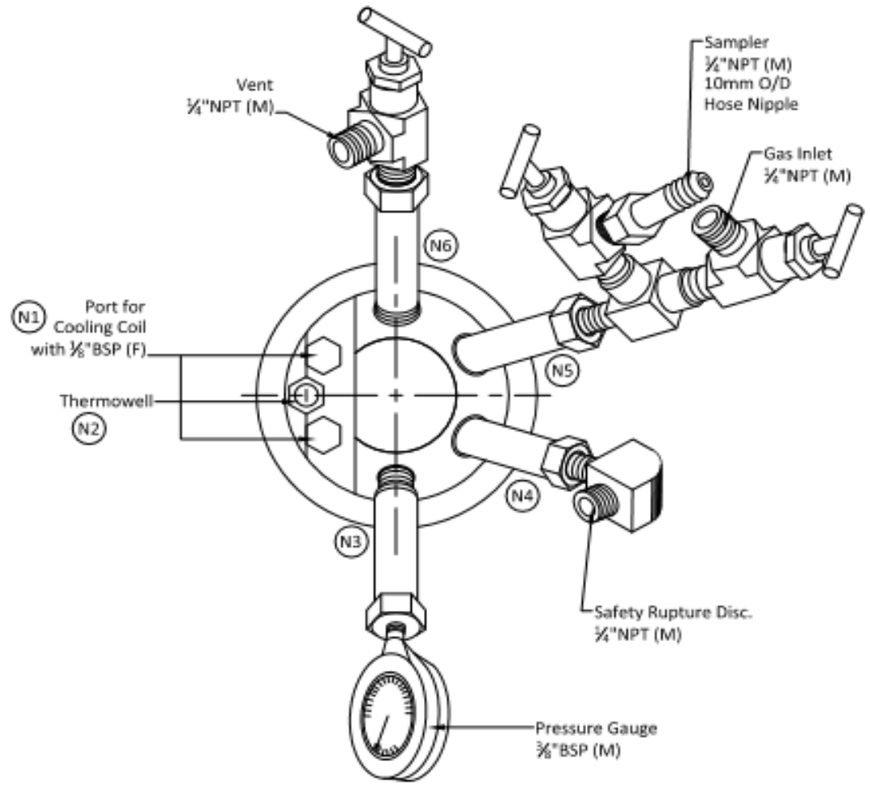
A high pressure non-stirred autoclave equipped with heating arrangement was purchased from Celsius Scientific and manufactured by AmAr Equipments PVT. LTD in India. The full engineering drawing with all specifications can be seen in Figure B.1 below

Design Data	
Design Pressure	100 barg
Design Temperature	250°C
All other Wetted Parts	S.S.316
Hydro Test Pressure	150 barg

Notes :-
1, All Valves with NPT Threaded of S.S.316.



Top view of Head assembly for Lab. Autoclave



Nozzle Plan			
Nozzle	Description	Size	Valve & Fitting
N1	Port For Cooling Coil	1/8"BSP (F)	With Dead Plug 1/8" BSP (M) - 2Nos.
N2	Thermowell	Ø10	Temp. Sensor in Client's Scope
N3	Pr. Gauge	1/4"BSP (F)	Pr. Gauge Ø4", 0 to 100Bar, 3/8"BSP (M)
N4	Safety Rupture Disc.	3/8"BSP (F)	Ø10 / Ø1/4" R.Disc. [100Bar].
N5	Sampler/Gas Inlet	1/4"BSP (F)	1/4"NPT (M) Needle Valve - 2Nos. with Dip Tube.
N6	Vent	1/4"BSP (F)	1/4"NPT (M) Needle Valve.

Rev.No.	Date	Client : CELSIUS SCIENTIFIC CC	This print is the property and copyright of AMAR EQUIPMENTS PVT. LTD. MUMBAI - 400 070.
		Equipment : 450ml Non - Stirred Autoclave	
		Title : General Arrangement Drawing	
		P. O. No. : ORDER-284/14, 18/06/2014	Drg No. : PP-400ml-3030-00 / Sheet No. :
		Note : 1, All dimension are in mm unless & otherwise specified. 2, Remove all burrs & sharp corners R-0.5 to R-1. 3, All surfaces degrease & clean.	Scale : N.T.S. / Angle / Drn. TAFAZZUL 20/06/14
			Job No. : AE-3030 / Chkd. / Appd.

Form # ISO-DSG-01 Rev.-01 10/11/2008

Figure B.1: Engineering drawing of the autoclave.

B.2 Standard operating procedure

Given below is a summary of the standard operating procedure for the autoclave as provided by the manufacturers (AmAr Equipments PVT. LTD., n.d.)

B.2.1 Charging the autoclave:

- Open vent valve to release any internal pressure.
- Using the spanner provided loosen the clamp bolts in a criss-cross manner and then unlock the latch.
- Remove the body clamp section and carefully lift out the head from the body. The head placed on the stand to prevent damage.
- Charge the autoclave with desired reactants (never exceeding ¾ of the vessel volume).

B.2.2 Closing the autoclave:

- Examine all fittings and Teflon gasket to ensure they are in the right position and without wear and tear. If necessary replace Teflon gasket.
- Carefully replace the head on the vessel, ensuring that it is properly in position.
- Slide on clamps and latch the two together.
- Using a torque wrench and following the same criss-cross manner, tighten the clamp bolts initially to 15 N. Then starting at one bolt and working clockwise, tighten the bolts further to 18 N until all bolts have been tightened.

B.2.3 Pressurising the autoclave:

- Ensure all valves are closed properly and attach the high pressure gas carrier pipe (equipped with regulator and reverse flow seal) to the gas inlet valve.
- Gas cylinder pressure must be greater than that of the autoclave to prevent back flow.
- Gas pressure regulator handle should initially be in the totally unscrewed position.

- The gas cylinder valve should be opened and the regulator handle rotated clockwise to allow the gas to flow and pressurise the line (DO NOT open the gas inlet valve).
- Once the line pressure is greater than the autoclave pressure the gas inlet valve can be opened and the reactor charged to the desired pressure. The valve must be closed as soon as the desired pressure is achieved.
- Detach the gas carrier pipe.

B.2.4 Releasing the gas:

- Use only the gas vent valve and vent gas away from body, preferably though tubing into a fume hood.
- DO NOT use liquid sampling valve as liquid will flow out of the reactor.

B.3 Autoclave commissioning

The autoclave was commissioned as per the instructions given by the manufacturer (summarised above). All parts were checked to be in the right working order and all safety precautions followed. The reactor was originally tested using 200 mL water and nitrogen gas (never exceeding 6000 kPa to ensure maximum pressure was never exceeded). The water was heated and cooled repeatedly to ensure that the heating jacket and thermocouples were functioning properly. The nitrogen was used to test all the seals and ensure no pressure leaks were experienced.

The temperature of the internal solution was best controlled by controlling the temperature of the heating jacket rather than controlling the internal solution which heated too quickly but cooled very slowly. This change in heating and cooling rates could not be accurately counted by the temperature controllers.

B.4 Heating rates and conditions

All experiments were heated following the procedures below based on the desired reaction temperature. Each experiment was heated for an hour and the final control temperature of the heating jacket adjusted to maintain a ±2 °C variation on the desired temperature. The heating jacket temperature was set to different temperatures for time intervals of 30, 10, 10, 5 and 5 min (total 1 h) as shown in Table B.1 below. The last 10 min temperatures given are an estimate as the set

temperature was set higher or lower depending on how hot the internal solution was at the time. If the solution was heating up faster then the jacket temperature would be decreased further but if slower then it would be slightly higher.

Table B.1: Heating jacket heating conditions.

Desired reaction temperature (°C)	120	140	150	160	180	220
Heating times (min)	Heating jacket set temperature (°C)					
30	100	100	100	120	150	200
10	130	150	150	170	200	250
10	160	180	200	220	230	270
5	100	170	150	150	150	230
5	100	140	155	150	185	200

B.5 Safety precautions

The autoclave was operated under high pressures and high temperatures. Hence, all safety precautions needed to be followed during every stage, i.e. loading, while the reactor was in operation and when it was turned off and the gases vented. In addition to the information given above the following safety precautions were put in place:

- Autoclave was operated inside a fume cupboard in case there were any leaks.
- Autoclave was equipped with a safety rupture disk in case the design pressure was exceeded.
- Operating temperatures were always kept below that of the design temperature allowing a safety margin of more than 30 °C. This prevents a possibility of pressure increasing too much and exceeding the design pressure.
- The nitrogen gas feed was always turned off once the reactor was loaded and the feed lines disconnected.
- Correct PPE was worn at all times. This included safety goggles, lab gloves and lab coat, closed shoes and when dealing with the hot surfaces then heatproof safety gloves were used.

APPENDIX C: SPECTROQUANT ANALYSIS

The analysis of all samples were done using a Spectroquant Pharo 300 Spectrophotometer. The standards were made according to the following procedure.

C.1 Stock solution:

The first standard required was an 800 ppm Fe made from iron(III) acetylacetonate crystals (>99.9 %) based on the following calculations:

Using a 200 mL volumetric flask that would make the mass of iron needed:

$$m_{Fe} = C_{Fe}V = 0.800\ \frac{g}{L} \times 0.200\ L = 0.160\ g \qquad (C.1)$$

Converting the mass of iron to the mass of iron(III) acetylacetonate required:

$$m_{Fe(acac)_3} = \frac{M_{Fe(acac)_3}}{M_{Fe}} \times m_{Fe}$$

$$= \frac{353.17\ g.mol^{-1}}{55.847\ g.mol^{-1}} \times 0.1600\ g \qquad (C.2)$$

$$= 1.0118\ g$$

Thus the total mass of iron(III) acetylacetonate crystals required is 1.0118 g into the 200 mL volumetric flask and then the remaining volume would be pure ethanol.

The above stock solution was then used to create ethanol based working standards to be used in the Spectroquant.

C.2 Spectroquant (UV-Vis) working standards:

The Spectroquant requires standards and solutions that are lower in concentration to increase the accuracy of the absorbance readings thus standards lower than 16 ppm Fe were created and solutions were diluted 1000 times.

Initially, the 800 ppm solution was diluted to 100 ppm Fe, this was done using a 100 mL volumetric flask and an 8 times dilution factor into pure ethanol. The required volume of the original 800 ppm solution was calculated as follows:

$$V = \frac{C_1 V_1}{C} = \frac{(100\ ppm\ Fe)(100\ mL)}{(800\ ppm\ Fe)} = 12.5\ mL \qquad (C.3)$$

Thus 12.5 mL of the 800 ppm Fe standard was used to make the 100 ppm solution.

The 100 ppm solution was then diluted further and combined with 0.05 mL (explanation given in Sample preparation below) of acetylacetone such that the standards were similar in composition and make-up as the solutions to be analysed. The working standards were made following the following method:

$$V = \frac{C_1 V_1}{C} = \frac{(2\ ppm\ Fe)(50\ mL)}{(100\ ppm\ Fe)} = 1\ mL \qquad (C.4)$$

Standards were made with 2, 4, 6, 8, 10, 12, 14 and 16 ppm Fe concentrations as can be seen in Table C.1 below.

Table C.1: Volume of 100 ppm Fe solution required to make the desired Spectroquant standard solutions.

Iron concentration (ppm Fe)	Volume of the 100 ppm Fe solution required (mL)	Iron concentration (ppm Fe)	Volume of the 100 ppm Fe solution required (mL)
2	1.000	10	5.000
4	2.000	12	6.000
6	3.000	14	7.000
8	4.000	16	8.000

These standards were then analysed after the machine was blanked, per each new analysis set, to give the standard calibration curves. The blank was made of 0.05 mL acetylacetone and combined with pure ethanol into a 50 mL volumetric flask.

C.3 Sample preparation

All samples were prepared identically and diluted into ethanol by a dilution ratio of 1000 times where dilution ratio is given by:

$$D = \frac{Total\ volume\ of\ diluted\ solution}{volume\ of\ solute\ used} \qquad (C.5)$$

The procedure followed is given below:

Stage 1: 1.000 mL of the original sample volume is pipetted into a 50 mL volumetric flask and filled with ethanol (i.e. $D = 50\ mL/1\ mL = 50$).

Stage 2: 2.500 mL of the 50 times diluted solution (i.e. stage 1 solution) is pipetted into a 50 mL volumetric flask and filled with ethanol (i.e. $D = 50\ mL/2.500\ mL = 20$ thus giving an overall dilution of $50 \times 20 = 1\ 000$)

This means that roughly 0.05 mL of acetylacetone is present in the final diluted sample solution (assuming water content is minimal) hence the amount used in the blank and standards above. This was calculated by:

$$Amount\ of\ acetylacetone\ present = \frac{1\ mL}{50\ mL} \times 2.500\ mL = 0.05\ mL \qquad (C.6)$$

All solutions were well shaken.

APPENDIX D: SOLUBILITY RESULTS

The solubility results used to generate the curves shown in Chapter 4 are shown below.

Table D.1: Solubility of iron(III) acetylacetonate in acetylacetone performed with two different light bulbs (i.e. energy saver 9 W bulb and a 100 W bulb).

Volume Hacac (mL)	Mass $Fe(acac)_3$ (g)	Solubility (g/ 100 mL)	Temperature (°C)
Energy saver bulb (9 W)			
10	1.201	12.01	25.4
10	1.404	14.04	29.7
10	1.502	15.02	31.8
10	1.604	16.04	34.2
10	2.003	20.03	43.7
100 W bulb (first results)			
10	2.003	20.03	51.3
10	2.502	25.02	66.2
10	3.001	30.01	83.8
100 W bulb (second results)			
10	1.503	15.03	51
10	2.016	20.16	73
10	2.501	25.01	91

APPENDIX E: VAPOUR PRESSURE RESULTS AND CALCULATIONS

The experimental results for the vapour pressure experiments is given below. The standard deviation and relative deviation of the repeated experiments was calculated.

Table E.1: Vapour pressure results for acetylacetone and water mixture (9:1 acetylacetone:water) in presence on N_2.

Pressure (kPag)	Temperature (°C)			Mean ($\bar{X}$)	Std dev. (S_x)	Rel. std dev. (%)
	Exp. 1	Exp. 2	Exp. 3			
1900	234.8	233.0	238.3	235.4	2.2	0.9
1880	234.2	232.2	237.4	234.6	2.1	0.9
1860	233.7	231.4	236.7	233.9	2.2	0.9
1840	233.0	230.9	235.9	233.3	2.0	0.9
1820	232.2	230.0	235.1	232.4	2.1	0.9
1800	231.6	229.2	234.5	231.8	2.2	0.9
1780	230.8	228.6	233.8	231.1	2.1	0.9
1760	230.0	227.9	233.0	230.3	2.1	0.9
1740	229.2	227.1	232.2	229.5	2.1	0.9
1720	228.6	226.3	231.3	228.7	2.0	0.9
1700	227.8	225.3	230.6	227.9	2.2	0.9
1680	227.2	224.7	230.0	227.3	2.2	1.0
1660	226.2	223.8	229.0	226.3	2.1	0.9
1640	225.6	223.1	228.4	225.7	2.2	1.0
1620	225.0	222.2	227.7	225.0	2.2	1.0
1600	224.3	221.5	226.9	224.2	2.2	1.0
1580	223.6	220.6	226.1	223.4	2.2	1.0
1560	222.9	219.5	225.3	222.6	2.4	1.1
1540	222.1	218.9	224.5	221.8	2.3	1.0
1520	221.1	218.1	223.6	220.9	2.2	1.0
1500	220.2	217.3	222.6	220.0	2.2	1.0
1480	219.2	216.4	221.5	219.0	2.1	1.0
1460	218.4	215.8	220.8	218.3	2.0	0.9
1440	217.7	215.0	220.0	217.6	2.0	0.9
1420	217.0	214.2	219.3	216.8	2.1	1.0
1400	216.2	213.4	218.3	216.0	2.0	0.9
1380	215.3	212.6	217.4	215.1	2.0	0.9
1360	214.2	211.8	216.3	214.1	1.8	0.9

Pressure (kPag)	Temperature (°C)			Mean ($\bar{X}$)	Std dev. (S_x)	Rel. std dev. (%)
	Exp. 1	Exp. 2	Exp. 3			
1340	213.3	210.9	215.6	213.3	1.9	0.9
1320	212.4	210.1	214.8	212.4	1.9	0.9
1300	211.4	209.1	213.7	211.4	1.9	0.9
1280	210.6	208.2	212.8	210.5	1.9	0.9
1260	209.6	207.2	211.8	209.5	1.9	0.9
1240	208.7	206.3	210.7	208.6	1.8	0.9
1220	207.7	205.2	209.7	207.5	1.8	0.9
1200	206.9	204.3	208.9	206.7	1.9	0.9
1180	205.9	203.3	207.9	205.7	1.9	0.9
1160	204.9	202.3	206.9	204.7	1.9	0.9
1140	204.1	201.2	206.0	203.8	2.0	1.0
1120	203.0	200.0	204.7	202.6	1.9	1.0
1100	201.9	199.2	203.8	201.6	1.9	0.9
1080	201.0	198.2	202.8	200.7	1.9	0.9
1060	199.9	197.2	201.7	199.6	1.8	0.9
1040	198.8	196.0	200.4	198.4	1.8	0.9
1020	197.7	194.9	199.4	197.3	1.9	0.9
1000	196.7	193.9	198.2	196.3	1.8	0.9
980	195.7	192.9	197.1	195.2	1.7	0.9
960	194.5	191.8	195.7	194.0	1.6	0.8
940	193.5	190.8	194.6	193.0	1.6	0.8
920	192.4	189.7	193.4	191.8	1.6	0.8
900	191.4	188.5	192.1	190.7	1.6	0.8
880	190.5	187.2	190.9	189.5	1.7	0.9
860	188.8	185.7	189.7	188.1	1.7	0.9
840	187.7	184.7	188.3	186.9	1.6	0.8
820	186.5	183.7	187.2	185.8	1.5	0.8
800	185.2	182.5	185.7	184.5	1.4	0.8
780	183.7	180.8	184.2	182.9	1.5	0.8
760	182.8	179.2	183.2	181.7	1.8	1.0
740	181.8	177.7	181.9	180.5	2.0	1.1
720	180.7	176.4	180.6	179.2	2.0	1.1
700	179.1	175.0	179.3	177.8	2.0	1.1
680	177.8	173.7	178.1	176.5	2.0	1.1
660	176.2	172.2	176.8	175.1	2.0	1.2
640	175.0	170.3	175.4	173.6	2.3	1.3
620	173.5	168.4	174.0	172.0	2.5	1.5
600	171.3	166.2	171.9	169.8	2.6	1.5
580	169.8	164.7	170.5	168.3	2.6	1.5

Pressure (kPag)	Temperature (°C)			Mean ($\bar{X}$)	Std dev. (S_x)	Rel. std dev. (%)
	Exp. 1	Exp. 2	Exp. 3			
560	168.4	163.1	168.7	166.7	2.6	1.5
540	166.8	161.3	167.3	165.1	2.7	1.6
520	165.2	159.7	165.5	163.5	2.7	1.6
500	163.3	158.2	163.3	161.6	2.4	1.5
480	161.4	156.3	161.7	159.8	2.5	1.6
460	159.6	154.3	159.8	157.9	2.5	1.6
440	157.7	152.4	158.1	156.1	2.6	1.7
420	155.3	149.8	155.6	153.6	2.7	1.7
400	153.6	147.8	153.2	151.5	2.6	1.7
380	151.2	145.6	151.0	149.3	2.6	1.7
360	149.2	143.1	148.2	146.8	2.7	1.8
340	146.4	139.9	145.4	143.9	2.9	2.0
320	143.5	137.4	142.6	141.2	2.7	1.9
300	141.1	134.8	140.5	138.8	2.8	2.0
280	138.5	132.0	138.0	136.2	3.0	2.2
260	135.3	128.7	135.4	133.1	3.1	2.4
240	131.8	125.6	132.8	130.1	3.2	2.4
220	128.6	122.1	129.3	126.7	3.2	2.6
200	125.6	118.8	125.6	123.3	3.2	2.6
180	122.0	115.2	121.8	119.7	3.2	2.6
160	116.8	110.0	116.8	114.5	3.2	2.8
140	112.5	105.7	112.0	110.1	3.1	2.8
120	107.7	100.6	106.9	105.1	3.2	3.0
100	102.6	94.6	100.6	99.3	3.4	3.4
80	96.2	87.6	94.7	92.8	3.8	4.0
60	88.1	78.9	85.8	84.3	3.9	4.6
40	78.5	66.4	76.2	73.7	5.2	7.1

Table E.2: Vapour pressure results for acetylacetone in presence on N_2.

Pressure (kPag)	Temperature (°C)			Mean ($\bar{X}$)	Std dev. (S_x)	Rel. std dev. (%)
	Exp. 1	Exp. 2	Exp. 3			
560	235.1	235.1	234.7	235.0	0.2	0.1
540	233.0	233.3	232.8	233.0	0.2	0.1
520	231.2	231.3	230.9	231.1	0.2	0.1
500	229.4	229.6	228.5	229.2	0.5	0.2
480	227.3	227.7	226.4	227.1	0.5	0.2
460	225.1	225.3	223.8	224.7	0.7	0.3
440	222.5	222.6	221.4	222.2	0.5	0.2
420	219.6	219.7	218.4	219.2	0.6	0.3
400	216.8	217.4	215.6	216.6	0.7	0.3
380	214.2	214.7	212.9	213.9	0.8	0.4
360	211.6	211.8	209.6	211.0	1.0	0.5
340	207.6	208.1	205.7	207.1	1.0	0.5
320	204.0	204.4	202.6	203.7	0.8	0.4
300	199.9	200.4	198.8	199.7	0.7	0.3
280	196.0	196.5	195.0	195.8	0.6	0.3
260	192.2	192.6	190.7	191.8	0.8	0.4
240	188.0	188.8	186.1	187.6	1.1	0.6
220	183.8	184.2	180.6	182.9	1.6	0.9
200	179.3	179.6	176.0	178.3	1.6	0.9
180	174.8	175.1	171.5	173.8	1.6	0.9
160	167.8	168.4	164.7	167.0	1.6	1.0
140	161.3	162.0	158.7	160.7	1.4	0.9
120	152.9	155.7	151.6	153.4	1.7	1.1
100	145.6	147.2	144.4	145.7	1.1	0.8
80	136.6	137.8	135.3	136.6	1.0	0.7
60	123.5	125.0	122.8	123.8	0.9	0.7
40	110.1	111.7	109.7	110.5	0.9	0.8

Table E.3: Vapour pressure results for water in presence on N_2.

Pressure (kPag)	Temperature (°C)			Mean ($\bar{X}$)	Std dev. (S_x)	Rel. std dev. (%)
	Exp. 1	Exp. 2	Exp. 3			
2740	235.3	235.3	235.3	235.3	0.0	0.0
2720	234.7	234.8	234.7	234.7	0.0	0.0
2700	234.4	234.4	234.4	234.4	0.0	0.0
2680	234.0	234.0	234.0	234.0	0.0	0.0
2660	233.7	233.6	233.7	233.7	0.0	0.0
2640	233.3	233.2	233.4	233.3	0.1	0.0
2620	233.0	232.9	232.9	232.9	0.0	0.0
2600	232.6	232.4	232.4	232.5	0.1	0.0
2580	232.3	232.2	232.2	232.2	0.0	0.0
2560	231.8	231.7	231.7	231.7	0.0	0.0
2540	231.2	231.3	231.3	231.3	0.0	0.0
2520	230.9	230.9	230.9	230.9	0.0	0.0
2500	230.5	230.4	230.4	230.4	0.0	0.0
2480	230.0	230.0	230.0	230.0	0.0	0.0
2460	229.5	229.5	229.5	229.5	0.0	0.0
2440	229.2	229.1	229.1	229.1	0.0	0.0
2420	228.6	228.7	228.5	228.6	0.1	0.0
2400	228.0	228.2	228.1	228.1	0.1	0.0
2380	227.7	227.8	227.8	227.8	0.0	0.0
2360	227.2	227.2	227.1	227.2	0.0	0.0
2340	226.9	226.8	226.8	226.8	0.0	0.0
2320	226.5	226.5	226.4	226.5	0.0	0.0
2300	226.0	226.0	226.0	226.0	0.0	0.0
2280	225.4	225.5	225.4	225.4	0.0	0.0
2260	225.0	225.1	225.1	225.1	0.0	0.0
2240	224.6	224.5	224.5	224.5	0.0	0.0
2220	224.3	224.1	224.2	224.2	0.1	0.0
2200	223.7	223.8	223.7	223.7	0.0	0.0
2180	223.3	223.3	223.3	223.3	0.0	0.0
2160	222.7	222.8	222.9	222.8	0.1	0.0
2140	222.4	222.4	222.4	222.4	0.0	0.0
2120	222.0	221.9	222.0	222.0	0.0	0.0
2100	221.5	221.5	221.4	221.5	0.0	0.0
2080	221.0	221.0	220.9	221.0	0.0	0.0
2060	220.5	220.5	220.6	220.5	0.0	0.0
2040	219.9	220.1	220.1	220.0	0.1	0.0
2020	219.5	219.5	219.7	219.6	0.1	0.0

Pressure (kPag)	Temperature (°C)			Mean ($\bar{X}$)	Std dev. (S_x)	Rel. std dev. (%)
	Exp. 1	Exp. 2	Exp. 3			
2000	219.2	218.8	219.0	219.0	0.2	0.1
1980	218.6	218.3	218.4	218.4	0.1	0.1
1960	218.1	217.8	218.0	218.0	0.1	0.1
1940	217.5	217.4	217.5	217.5	0.0	0.0
1920	216.9	216.8	217.0	216.9	0.1	0.0
1900	216.3	216.3	216.4	216.3	0.0	0.0
1880	215.8	215.8	215.9	215.8	0.0	0.0
1860	215.3	215.4	215.3	215.3	0.0	0.0
1840	214.9	214.8	214.9	214.9	0.0	0.0
1820	214.3	214.3	214.2	214.3	0.0	0.0
1800	213.4	213.7	213.7	213.6	0.1	0.1
1780	212.9	213.2	213.3	213.1	0.2	0.1
1760	212.4	212.7	212.6	212.6	0.1	0.1
1740	211.9	212.2	212.0	212.0	0.1	0.1
1720	211.3	211.5	211.5	211.4	0.1	0.0
1700	211.0	211.0	211.0	211.0	0.0	0.0
1680	210.3	210.4	210.4	210.4	0.0	0.0
1660	209.9	209.8	209.9	209.9	0.0	0.0
1640	209.3	209.4	209.4	209.4	0.0	0.0
1620	208.6	208.8	208.9	208.8	0.1	0.1
1600	208.2	208.4	208.2	208.3	0.1	0.0
1580	207.6	207.7	207.7	207.7	0.0	0.0
1560	207.2	207.1	207.1	207.1	0.0	0.0
1540	206.6	206.3	206.6	206.5	0.1	0.1
1520	205.9	205.9	205.9	205.9	0.0	0.0
1500	205.3	205.1	205.3	205.2	0.1	0.0
1480	204.5	204.5	204.6	204.5	0.0	0.0
1460	204.0	204.0	204.0	204.0	0.0	0.0
1440	203.3	203.2	203.2	203.2	0.0	0.0
1420	202.7	202.7	202.7	202.7	0.0	0.0
1400	202.2	202.1	201.9	202.1	0.1	0.1
1380	201.4	201.4	201.4	201.4	0.0	0.0
1360	200.6	200.8	200.7	200.7	0.1	0.0
1340	200.1	200.1	200.0	200.1	0.0	0.0
1320	199.5	199.4	199.4	199.4	0.0	0.0
1300	198.8	198.7	198.7	198.7	0.0	0.0
1280	198.1	198.2	197.9	198.1	0.1	0.1
1260	197.5	197.5	197.3	197.4	0.1	0.0
1240	196.7	196.7	196.6	196.7	0.0	0.0

Pressure (kPag)	Temperature (°C)			Mean ($\bar{X}$)	Std dev. (S_x)	Rel. std dev. (%)
	Exp. 1	Exp. 2	Exp. 3			
1220	196.0	196.0	195.8	195.9	0.1	0.0
1200	195.3	195.3	195.2	195.3	0.0	0.0
1180	194.7	194.6	194.5	194.6	0.1	0.0
1160	194.0	193.8	193.9	193.9	0.1	0.0
1140	193.4	193.1	193.0	193.2	0.2	0.1
1120	192.4	192.3	192.3	192.3	0.0	0.0
1100	191.8	191.6	191.5	191.6	0.1	0.1
1080	191.1	190.9	190.8	190.9	0.1	0.1
1060	190.4	190.1	190.0	190.2	0.2	0.1
1040	189.5	189.2	189.1	189.3	0.2	0.1
1020	188.5	188.3	188.2	188.3	0.1	0.1
1000	187.9	187.6	187.5	187.7	0.2	0.1
980	186.9	186.8	186.5	186.7	0.2	0.1
960	186.1	185.8	185.8	185.9	0.1	0.1
940	185.3	185.1	184.8	185.1	0.2	0.1
920	184.4	184.3	183.9	184.2	0.2	0.1
900	183.4	183.5	183.1	183.3	0.2	0.1
880	182.5	182.5	182.6	182.5	0.0	0.0
860	181.6	181.3	181.4	181.4	0.1	0.1
840	180.7	180.6	180.3	180.5	0.2	0.1
820	179.7	179.5	179.2	179.5	0.2	0.1
800	178.8	178.6	178.1	178.5	0.3	0.2
780	177.8	177.6	176.9	177.4	0.4	0.2
760	176.7	176.7	175.9	176.4	0.4	0.2
740	175.7	175.7	174.9	175.4	0.4	0.2
720	174.8	174.7	173.9	174.5	0.4	0.2
700	173.7	173.6	172.9	173.4	0.4	0.2
680	172.9	172.7	171.7	172.4	0.5	0.3
660	171.9	171.8	170.5	171.4	0.6	0.4
640	170.9	170.5	169.4	170.3	0.6	0.4
620	169.8	169.4	168.3	169.2	0.6	0.4
600	168.3	167.8	166.4	167.5	0.8	0.5
580	167.0	166.9	165.2	166.4	0.8	0.5
560	165.7	165.6	163.9	165.1	0.8	0.5
540	164.1	164.2	162.6	163.6	0.7	0.4
520	163.3	162.6	160.8	162.2	1.1	0.6
500	162.1	160.8	159.0	160.6	1.3	0.8
480	160.5	159.1	157.6	159.1	1.2	0.7
460	159.0	157.8	156.2	157.7	1.1	0.7

Pressure (kPag)	Temperature (°C)			Mean ($\bar{X}$)	Std dev. (S_x)	Rel. std dev. (%)
	Exp. 1	Exp. 2	Exp. 3			
440	157.7	156.4	154.5	156.2	1.3	0.8
420	155.7	154.2	152.5	154.1	1.3	0.8
400	154.0	152.6	150.4	152.3	1.5	1.0
380	152.9	150.7	148.3	150.6	1.9	1.2
360	151.3	148.9	146.2	148.8	2.1	1.4
340	149.0	146.5	144.0	146.5	2.0	1.4
320	146.8	144.3	142.0	144.4	2.0	1.4
300	144.5	141.9	139.9	142.1	1.9	1.3
280	142.3	139.7	137.7	139.9	1.9	1.3
260	140.3	137.4	135.5	137.7	2.0	1.4
240	137.6	135.0	132.8	135.1	2.0	1.5
220	134.7	132.3	130.2	132.4	1.8	1.4
200	131.8	129.4	127.0	129.4	2.0	1.5
180	128.8	126.4	123.2	126.1	2.3	1.8
160	124.8	122.0	119.1	122.0	2.3	1.9
140	120.4	118.9	115.5	118.3	2.0	1.7
120	115.9	115.0	111.2	114.0	2.0	1.8
100	111.2	110.1	105.8	109.0	2.3	2.1
80	105.8	103.9	99.0	102.9	2.9	2.8
60	97.7	96.6	89.9	94.7	3.4	3.6
40	86.4	87.7	80.5	84.9	3.1	3.7

The standard deviation was calculated using the following formula (Lazić, 2004):

$$S_x = \sqrt{\frac{1}{N}\sum_{i=0}^{N}(X_i - \bar{X})^2} \qquad (E.1)$$

where S_x is the standard deviation, N is the number of terms, X_i is any given value from the sample and $\bar{X}$ is the mean given by $\sum(X_i/N)$.

The relative standard deviation is given by (Lazić, 2004):

$$Relative\ standard\ deviation(\%) = \frac{S_x}{\bar{X}} \qquad (E.2)$$

APPENDIX F: RESULTS AND CALCULATIONS

The sections that follow contain all the results and calculations relating to the results of the calibration of the Spectroquant and the different reactions that were done inside the autoclave.

F.1 Iron standard calibration results

The iron(III) acetylacetonate standards were scanned using the Spectroquant Pharo 300 Spectrophotometer with software version 2.03-Merck-2.01. They were scanned over the wavelength range of 190 – 600 nm and peak readings taken at 351 nm to construct the calibration curves. An example of the UV-Vis scan is given below in Figure F.1 and the results given in Table F.1. Everytime that samples were analysed the Spectroquant was calibrated and the results are given in Tables F.2 – F.13.

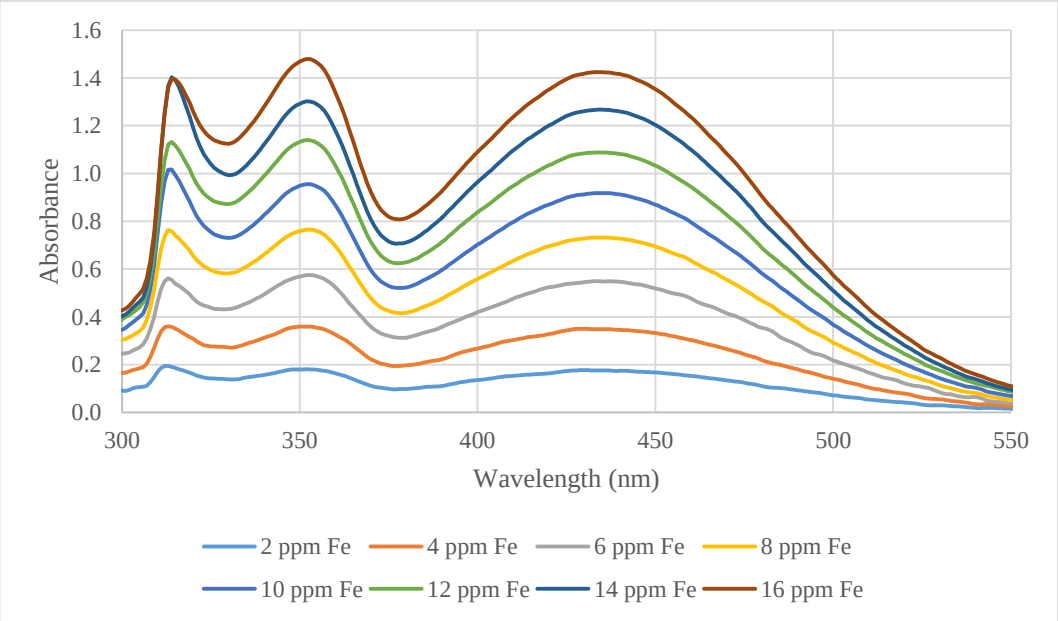


Figure F.1: UV-Vis scan results for the iron(III) acetylacetonate standards shown in terms of iron concentrations (scanned on 06/01/2016).

It can be seen in Figure F.1 that there are three main peaks. The peak at 310 nm is the peak that represents acetylacetone (Abood et al., 1992) (acetylacetone concentration effect shown in Section F.2.5), while the peaks at 351 and 438 nm

are representative of iron(III) acetylacetonate (Meneses et al., 2014). Hence, the absorbance reading was taken at 351 nm as mentioned.

Table F.1: Iron(III) acetylacetonate standard calibration results (scanned on 06/01/2016).

Vial	Std conc. (ppm Fe)	Volume of 100 ppm Fe solution required (mL)	Absorbance at λ = 351 nm			
			Reading 1	Reading 2	Reading 3	Average
3	2	1.000	0.182	0.180	0.179	0.180
4	4	2.000	0.361	0.360	0.359	0.360
5	6	3.000	0.574	0.572	0.571	0.572
6	8	4.000	0.763	0.762	0.763	0.763
7	10	5.000	0.953	0.954	0.952	0.953
8	12	6.000	1.139	1.137	1.136	1.137
9	14	7.000	1.300	1.298	1.296	1.298
10	16	8.000	1.477	1.478	1.472	1.476

These results were then used to construct the calibration curve below.

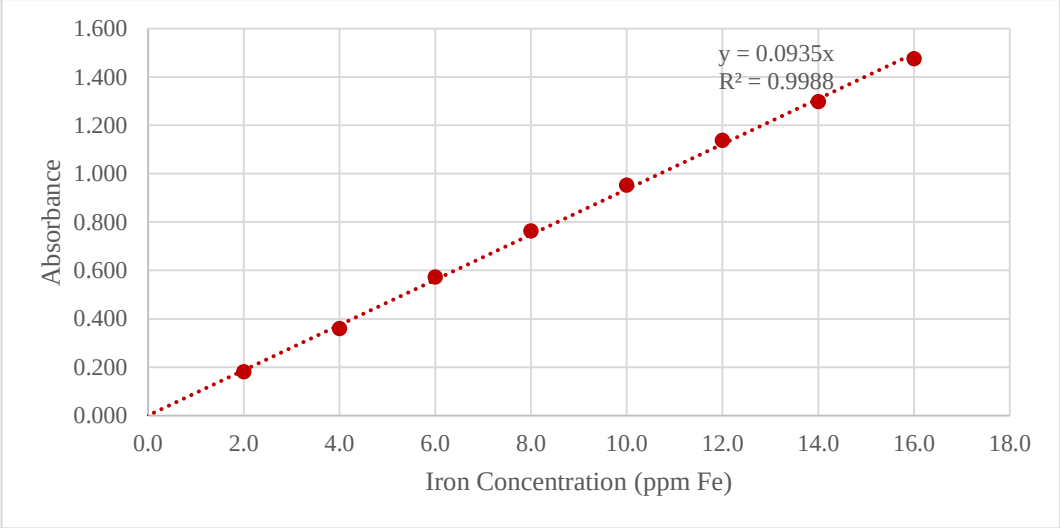


Figure F.2: Calibration curve for the iron(III) acetylacetonate standards represented in terms of iron concentration present (scanned on 06/01/2016).

The curve has an equation of $y = 0.0935x$ this is equivalent to $Absorbance = 0.0935\ (iron\ conc.\ [ppm\ Fe])$ which can be rearranged to:

$$Iron\ conc.[ppm\ Fe] = 10.693\ (Absorbance) \qquad (F.1)$$

This equation makes it easier to determine the unknown concentration of iron in the sample solutions. The rearranged calibration equation is given at the bottom of each calibration table below.

Table F.2: Iron(III) acetylacetonate standard calibration results (scanned on 08/01/2016).

Vial	Std conc. (ppm Fe)	Volume of 100 ppm Fe solution required (mL)	Absorbance at λ = 351 nm			
			Reading 1	Reading 2	Reading 3	Average
3	2	1.000	0.174	0.176	0.175	0.175
4	4	2.000	0.346	0.345	0.345	0.345
5	6	3.000	0.562	0.561	0.560	0.561
6	8	4.000	0.754	0.753	0.755	0.754
7	10	5.000	0.942	0.940	0.939	0.940
8	12	6.000	1.121	1.115	1.115	1.117
9	14	7.000	1.296	1.293	1.293	1.294
10	16	8.000	1.457	1.456	1.452	1.455
Calibration equation (with R^2 = 0.9987) : Concentration of iron (ppm Fe) = 10.829 × Absorbance						

Table F.3: Iron(III) acetylacetonate standard calibration results (scanned on 15/01/2016).

Vial	Std conc. (ppm Fe)	Volume of 100 ppm Fe solution required (mL)	Absorbance at λ = 351 nm			
			Reading 1	Reading 2	Reading 3	Average
3	2	1.000	0.181	0.177	0.176	0.178
4	4	2.000	0.369	0.368	0.367	0.368
5	6	3.000	0.572	0.571	0.569	0.571
6	8	4.000	0.786	0.784	0.783	0.784
7	10	5.000	0.936	0.933	0.933	0.934
8	12	6.000	1.137	1.134	1.132	1.134
9	14	7.000	1.341	1.340	1.336	1.339
10	16	8.000	1.468	1.462	1.461	1.464
Calibration equation (with R^2 = 0.9977) : Concentration of iron (ppm Fe) = 10.642 × Absorbance						

Table F.4: Iron(III) acetylacetonate standard calibration results (scanned on 22/01/2016).

Vial	Std conc. (ppm Fe)	Volume of 100 ppm Fe solution required (mL)	Absorbance at λ = 351 nm			
			Reading 1	Reading 2	Reading 3	Average
3	2	1.000	0.174	0.173	0.173	0.173
4	4	2.000	0.367	0.366	0.366	0.366
5	6	3.000	0.532	0.530	0.529	0.530
6	8	4.000	0.716	0.714	0.712	0.714
7	10	5.000	0.879	0.877	0.877	0.878
8	12	6.000	1.057	1.054	1.052	1.054
9	14	7.000	1.243	1.236	1.234	1.238
10	16	8.000	1.452	1.448	1.446	1.449
Calibration equation (with $R^2 = 0.9991$) : Concentration of iron (ppm Fe) = 11.231 × Absorbance						

Table F.5: Iron(III) acetylacetonate standard calibration results (scanned on 29/01/2016).

Vial	Std conc. (ppm Fe)	Volume of 100 ppm Fe solution required (mL)	Absorbance at λ = 351 nm			
			Reading 1	Reading 2	Reading 3	Average
3	2	1.000	0.185	0.183	0.184	0.184
4	4	2.000	0.364	0.361	0.362	0.362
5	6	3.000	0.524	0.524	0.522	0.523
6	8	4.000	0.718	0.716	0.717	0.717
7	10	5.000	0.873	0.868	0.867	0.869
8	12	6.000	1.053	1.049	1.049	1.050
9	14	7.000	1.239	1.234	1.234	1.236
10	16	8.000	1.453	1.448	1.445	1.449
Calibration equation (with $R^2 = 0.9988$) : Concentration of iron (ppm Fe) = 11.257 × Absorbance						

Table F.6: Iron(III) acetylacetonate standard calibration results (scanned on 04/02/2016).

Vial	Std conc. (ppm Fe)	Volume of 100 ppm Fe solution required (mL)	Absorbance at λ = 351 nm			
			Reading 1	Reading 2	Reading 3	Average
3	2	1.000	0.179	0.179	0.178	0.179
4	4	2.000	0.362	0.316	0.360	0.346
5	6	3.000	0.531	0.531	0.529	0.530
6	8	4.000	0.731	0.729	0.730	0.730
7	10	5.000	0.879	0.877	0.876	0.877
8	12	6.000	1.068	1.065	1.064	1.066
9	14	7.000	1.269	1.268	1.270	1.269
10	16	8.000	1.472	1.472	1.465	1.470
Calibration equation (with R^2 = 0.9985) : Concentration of iron (ppm Fe) = 11.083 × Absorbance						

Table F.7: Iron(III) acetylacetonate standard calibration results (scanned on 19/02/2016).

Vial	Std conc. (ppm Fe)	Volume of 100 ppm Fe solution required (mL)	Absorbance at λ = 351 nm			
			Reading 1	Reading 2	Reading 3	Average
3	2	1.000	0.194	0.194	0.194	0.194
4	4	2.000	0.374	0.365	0.364	0.368
5	6	3.000	0.521	0.520	0.520	0.520
6	8	4.000	0.784	0.780	0.779	0.781
7	10	5.000	0.875	0.869	0.869	0.871
8	12	6.000	1.070	1.067	1.064	1.067
9	14	7.000	1.260	1.258	1.255	1.258
10	16	8.000	1.459	1.456	1.453	1.456
Calibration equation (with R^2 = 0.9959) : Concentration of iron (ppm Fe) = 11.071 × Absorbance						

Table F.8: Iron(III) acetylacetonate standard calibration results (scanned on 26/02/2016).

Vial	Std conc. (ppm Fe)	Volume of 100 ppm Fe solution required (mL)	Absorbance at λ = 351 nm			
			Reading 1	Reading 2	Reading 3	Average
3	2	1.000	0.175	0.176	0.174	0.175
4	4	2.000	0.366	0.365	0.364	0.365
5	6	3.000	0.532	0.530	0.530	0.531
6	8	4.000	0.720	0.713	0.713	0.715
7	10	5.000	0.877	0.873	0.872	0.874
8	12	6.000	1.075	1.073	1.070	1.073
9	14	7.000	1.253	1.248	1.246	1.249
10	16	8.000	1.413	1.407	1.405	1.408
Calibration equation (with $R^2 = 0.9996$) : Concentration of iron (ppm Fe) = 11.278 × Absorbance						

Table F.9: Iron(III) acetylacetonate standard calibration results (scanned on 03/03/2016).

Vial	Std conc. (ppm Fe)	Volume of 100 ppm Fe solution required (mL)	Absorbance at λ = 351 nm			
			Reading 1	Reading 2	Reading 3	Average
3	2	1.000	0.179	0.179	0.179	0.179
4	4	2.000	0.361	0.360	0.361	0.361
5	6	3.000	0.551	0.551	0.551	0.551
6	8	4.000	0.717	0.717	0.717	0.717
7	10	5.000	0.913	0.911	0.910	0.911
8	12	6.000	1.098	1.094	1.095	1.096
9	14	7.000	1.234	1.232	1.231	1.232
10	16	8.000	1.431	1.427	1.425	1.428
Calibration equation (with $R^2 = 0.9990$) : Concentration of iron (ppm Fe) = 11.145 × Absorbance						

Table F.10: Iron(III) acetylacetonate standard calibration results (scanned on 07/03/2016).

Vial	Std conc. (ppm Fe)	Volume of 100 ppm Fe solution required (mL)	Absorbance at λ = 351 nm			
			Reading 1	Reading 2	Reading 3	Average
3	2	1.000	0.175	0.175	0.175	0.175
4	4	2.000	0.351	0.350	0.349	0.350
5	6	3.000	0.541	0.540	0.539	0.540
6	8	4.000	0.715	0.713	0.714	0.714
7	10	5.000	0.903	0.901	0.900	0.901
8	12	6.000	1.084	1.081	1.080	1.082
9	14	7.000	1.220	1.223	1.215	1.219
10	16	8.000	1.423	1.418	1.416	1.419
Calibration equation (with R^2 = 0.9992) : Concentration of iron (ppm Fe) = 11.258 × Absorbance						

Table F.11: Iron(III) acetylacetonate standard calibration results (scanned on 08/03/2016).

Vial	Std conc. (ppm Fe)	Volume of 100 ppm Fe solution required (mL)	Absorbance at λ = 351 nm			
			Reading 1	Reading 2	Reading 3	Average
3	2	1.000	0.186	0.185	0.186	0.186
4	4	2.000	0.363	0.361	0.361	0.362
5	6	3.000	0.555	0.552	0.552	0.553
6	8	4.000	0.736	0.733	0.733	0.734
7	10	5.000	0.920	0.923	0.916	0.920
8	12	6.000	1.099	1.097	1.095	1.097
9	14	7.000	1.237	1.234	1.231	1.234
10	16	8.000	1.442	1.437	1.435	1.438
Calibration equation (with R^2 = 0.9988) : Concentration of iron (ppm Fe) = 11.076 × Absorbance						

Table F.12: Iron(III) acetylacetonate standard calibration results (scanned on 11/03/2016).

Vial	Std conc. (ppm Fe)	Volume of 100 ppm Fe solution required (mL)	Absorbance at λ = 351 nm			
			Reading 1	Reading 2	Reading 3	Average
3	2	1.000	0.195	0.194	0.194	0.194
4	4	2.000	0.366	0.366	0.364	0.365
5	6	3.000	0.560	0.558	0.557	0.558
6	8	4.000	0.743	0.742	0.740	0.742
7	10	5.000	0.901	0.899	0.897	0.899
8	12	6.000	1.095	1.093	1.091	1.093
9	14	7.000	1.273	1.268	1.266	1.269
10	16	8.000	1.476	1.473	1.470	1.473
Calibration equation (with $R^2 = 0.9994$) : Concentration of iron (ppm Fe) = 10.941 × Absorbance						

Table F.13: Iron(III) acetylacetonate standard calibration results (scanned on 16/03/2016).

Vial	Std conc. (ppm Fe)	Volume of 100 ppm Fe solution required (mL)	Absorbance at λ = 351 nm			
			Reading 1	Reading 2	Reading 3	Average
3	2	1.000	0.186	0.187	0.186	0.186
4	4	2.000	0.365	0.365	0.364	0.365
5	6	3.000	0.564	0.562	0.563	0.563
6	8	4.000	0.710	0.708	0.706	0.708
7	10	5.000	0.908	0.906	0.905	0.906
8	12	6.000	1.102	1.100	1.099	1.100
9	14	7.000	1.298	1.289	1.288	1.292
10	16	8.000	1.485	1.482	1.477	1.481
Calibration equation (with $R^2 = 0.9994$) : Concentration of iron (ppm Fe) = 10.941 × Absorbance						

These calibration results were used to calculate all the unknown concentrations of the sample results that follow.

F.2 Sample results

The samples were all prepared to a 1000 times dilution ratio (as mentioned previously) and with the use of the calibration data the concentrations of iron

present in each of the solutions could be found. However, more calculations were needed to calculate the conversion percentage of iron in iron oxide to iron in iron(III) acetylacetonate. The concentration of iron in the sample ($C_{Fe_{(sample)}}$) was calculated from the concentration of iron in the diluted solution ($C_{Fe_{(dil)}}$) using the following equation:

$$C_{Fe_{(sample)}} = C_{Fe_{(dil)}} \times D \qquad (F.2)$$

Once the concentration of iron in the sample was calculated it was converted to mass of iron present in the sample ($m_{Fe_{(sample)}}$) by multiplying it with the volume of the sample ($V_{(sample)}$). This followed the following equation:

$$m_{Fe_{(sample)}} = C_{Fe_{(sample)}} \times V_{(sample)} \qquad (F.3)$$

Using the mass of iron in the sample and the mass of iron present in the original loaded solution ($m_{Fe_{(loaded)}}$) it was possible to calculate the percentage of iron in the iron oxide loaded that was converted to iron in the iron(III) acetylacetonate. This is given by:

$$\%\ Iron\ converted = \frac{m_{Fe_{(sample)}}}{m_{Fe_{(loaded)}}} \times 100 \qquad (F.4)$$

Where $m_{Fe_{(loaded)}}$ is given in terms of the mass of synthetic iron oxide ($m_{Fe_2O_3\,syn}$) (>95 %):

$$m_{Fe_{(loaded)}} = 0.95 \times m_{Fe_2O_3\,syn} \times \frac{2 \times M_{Fe}}{M_{Fe_2O_3}} \qquad (F.5)$$

Or alternately in terms of the mass of iron ore fines ($m_{Fe_2O_3\,fines}$) (>93 %):

$$m_{Fe_{(loaded)}} = 0.93 \times m_{Fe_2O_3\,fines} \times \frac{2 \times M_{Fe}}{M_{Fe_2O_3}} \qquad (F.6)$$

Where M_{Fe} is the molecular weight of iron (55.847 g/mol) and $M_{Fe_2O_3}$ is the molecular weight of iron(III) oxide (159.69 g/mol).

F.2.1 Example calculation

Taking an example of an average absorbance reading of 0.617 and using Equations F.1 – F.6 the percentage of iron converted is calculated as follows:

$$Iron\ conc. = 10.693\ (Absorbance) = 10.693\ (0.617) = 6.597\ ppm\ Fe$$

Hence, the unknown concentration of iron in the diluted solution is $C_{Fe_{(dil)}} = 6.597\ ppm\ Fe$. Now it is possible to calculate the concentration of the sample solution.

$$C_{Fe_{(sample)}} = C_{Fe_{(dil)}} \times D = (6.597\ ppm\ Fe) \times (1000) = 6597\ ppm\ Fe$$

Hence, the mass of iron present in the sample solution is (remembering 1 ppm = 1 mg/L = 10^{-6} g/mL):

$$m_{Fe_{(sample)}} = C_{Fe_{(sample)}} \times V_{(sample)} = \left(6\,597\ \times 10^{-6}\frac{g\ Fe}{mL}\right) \times (250\ mL)$$
$$= 1.649\ g\ Fe$$

First, calculating the mass of iron loaded in the original sample. Taking a mass of synthetic iron oxide of 5.0032 g this gives:

$$m_{Fe_{(loaded)}} = 0.95 \times m_{Fe_2O_3\,syn} \times \frac{2 \times M_{Fe}}{M_{Fe_2O_3}}$$
$$= 0.95 \times (5.0032\ g) \times \frac{2 \times (55.847)}{(159.69)} = 3.324\ g\ Fe$$

Thus, the percentage of iron converted from iron oxide to iron acetylacetonate is:

$$\%\ Iron\ converted = \frac{m_{Fe_{(sample)}}}{m_{Fe_{(loaded)}}} \times 100 = \frac{1.649\ g\ Fe}{3.324\ g\ Fe} \times 100 = 49.6\ \%$$

This means that 49.6 % of the original iron in the iron ore fines was converted to iron present in the iron(III) acetylacetonate.

This type of calculation was performed per each of the sample results that follow.

F.2.2 Initial extraction of iron from iron ore fines

The initial testing results of iron ore fines at varying pressures of 1000, 2000 and 3000 kPa nitrogen loaded are shown below.

Table F.14: Results for the initial study at varying N_2 loaded pressures of 7.5 g of iron ore fines (>93 %) at 220 °C with 300 mL solution (270 mL acetylacetone and 30 mL water), solid to liquid ratio of 0.025 g:1 mL, total time 18 h, particle size of +106 -150 µm and stirrer speed of 375 rpm.

Temperature (°C)	Nitrogen pressure (kPa)	Mass iron oxide (g)	Final sample volume (mL)	Dilution ratio	Average absorbance (@ λ = 351 nm)	Diluted iron concentration (ppm Fe)	Sample concentration (ppm Fe)	Mass of iron extracted (g)	Iron extracted/ converted (%)
220	1000	7.503	250	1000	-	-	-	-	-
220	2000	7.501	250	1000	-	-	-	-	-
220	3000	7.502	250	1000	-	-	-	-	-

F.2.3 Extraction of iron from synthetic iron(III) oxide

The results from the temperature study on the synthetic iron oxide are shown below for varying temperatures of 120, 140, 150, 160, 180 and 220 °C at times of 3, 4, 6, 8, 10 and 18 h when deemed necessary.

Table F.15: Results for the temperature study of 5 g of synthetic iron oxide (>95 %) with 200 mL solution (180 mL acetylacetone and 20 mL water), 1010 kPa N_2 loaded, solid to liquid ratio of 0.025 g:1 mL and stirrer speed of 375 rpm.

Temperature (°C)	Total time (h)	Mass iron oxide (g)	Final sample volume (mL)	Dilution ratio	Average absorbance (@ λ = 351 nm)	Diluted iron concentration (ppm Fe)	Sample concentration (ppm Fe)	Mass of iron extracted (g)	Iron extracted/ converted (%)
220	8	5.0022	250	1000	-	-	-	-	-
220	6	5.0025	250	1000	-	-	-	-	-
220	4	5.0034	250	1000	-	-	-	-	-
220	3	5.0032	250	1000	-	-	-	-	-
180	8	5.0033	250	1000	-	-	-	-	-
180	6	5.0028	250	1000	-	-	-	-	-
180	4	5.0010	250	1000	-	-	-	-	-
180	3	5.0037	250	1000	0.578	6.297	6297	1.574	47.4
160	10	5.0032	250	1000	-	-	-	-	-
160	8	5.0026	250	1000	0.446	4.943	4943	1.236	37.2
160	6	5.0038	250	1000	0.556	6.162	6162	1.541	46.3
160	4	5.0017	250	1000	0.563	6.275	6275	1.569	47.2
160	3	5.0020	250	1000	0.569	6.338	6338	1.584	47.7
150	18	5.0020	250	1000	0.667	7.437	7437	1.859	55.9
150	10	5.0025	250	1000	0.650	7.078	7078	1.769	53.2
150	8	5.0026	250	1000	0.608	6.731	6731	1.683	50.6

Temperature (°C)	Total time (h)	Mass iron oxide (g)	Final sample volume (mL)	Dilution ratio	Average absorbance (@ λ = 351 nm)	Diluted iron concentration (ppm Fe)	Sample concentration (ppm Fe)	Mass of iron extracted (g)	Iron extracted/ converted (%)
150	6	5.0032	250	1000	0.569	6.299	6299	1.575	47.4
150	4	5.0030	250	1000	0.515	5.702	5702	1.425	42.9
150	3	5.0026	250	1000	0.360	4.008	4008	1.002	30.1
140	18	5.0025	250	1000	0.708	7.838	7838	1.960	59.0
140	10	5.0032	260	1000	0.648	7.281	7281	1.893	56.9
140	8	5.0030	250	1000	0.632	7.098	7098	1.774	53.4
140	6	5.0032	250	1000	0.617	6.597	6597	1.649	49.6
140	4	5.0026	250	1000	0.425	4.733	4733	1.183	35.6
140	3	5.0023	250	1000	0.331	3.693	3693	0.923	27.8
120	18	5.0026	250	1000	0.740	8.251	8251	2.063	62.1
120	10	5.0034	250	1000	0.625	7.019	7019	1.755	52.8
120	8	5.0029	250	1000	0.582	6.197	6197	1.549	46.6
120	6	5.0015	250	1000	0.499	5.407	5407	1.352	40.7
120	4	5.0029	250	1000	0.355	3.953	3953	0.988	29.7
120	3	5.0015	250	1000	0.088	0.977	977	0.244	7.3

F.2.4 Extraction of iron from iron ore fines

All the UV-Vis results are given before the conversion results for the iron ore fine studies below. These have been grouped by reaction rate, change in temperature and particle size, change in pressure of N_2 loaded, and change in solid to liquid ratio.

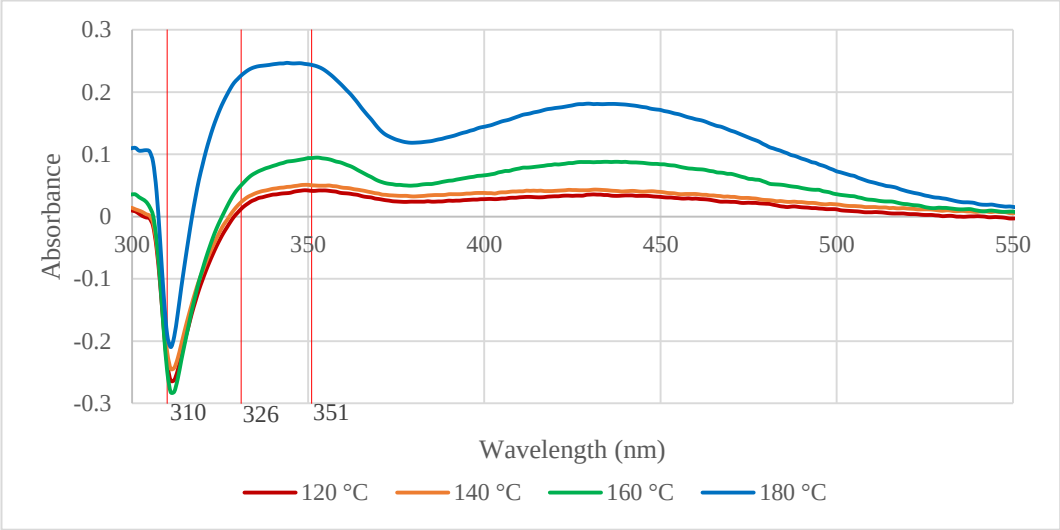


Figure F.3: UV-Vis analysis results temperature study of 5 g of iron ore fines (>93 %) with 200 mL solution (180 mL acetylacetone and 20 mL water), 1010 kPa N_2 loaded, solid to liquid ratio of 0.025 g:1 mL, particle size of +45-75 µm, total time 4 h and stirrer speed of 375 rpm.

Table F.16: Results for the reaction rate study of 5 g of iron ore fines (>93 %) at 140 °C with 200 mL solution (180 mL acetylacetone and 20 mL water), 1010 kPa N_2 loaded, solid to liquid ratio of 0.025 g:1 mL, particle size of +106 -150 µm and stirrer speed of 375 rpm.

Temperature (°C)	Total time (h)	Mass iron oxide (g)	Final sample volume (mL)	Dilution ratio	Average absorbance (@ λ = 351 nm)	Diluted iron concentration (ppm Fe)	Sample concentration (ppm Fe)	Mass of iron extracted (g)	Iron extracted/ converted (%)
140	10	5.0034	250	1000	0.093	1.051	1051	0.263	8.1
140	8	5.0034	250	1000	0.083	0.931	931	0.233	7.1
140	6	5.0032	260	1000	0.064	0.720	720	0.187	5.8
140	4	5.0038	250	1000	0.048	0.537	537	0.134	4.1

Table F.17: Results for the particle size and temperature study of 5 g of iron ore fines (>93 %) with 200 mL solution (180 mL acetylacetone and 20 mL water), 1010 kPa N_2 loaded, solid to liquid ratio of 0.025 g:1 mL, total time 4 h and stirrer speed of 375 rpm.

Temperature (°C)	Particle size (µm)	Mass iron oxide (g)	Final sample volume (mL)	Dilution ratio	Average absorbance (@ λ = 351 nm)	Diluted iron concentration (ppm Fe)	Sample concentration (ppm Fe)	Mass of iron extracted (g)	Iron extracted/ converted (%)
120	+45-75	5.0022	250	1000	0.041	0.465	465	0.116	3.6
140	+45-75	5.0015	250	1000	0.051	0.570	570	0.143	4.4
160	+45-75	5.0031	250	1000	0.094	1.041	1041	0.260	8.0
180	+45-75	5.0014	250	1000	0.244	2.699	2699	0.675	20.7
120	+106-150	5.0019	250	1000	0.030	0.334	334	0.084	2.6
140	+106-150	5.0038	250	1000	0.048	0.537	537	0.134	4.1
160	+106-150	5.0021	250	1000	0.083	0.931	931	0.233	7.2
180	+106-150	5.0032	250	1000	0.213	2.394	2394	0.599	18.4
180	+212-300	5.0015	250	1000	0.202	2.234	2234	0.558	17.2

Table F.18: Results for the pressure study of 5 g of iron ore fines (>93 %) at 180 °C with 200 mL solution (180 mL acetylacetone and 20 mL water), solid to liquid ratio of 0.025 g:1 mL, particle size of +45-75 µm, total time 4 h and stirrer speed of 375 rpm.

Temperature (°C)	Nitrogen pressure (kPa)	Mass iron oxide (g)	Final sample volume (mL)	Dilution ratio	Average absorbance (@ λ = 351 nm)	Diluted iron concentration (ppm Fe)	Sample concentration (ppm Fe)	Mass of iron extracted (g)	Iron extracted/ converted (%)
180	0	5.0021	250	1000	0.204	2.232	2232	0.558	17.1
180	1010	5.0014	250	1000	0.244	2.699	2699	0.675	20.7
180	2010	5.0015	250	1000	0.208	2.272	2272	0.568	17.5
180	3010	5.0015	250	1000	0.155	1.696	1696	0.424	13.0

Table F.19: Results for the solid to liquid ratio study of iron ore fines (>93 %) at 180 °C with 200 mL solution (180 mL acetylacetone and 20 mL water), 1010 kPa N_2 loaded, particle size of +45-75 µm, total time 4 h, and stirrer speed of 375 rpm.

Temperature (°C)	Solid to liquid ratio (g:mL)	Mass iron oxide (g)	Final sample volume (mL)	Dilution ratio	Average absorbance (@ λ = 351 nm)	Diluted iron concentration (ppm Fe)	Sample concentration (ppm Fe)	Mass of iron extracted (g)	Iron extracted/ converted (%)
180	0.025:1	5.0014	250	1000	0.244	2.699	2699	0.675	20.7
180	0.050:1	10.0026	250	1000	0.362	3.961	3961	0.990	15.2
180	0.100:1	20.0026	250	1000	0.505	5.529	5529	1.382	10.6

F.2.5 Acetylacetone UV-Vis scan peak results

It would be noted that the calibration UV-Vis curves have positive peaks at 310 nm while those of the samples have negative peaks in some cases. This is due to the concentration of acetylacetone present in the standards being slightly higher than that of the samples compared to the blank. This relationship can be seen in the UV-Vis curve below of varying acetylacetone volumes (0, 0.0125, 0.0250, 0.0500, 0.0750, 0.0875 and 0.1000 mL) added to pure ethanol (in a 50 mL volumetric flask) and run against the blank with 0.05 mL acetylacetone.

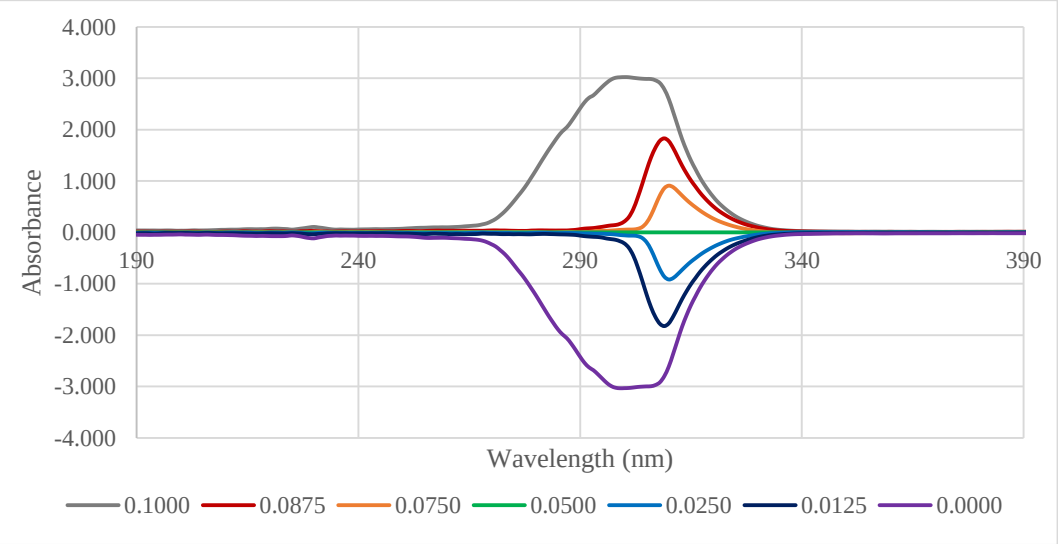


Figure F.4: UV-Vis scan results of varying acetylacetone volumes into ethanol with solution total volume of 50 mL.

It can be seen in Figure F.4 if the concentration of acetylacetone is higher than the blank then the peak is positive while if the concentration of acetylacetone is lower than the blank then the peak would be negative. The absorbance values at 351 nm are plotted on the graph below.

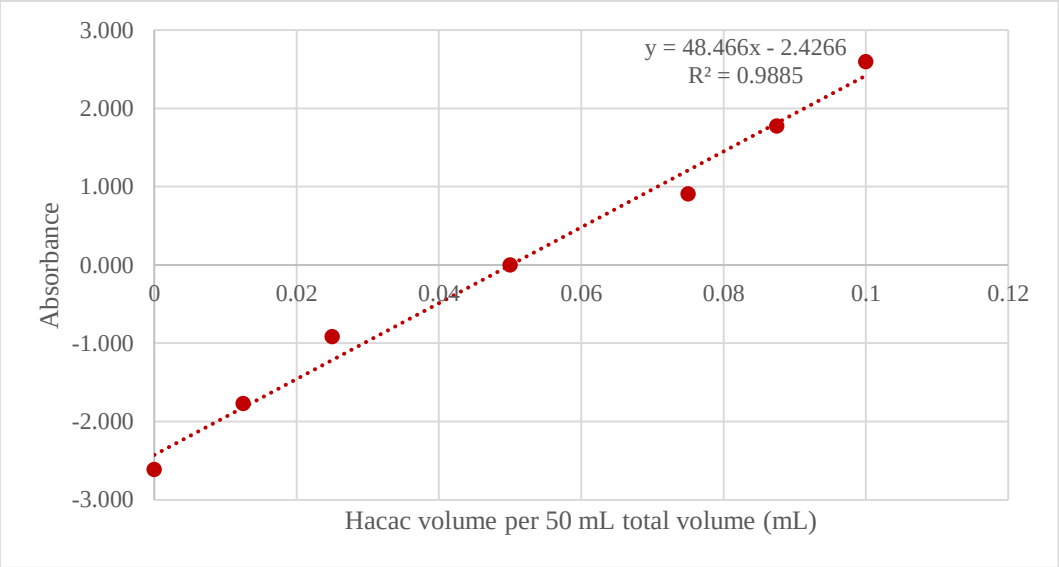


Figure F.5: Results of varying acetylacetone volumes into ethanol with solution total volume of 50 mL.

F.3 FTIR results

The FTIR scan results for the synthetic iron oxide experiments performed at 140 °C and total time of 8 h, and 180 °C and total time of 4 h are shown below.

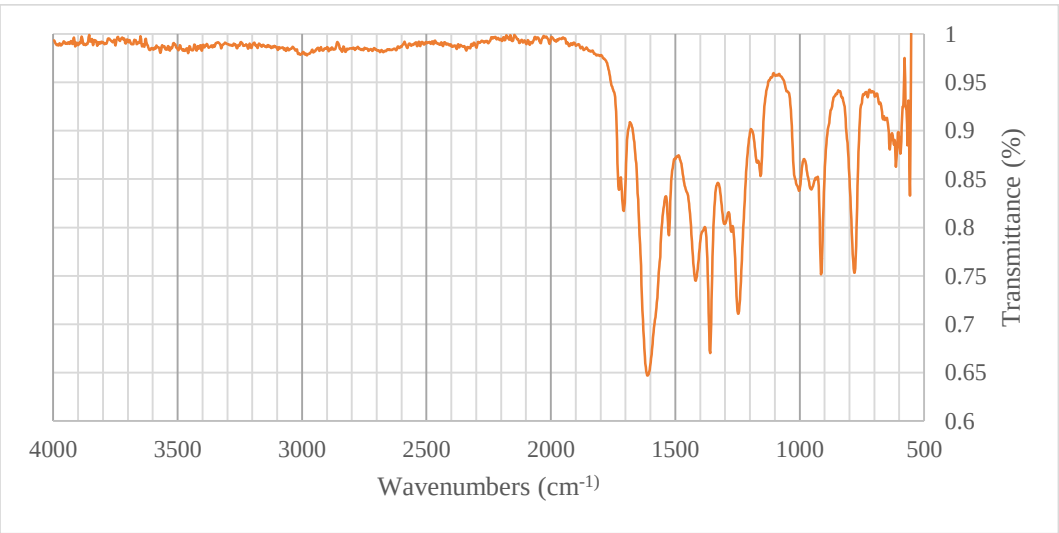


Figure F.6: FTIR scan results for the synthetic iron oxide experiment performed at 140 °C, total time of 8 h, 9:1 ratio of acetylacetone: water, 0.025 g/mL and 5 g of iron oxide.

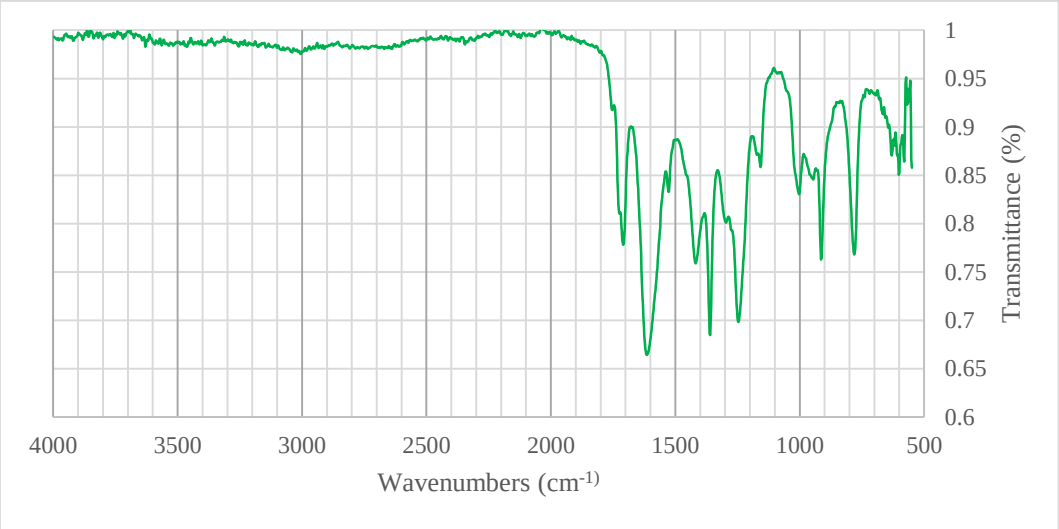


Figure F.7: FTIR scan results for the synthetic iron oxide experiment performed at 140 °C, total time of 4 h, 9:1 ratio of acetylacetone: water, 0.025 g/mL and 5 g of iron oxide.

F.4 Recovery results and calculations

The samples were recovered using the Heidolph Rotary Evaporator. The following calculations were made to estimate the amount of iron(III) acetylacetonate that was expected and the actual amount produced.

The expected amount of iron(III) acetylacetonate formed $\left(m_{Fe(acac)_{3(calc)}}\right)$ based on the amount of iron present in the solution was calculated using the following formula:

$$m_{Fe(acac)_{3(calc)}} = m_{Fe} \times \frac{M_{Fe(acac)_3}}{M_{Fe}} \qquad (F.7)$$

Where $M_{Fe(acac)_3}$ is the molar mass of iron(III) acetylacetonate = 353.17 g/mol.

The actual amount of iron(III) acetylacetonate formed $\left(m_{Fe(acac)_{3(actual)}}\right)$ was based on the mass of crystals weighed $\left(m_{Fe(acac)_{3(weighed)}}\right)$ and multiplied by the volume factor. This is given by the following formula:

$$m_{Fe(acac)_{3(actual)}} = m_{Fe(acac)_{3(weighed)}} \times \frac{V_{sample}}{V_{recovery}} \qquad (F.8)$$

Where V_{sample} is the volume of the original sample (i.e. 250 mL) and $V_{recovery}$ is the volume of the amount of that solution that was used in the recovery (i.e. 200 mL).

This calculation was based on the fact that:

$$\frac{m}{m_1} = \frac{CV}{C_1V_1} \qquad (F.9)$$

But the concentration of the solutions are the same and thus cancel each other out yielding the formula above when rearranged.

The amount recovered was calculated based on the actual and the calculated weights given by the following:

$$Recovery\ (\%) = \frac{m_{Fe(acac)_{3(actual)}}}{m_{Fe(acac)_{3(calc)}}} \times 100 \qquad (F.10)$$

F.4.1 Solid to liquid ratio experimental calculated results

The calculated iron(III) acetylacetonate results for the solid to liquid ratio iron ore fines study are given below.

Table F.20: Calculated yield of iron(III) acetylacetonate for the solid to liquid ratio study of iron ore fines (>93 %) at 180 °C with 200 mL solution (180 mL acetylacetone and 20 mL water), 1010 kPa N_2 loaded, particle size of +45-75 µm, total time 4 h, and stirrer speed of 375 rpm.

Solid to liquid ratio (g:mL)	Mass of iron extracted (g)	Calculated iron(III) acetylacetonate formed (g)
0.025:1	0.675	4.27
0.050:1	0.990	6.26
0.100:1	1.382	8.74